AD-A121 681 OPTICAL WAVEGUIDE SPATIAL FILTERS(U) BATTELLE COLUMBUS LABS OH C M VERBER ET AL. 30 JUN 82 AFOSR-TR-82-1000 F49620-79-C-0044 1/2

UNCLASSIFIED F/G 20/6 NL

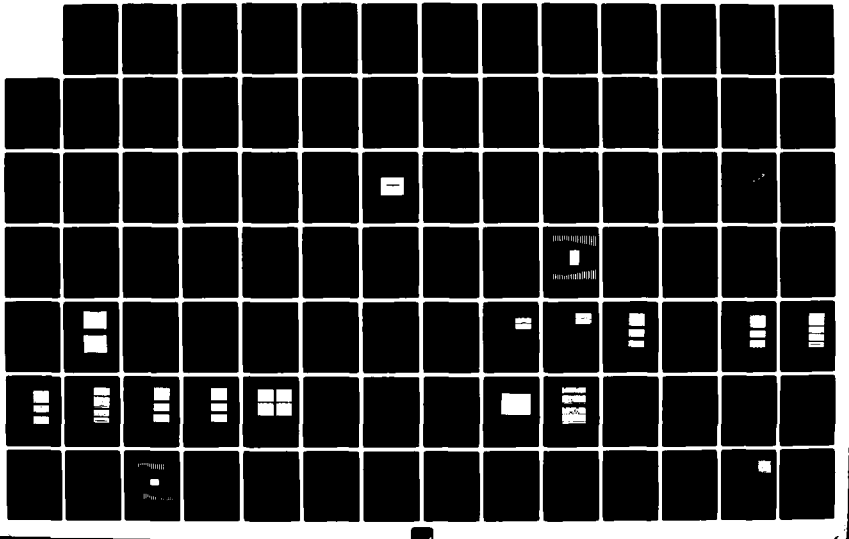

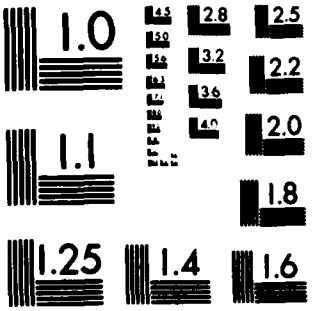

MICROCOPY RESOLUTION TEST CHART
NATIONAL BUREAU OF STANDARDS-1963-A

AD A121681

OPTICAL WAVEGUIDE SPATIAL FILTERS

ANNUAL TECHNICAL REPORT

on

AFOSR Contract No. F49620-79-C-0044

by

C. M. Verber, R. P. Kenan and J. R. Busch

June 30, 1982

Optical Sciences Group
Battelle Columbus Laboratories
505 King Avenue
Columbus, Ohio 43201

DTIC
ELECTE
NOV 22 1982
S
E
D

Approved for public release;
distribution unlimited.

DTIC FILE COPY

82 11 22 010

SECURITY CLASSIFICATION OF THIS PAGE (When Data Entered) UNCLASSIFIED

REPORT DOCUMENTATION PAGE

READ INSTRUCTIONS BEFORE COMPLETING FORM

1. REPORT NUMBER: AFOSR-TR- 82-1000	2. GOVT ACCESSION NO.: AD-A121681
3. RECIPIENT'S CATALOG NUMBER:	
4. TITLE (and Subtitle): OPTICAL WAVEGUIDE SPATIAL FILTERS	5. TYPE OF REPORT & PERIOD COVERED: Annual Technical Report
	6. PERFORMING ORG. REPORT NUMBER:
7. AUTHOR(s): C. M. Verber, R. P. Kenan and J. R. Busch	8. CONTRACT OR GRANT NUMBER(s): F49620-79-C-0044
9. PERFORMING ORGANIZATION NAME AND ADDRESS: Battelle Columbus Laboratories, 505 King Avenue, Columbus, Ohio 43201	10. PROGRAM ELEMENT, PROJECT, TASK AREA & WORK UNIT NUMBERS: 61102F 2305/B1
11. CONTROLLING OFFICE NAME AND ADDRESS: Air Force Office of Scientific Research/NE, Building 410, Bolling AFB, Washington, D.C. 20332	12. REPORT DATE: June 30, 1982 13. NUMBER OF PAGES: 237
14. MONITORING AGENCY NAME & ADDRESS (if different from Controlling Office)	15. SECURITY CLASS. (of this report): UNCLASSIFIED 15a. DECLASSIFICATION/DOWNGRADING SCHEDULE

16. DISTRIBUTION STATEMENT (of this Report)

Approved for public release; distribution unlimited.

17. DISTRIBUTION STATEMENT (of the abstract entered in Block 20, if different from Report)

18. SUPPLEMENTARY NOTES

19. KEY WORDS (Continue on reverse side if necessary and identify by block number)

Spatial light modulator
Integrated optics
Waveguides
Correlator
Grating array
Electrooptics

20. ABSTRACT (Continue on reverse side if necessary and identify by block number)

Research leading to the development of an Integrated-Optical Spatial Light Modulator (IOSLM) and its utilization as a component in a space-integrating correlator for binary words is presented. Principles of operation, design procedures, and characterization data are discussed. Other uses for the IOSLM are presented and commented upon. The full range of the research-from feasibility experiment through characterization of a 32 Mbit/sec correlator-is presented.

DD FORM 1 JAN 73 1473 EDITION OF 1 NOV 65 IS OBSOLETE

UNCLASSIFIED

SECURITY CLASSIFICATION OF THIS PAGE (When Data Entered)

AIR FORCE OFFICE OF SCIENTIFIC RESEARCH (AFSC)
NOTICE OF TRANSMITTAL TO DTIC
This technical report has been reviewed and is
approved for public release IAW AFR 190-12.
Distribution is unlimited.
MATTHEW J. KERPER
Chief, Technical Information Division

TABLE OF CONTENTS

TABLE OF CONTENTS
(Continued)

LIST OF FIGURES

LIST OF FIGURES
(Continued)

LIST OF FIGURES
(Continued)

LIST OF TABLES

APPENDIX

PUBLISHED PAPERS AND TECHNICAL PRESENTATIONS ARISING FROM THIS PROGRAM

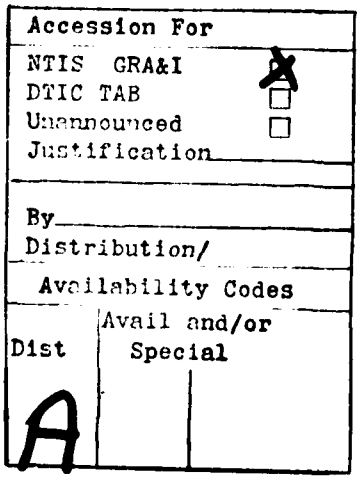

1. INTRODUCTION

MOTIVATION

This report summarizes the results of a three-year program whose motivation was provided by a 1968 paper by Shubert and Harris[1] in which the application of integrated-optics techniques to signal processing was discussed for the first time. In this paper it was suggested that integrated-optics techniques could be used to produce a general purpose one-dimensional Fourier-transform processor (Fig. 1-1). At the time of our rereading of the Shubert-Harris paper in 1978, all of the components required for such a correlator except the programmable spatial light modulator were in existence. It was the initial goal of this program to demonstrate such an integrated optical spatial light modulator (IOSLM).

The IOSLM is a programmable spatial filter whose purpose is to impose a spatial modulation upon the amplitude of the light traversing a given plane in the correlator. In the most general case, both the spatial and transmission characteristics of the filter are arbitrary analog functions. In all real systems the spatial response will have some resolution limit and the transmission function will be limited due to incomplete attenuation, incomplete transmission or both.

A versatile and easily implemented spatial modulator is a surface acoustic wave (SAW) modulator[2] as shown in Figure 1-2. Light incident upon the SAW at the Bragg angle θ_B will be deflected by $2\theta_B$. The Bragg angle is defined by

$$\sin\theta_B = \frac{\lambda}{2\Lambda} \tag{1-1}$$

where λ is the optical wavelength in the waveguide and Λ is the acoustic wavelength. Digital modulation of the SAW results in angular encoding of information on the light beam. As is discussed below, this angular encoding can be used to advantage in several types of data processing systems.

The diffraction efficiency of a thick phase grating such as that produced by a SAW is (at Bragg incidence)

$$\eta = \sin^2\left(\frac{\pi\Delta nd}{\lambda\cos\theta}\right) \tag{1-2}$$

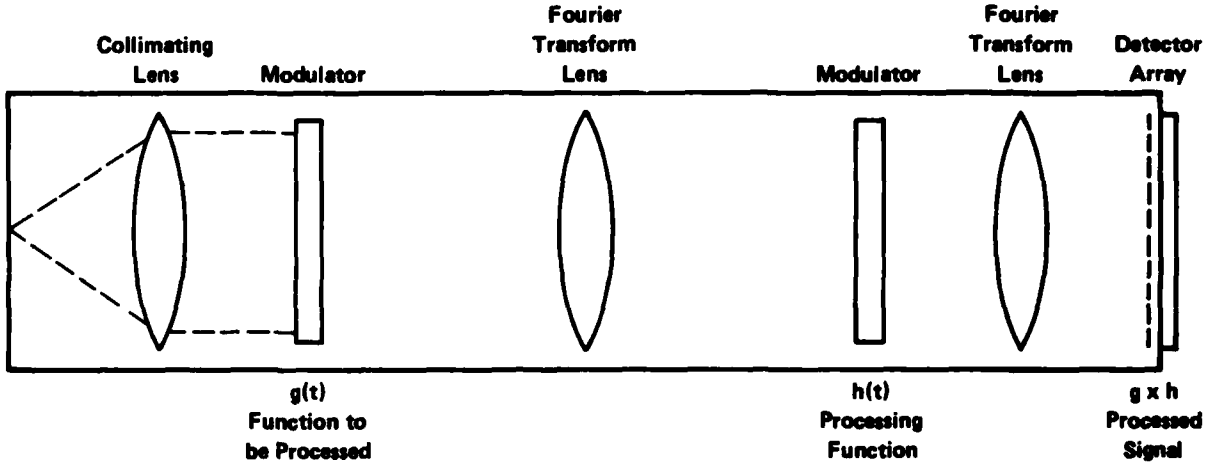

Figure 1-1. An integrated-optical Fourier transform correlator. All components except the programmable spatial light modulators have been available for some time.

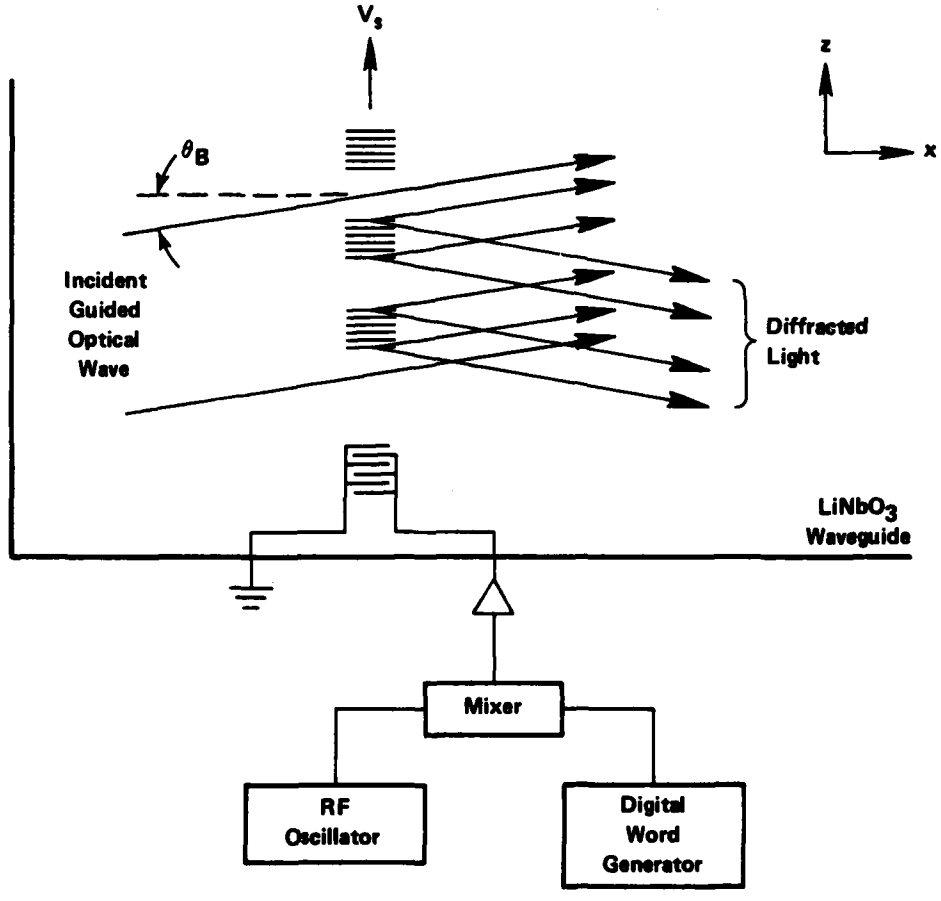

Figure 1-2. Digital (binary) modulation of a guided optical wave by a surface acoustic wave (SAW). The diffracted beam, separated from the incident light by an angle $2\theta_B$, is usually used as the encoded beam.

where Δn is the amplitude of the periodic index perturbation. In the case of the SAW modulator η can be an analog function, although in Figure 1-2, and in the remainder of this report only digital filtering is considered.

The pattern generated by a SAW device traverses the optical system at the acoustic velocity, some 10^5 cm/sec for most suitable materials. In order to perform the functions associated with the Fourier-transform correlator of Figure 1-1 it was decided to build a stationary but easily programmable SLM which could be used in the configuration of Fig. 1-1 or in conjunction with a SAW or with other integrated optical components.

PROGRAM SUMMARY

Several concepts were considered for implementing the IOSLM. It was decided that the most promising of those was a segmented, addressable electrooptic grating on the surface of a planar electrooptic waveguide. This structure was chosen because it could be easily fabricated and promised to yield high diffraction efficiencies and high modulation rates.

In considering a test configuration for demonstrating the IOSLM it was decided to abandon the complex structure of Fig. 1-1 and to use instead the simple correlator configuration discussed in Section 2, Device Concept. This correlator is composed simply of the IOSLM, a surface acoustic wave (SAW) transducer and associated external (i.e., nonintegrated) source, lens and detector. In addition to discussing the device concept, Section 2 also deals, in detail, with the theory of electrooptically induced Bragg gratings and their application to guided-wave structures.

Prior to fabricating the first programmable IOSLM, a static Feasibility Study (Section 3) was carried out in which a holographically-exposed, segmented photoresist grating took the place of the electrooptic transducer. Upon the successful completion of the feasibility study, two programmable correlators were designed and fabricated, a one-SAW device (Section 4) and a two-SAW correlator (Section 5) which was designed to overcome some flaws in the one-SAW device.

The bulk of this document deals with the two-SAW correlator which operates on a 32-bit digital word at the rate of 32 Mbit/sec. This device speed was chosen to be compatible with available test equipment and the word

length was selected for ease of fabrication. Both figures can be increased although there are practical limits to the data rate which are also discussed in Section 5. The work described in that Section is sufficient to demonstrate the potential of the correlator and to predict its performance in a variety of configurations. The next step of the correlator development would be to fabricate it as a hybrid integrated optical circuit with a butt-coupled diode laser, integrated collimating and output lenses, and integrated or butt-coupled detectors. However, this effort is properly deferred until the device design is optimized for a specific application.

In the course of the work on the correlator it was realized that there are a number of other functions which could be performed using grating arrays on planar waveguides. These are mainly computational operations and are discussed in Section 6.

The correlators which have been built during the course of this program are all space-integrating correlators. The outputs of a number of distinct computational channels are integrated by a lens and focused onto a single detector whose output presents the time history of the spatially integrated signals. In Section 7 we discuss some on-going work on an integrated-optical time-integrating correlator in which there are spatially discrete output channels for which the detector has a finite integration time. We show plans for the integrated optics version of such a device which was developed at Harry Diamond Laboratories in the bulk optical form. The integration scheme depends heavily upon the properties of fixed surface gratings and thus builds upon some of the work done on the space integrating device.

2. DEVICE CONCEPT

ELECTROOPTIC GRATINGS AS IOSLM

As described above, the mechanism selected for demonstration of an integrated optical spatial light modulator (IOSLM) was Bragg diffraction from a phase grating electrically induced in an electrooptic waveguide. Such gratings can be induced using simple, easy-to-fabricate interdigital electrode structures on the surface of the waveguide (Fig. 2-1). Standard photolithographic techniques are used in the fabrication of such structures and reasonably small periods are feasible using hard-contact optical photolithography. These structures are fairly small and can be driven to high diffraction efficiency using low voltages. For example, our first IOSLM had a period of 13.3 μm, was 2 mm in depth and reached a diffraction efficiency of 95% with a driving potential of 4 volts when the electrode structure was deposited directly onto the bare $LiNbO_3$ waveguide. When a thin buffer layer was used to prevent interaction of the optical beam with the metallic electrode structure, this voltage increased to 10 volts, still a usably small value.

An additional advantage of this type of IOSLM is the high speed at which it can be switched on and off. Switching speed is dominated by the capacitance of the electrode structure itself. For a 2 mm deep grating, one expects[4] approximately 1 picofarad of capacitance per finger pair in such electrode structures. Thus, for our first IOSLM, which used 15 finger pairs per segment, we would find a capacitance of about 15 picofarads for each segment, exclusive of the capacitance of the lead-in and connecting pad structure. If we arbitrarily doubled this figure to account for the lead-in and pad structure, we would find a switching speed of about 1.5 nsec when working into a 50-ohm load. Thus, even with this gross exaggeration of the capacitance, we would expect the device to be switchable at rates of the order of 300 MHz. Careful attention to drive circuitry should increase this value considerably.

The original IOSLM designed in this project made use of grating segments with a basic period of 13.3 μm having 15 periods per addressable segment. Thus, the basic resolution of the device was about 2-1/2 line pairs per millimeter, not very high. This choice was made in order to

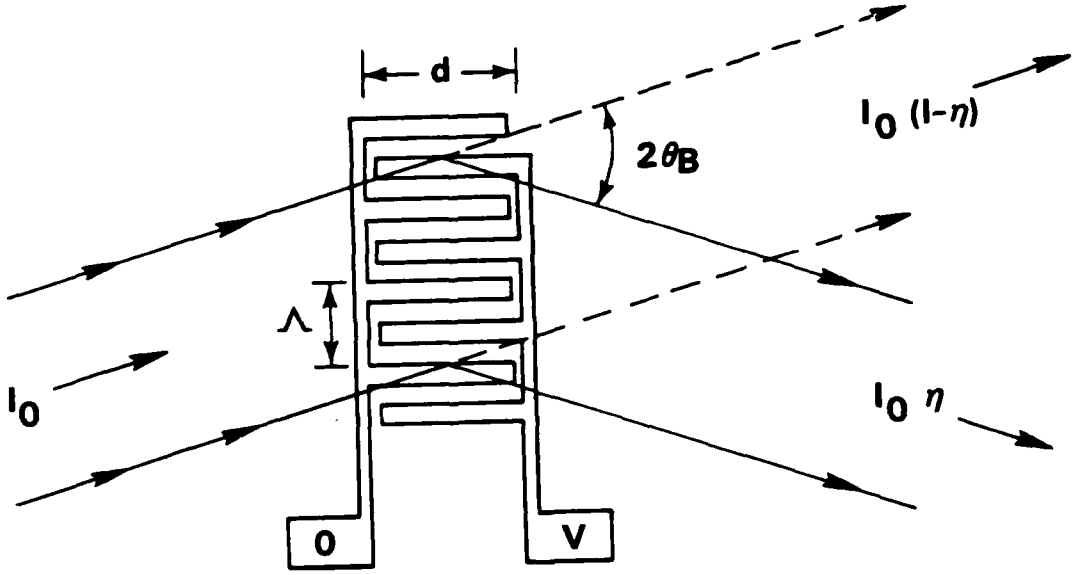

Figure 2-1. Interdigital surface electrode structure for inducing a phase grating into an electrooptic substrate

facilitate the implementation of the demonstration device, an acoustooptic correlator. For this type of device, it is very important to have extremely high diffraction efficiency in the electrooptic grating. In a device used primarily to impose phase information on an optical waveguided beam, one can basically use addressable segments of only one finger pair, i.e., one-half period. In that case, a photolithographic line width limitation of 1 μm (as is the case in our facilities), would allow basic grating periods of 4 μm. According to the Nyquist criterion, we must be able to address 2 points in each spatial period in order to be able unambiguously to resolve a given spatial frequency. Thus an IOSLM with a basic addressable span of 2 μm would have a period of 4 μm and a limiting spatial resolution of 250 line pairs per millimeter, a very respectable figure. The fly in this particular ointment is that such high resolution leads to very difficult leadout and connection problems in the device. Such high-resolution devices need to be used in a serial fashion. This implies the use of some suitably integrated, serially-addressed device such as a charge-coupled array. Unfortunately, such integration is not readily carried out using $LiNbO_3$ as substrate. As we demonstrate below however the current device with its limited resolution can be used to make potentially useful correlators and other devices.

CORRELATOR CONCEPT

As indicated in the opening section, we have chosen to illustrate the use of segmented electrooptic gratings as an integrated optical spatial light modulator by constructing a correlator. The object of the device is to calculate the correlation of two binary bit sequences. There are two principal reasons for chosing binary sequences for our correlator. First, the IOSLM is segmented into "windows" of finite length. Whatever the input is, the effects of this segmentation will always be to average over these "windows". Second, such sequences are encountered with ever increasing frequency in digital electronics. This means that such a device could prove quite useful in searching long strings of binary data for particular bit sequences. Our choice notwithstanding, it should always be understood that the devices we have constructed can just as well be used to calculate analog correlations.

The mathematical object known as a correlation is defined in Equation 2-1.

$$C(y) = \int_{-\infty}^{\infty} S(x + y)\, F(x)\, dx \qquad (2\text{-}1)$$

C(y) is the correlation of the two functions S and F, assumed here to be real. Equation 2-1 illustrates what is known as the "cross-correlation", because S and F are different functions. When S and F are the same function, the correlation is known as a "auto-correlation". A device which calculated the function of Equation 2-1 would be known as an "x-integrating" correlator, because whatever the coordinate x may represent, it is integrated out of the expression, and the correlation appears as a sequence along the y axis. Common correlators in practice are space-integrating correlators, which integrate over a space dimension and present the correlation itself as a time sequence; and time-integrating correlators which integrate over a finite time period and presents the correlation as a spatial light distribution.

In what follows we shall usually refer to the function S as the signal function and the function F as the filter function. We will always require that the function F should be 0 outside of a finite interval, because we associate this function with the IOSLM, which has a finite spatial extent. The filter function can therefore always be written in the form

$$F(x) = \sum_{i=1}^{N} F_i \, \mathrm{Rect}\left(\frac{x - x_i}{\Delta x}\right) \qquad (2\text{-}2)$$

where the F_i are amplitudes of the filter function within the window centered at x_i and having width Δx. The rectangular function is defined by

$$\mathrm{Rect}(x) = \begin{cases} 1 \text{ if } |x| \leq 1/2 \\ 0 \text{ otherwise} \end{cases} \qquad (2\text{-}3)$$

Since we are dealing with binary sequences, the F_i will always be either 0 or 1.

Looking back now at Equation 2-1, we see that the effect of the offset, y, is to shift the origin of the function S before multiplication by the functions F. Since y is fixed in the integration, the offset is constant throughout the integral. If we think of y as the time coordinate, and the

y-integration as occurring instantaneously, then as time evolves the correlation C (y) is presented sequentially in time. The function S simply slides by the function F with the integrations being carried out at each instant of time. In integrated optics we can carry out this motion of a signal S past a function F by using a surface acoustic wave modulated as in Figure 1-2. The binary pattern of the signal function is encoded into surface acoustic waves as shown, and interrogated by the light beam. If we arrange it that the diffracted beam falls upon the IOSLM at the proper Bragg angle, then light that is also diffracted from the IOSLM will represent at each instant of time the integrand of Equation 2-1. Of course, with these binary signals, the integrands are not continuous. If this twice-diffracted beam is now passed through a lens which collects all of the diffracted beam and focuses it onto a detector, then the lens-detector combination accomplishes the function of integration. The electrical signal from the detector is a time-dependent signal whose amplitude is proportional to the desired correlation. This is the basic idea of the correlators constructed in this project, both in the feasibility demonstration of Section 3, using a fixed filter signal, and in the single-SAW correlator of Section 4, using a programmable IOSLM.

Since the signal word is also a binary sequence, the function S(x) will have a form similar to that of Equation 2-2. In general, the upper limit on the sum for the signal word can be infinite, representing an arbitrarily long binary bit sequence. It is, however, convenient for experimentation to make the signal word and the filter word have the same physical length. We therefore define the binary signal word as in Equation 2-4:

$$S(x) = \sum_{i=1}^{N} S_i \, \mathrm{Rect}\left(\frac{x - x_i + L - vt}{\Delta x}\right) \qquad (2\text{-}4)$$

In this equation, the S_i are also either 0 or 1. The offset, y, has now been written as L-vt, where v is the acoustic velocity of the surface acoustic wave into which the signal word is encoded. If Equations 2-2 and 2-4 are inserted into Equation 2-1, there results a double summation over the products of the components of the signal and filter words with an integration representing the autocorrelation of a rectangular function. This autocorrelation is a triangular wave having maximum value equal to the segment length, Δx, and a total width of $2\,\Delta x$. The peaks of the triangle functions occur at those instants of time at which the surface acoustic wave grating segments and the IOSLM electro-optic grating segments are perfectly aligned. The characteristic peaks and valleys of the correlation function also occur at these times. We therefore choose to define the discrete correlation to be the values of the correlation at these same instants of time which are

$$t_{ij} = [L + (i-j)\,x]/v = \frac{L}{vN}\,[N + i-j] \tag{2-5}$$

It should be noted that all index pairs (i,j) having the same value of i-j correspond to the same time. We enumerate the correlation using the value in square brackets in the last equality of Eq. (2-5), that is, we define n to be

$$n = N + i - j; \quad 1 \leq n \leq 2N - 1 \tag{2-6}$$

We then find for the discrete correlation components

$$C_n = \Delta x \sum_{\text{Max}\ \{1,\ N-n+1\}}^{\text{Min}\ \{N,\ 2N-n\}} S_{j+n-N}\, F_j \tag{2-7}$$

The summation range in Equation (2-7) is illustrated in Figure 2-2.

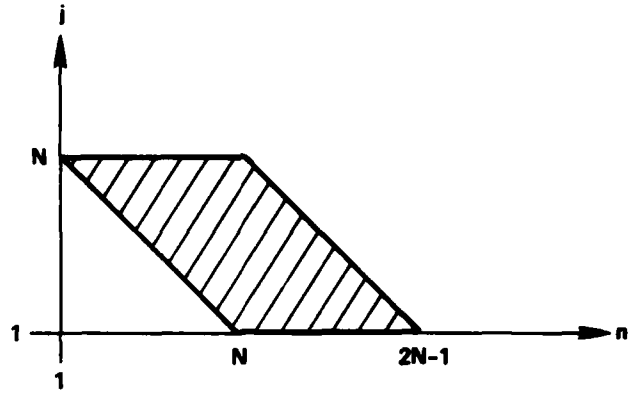

Figure 2-2. Illustration of the summation range for the discrete correlation.

Our choice of the instants of time at which to evaluate the correlation in its discrete version is, of course, arbitrary. As mentioned in the preceding paragraph, however, this choice does serve to pick out the points at which the principal features of the correlation occur. It is also very convenient for computer simulation. Such a computer simulation is discussed in Section 5.

Grating Theory

In this section we display a number of useful formulas relating to the operation of electrooptically induced Bragg diffraction gratings.

The Electrooptic Effect in $LiNbO_3$

The linear electrooptic effect can be expressed as

$$\Delta n = -\frac{1}{2} n^3 r E \tag{2-8}$$

where Δn is the refractive index change due to the field E, n is the refractive index in zero field, and r is an electrooptic coefficient. Formula (2-8) is is also approximately valid for the change in effective refractive index for a waveguide mode.

For $LiNbO_3$ the effective electrooptic coefficients[5] for TE_0 and TM_0 light propagating along the x-direction in a y-cut crystal are $r_{33} = 3.1 \times 10^{-5}$ (μm/V) and $r_{13} = 1.0 \times 10^{-5}$ (μm/V), respectively.

Fields From Surface Electrodes

The electric field in the half-space y<0 (see Fig. 2-3) due to a gap of width g in an infinite conducting sheet can be found using conformal mapping.[6] For y = 0, we have

$$\left.\begin{aligned} E_y &= 0 \\ E_z &= \left(\frac{2}{\pi}\right)\left(\frac{V}{g}\right) \frac{1}{\sqrt{1 - \left(\frac{2z}{g}\right)^2}} \end{aligned}\right\} \tag{2-9}$$

while for z = 0,

$$\begin{aligned} E_y &= 0 \\ E_z &= \frac{2V}{\pi g} \frac{1}{\sqrt{1 + \left(\frac{2y}{g}\right)^2}} \end{aligned} \tag{2-10}$$

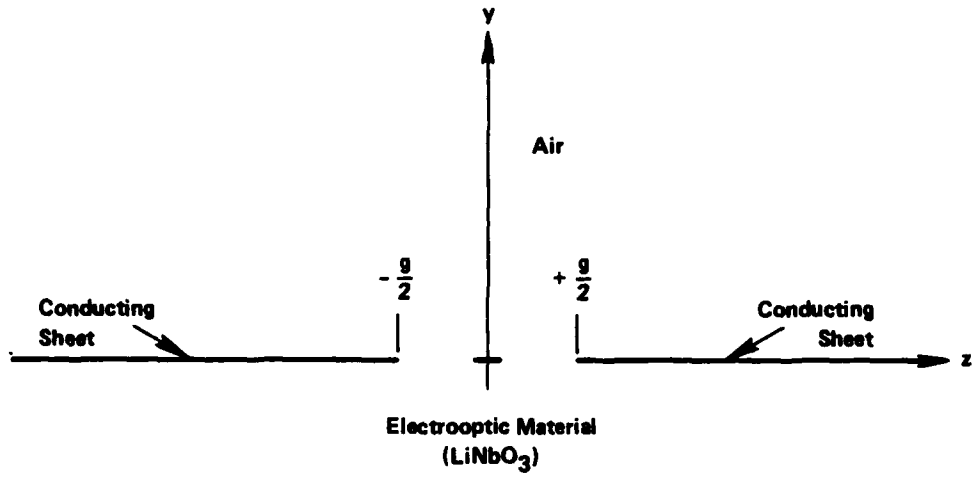

Figure 2-3. Geometry and notation for a single gap of width g in a conducting sheet.

For a periodic system of surface electrodes having equal gap and finger widths, the field everywhere in the y<0 half space can be written as a Fourier series. According to Engan[7]

$$E_z = 0.847\ (\frac{V_o}{g}) \sum_{\ell=o}^{\infty} (-1)^{\ell} A_{\ell} \cos(4\ell+1)\frac{\pi z}{2g}\ \exp[(4\ell+1)\pi\varepsilon_r y/2g]$$

$$E_y = 0.847\ (\frac{V_o}{g}) \sum_{\ell=o}^{\infty} (-1)^{\ell} A_{\ell} \sin(4\ell+1)\frac{\pi z}{2g}\ \exp[(4\ell+1)\pi\varepsilon_r y/2g] \qquad (2\text{-}11)$$

where

$$A_{\ell} = 2^{-2\ell}\binom{2\ell}{\ell} \qquad (2\text{-}12)$$

$$\varepsilon_r = \sqrt{\frac{\varepsilon_{zz}}{\varepsilon_{yy}}} \approx 0.6 \qquad (2\text{-}13)$$

For most purposes, the fundamental (ℓ=0) field component is the most important. Further, for shallow guides, only the field near y = 0 need be considered.

It is interesting to note that since

$$\sum_{\ell=0}^{\infty} (-1)^{\ell} 2^{-2\ell} \binom{2\ell}{\ell} x^{\ell} = \frac{1}{\sqrt{1+x}} \tag{2-14}$$

the summations in Eq. (2-11) can be carried out formally, giving

$$E_z = 0.847 \left(\frac{V_o}{g}\right) \mathrm{Re}\left\{1/\sqrt{2\cos\left(\frac{\pi \hat{z}}{g}\right)}\right\} \tag{2-15}$$

$$E_y = 0.847 \left(\frac{V_o}{g}\right) \mathrm{Im}\left\{1/\sqrt{2\cos\left(\frac{\pi \hat{z}}{g}\right)}\right\} \tag{2-16}$$

where $\hat{z} = y + iz$. Eq. (2-16) shows that E_y vanishes for both $y = 0$ and $z = 0$.

Diffraction Efficiency

A long unslanted diffraction grating of depth d is illustrated in Fig. 2-4. For this kind of grating, Kogelnik[8] has shown that for weak modulation the efficiency, η, can be written in the form

$$\eta = \sin^2 \sqrt{\nu^2 + \xi^2} \,/\, (1 + \xi^2/\nu^2) \tag{2-17}$$

where ν and ξ are dimensionless combinations of parameters:

$$\nu = \pi \frac{\Delta n\, d}{\lambda_o \cos\theta_B} \tag{2-18}$$

$$\xi = \frac{\Xi\, d}{2\cos\theta_B} \tag{2-19}$$

Ξ is the "dephasing" factor,

$$\Xi = \frac{2}{\Lambda} [\sin\theta - \sin\theta_B]$$

$$\simeq \frac{2\pi}{\Lambda} \cos\theta_B \, \Delta\theta \tag{2-20}$$

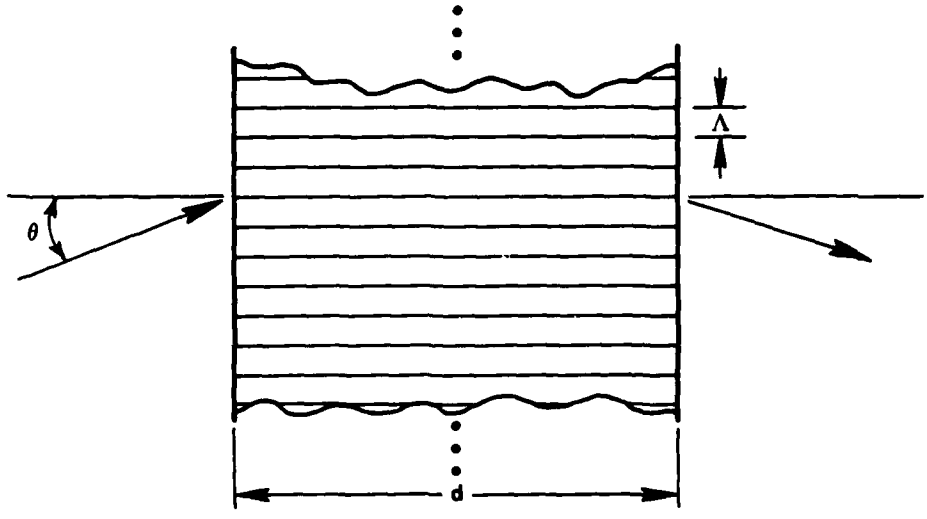

Figure 2-4. Geometry and notation for an unslanted thick phase grating having an infinite height.

where $\Delta\theta = \theta - \theta_B$. Ξ measures the phase mismatch caused by moving the angle of incidence away from the Bragg angle.

The Bragg angle is determined from

$$\sin\theta_B = \frac{\lambda}{2\Lambda} = \frac{\lambda_o}{2n\Lambda} \tag{2-21}$$

When $\theta = \theta_B$, the efficiency is

$$\eta = \sin^2\nu \tag{2-22}$$

and $\eta = 1$ when $\nu = \frac{\pi}{2}$.

Using these relations and taking note of the fact that, because of photolithographic limitations, $\lambda << \Lambda$ so $\cos\theta_B \simeq 1$, we can write n in terms of

$$\xi/\nu \simeq \frac{\lambda_o \Delta\theta}{\Lambda\ \Delta n} \tag{2-23}$$

as

$$\eta = \sin^2\sqrt{1 + \left(\frac{\lambda_o\Delta\theta}{\Lambda\ \Delta n}\right)^2}\ /\ \left[1 + \left(\frac{\lambda_o\Delta\theta}{\Lambda\ \Delta n}\right)^2\right] \tag{2-24}$$

Acceptance Angle

For a grating of 100% efficiency, Eq. (2-18) gives us

$$\nu = \frac{\pi}{2} = \frac{\Delta n\, d}{\lambda_o \cos\theta_B} \approx \frac{\Delta n d}{\lambda_o} \tag{2-25}$$

Hence, for this case

$$\xi/\nu = 2\left(\frac{d}{\Lambda}\right)\Delta\theta \tag{2-26}$$

The diffraction efficiency vanishes if

$$\sqrt{\nu^2 + \xi^2} = m\pi \qquad m = \pm 1, \pm 2, \ldots \tag{2-27}$$

For our case, this means

$$1 + \left[2\left(\frac{d}{\Lambda}\right)\Delta\theta\right]^2 = (2m)^2 \tag{2-28}$$

where m is an integer, m = 1, 2, 3,...

$$\Delta\theta(m) = \frac{1}{2}\sqrt{(2m)^2 - 1}\ \left(\frac{\Lambda}{d}\right) \tag{2-29}$$

The first such zero occurs for m = 1 or

$$\Delta\theta(1) = \frac{\sqrt{3}}{2}\left(\frac{\Lambda}{d}\right) \approx 0.9\left(\frac{\Lambda}{d}\right) \tag{2-30}$$

Table I lists the first 9 values of d for $\Lambda = 8.41\ \mu m$, $\Delta\theta = .0378$ rad (corresponding to the electrooptic gratings for the 2-SAW correlator). Also listed is the peak diffraction efficiency between the zeros.

The full width of the central peak of the diffraction efficiency is $2\Delta\theta(1)$. The acceptance width is more commonly given as the full width of the diffraction curve at the angle where the efficiency is half of its peak value. This value depends on ν, of course. For $\nu = \frac{\pi}{2}$, it is $0.80\left(\frac{\Lambda}{d}\right)$ while for ν near zero it is $0.88\left(\frac{\Lambda}{d}\right)$.

TABLE I. GRATING DEPTHS FOR ADDRESS AT A ZERO OF DIFFRACTION EFFICIENCY[a]

Index ℓ	Depth $d(\ell)$ (μm)	Efficiency[b] η (%)
0	--	100[c]
1	192.7	4.7
2	431.0	1.6
3	658.4	0.8
4	883.3	0.5
5	1107.3	0.3
6	1330.8	0.2
7	1554.0	0.2
8	1777.0	0.1
9	2000.0	

a Design data from Table II are used.

b Efficiencies at the efficiency peaks between the zeros are shown in this column.

c Diffraction efficiency at Bragg incidence assumed to be 100%.

Effect of Finite Length of Grating Segments

The formulas discussed above are derived for a grating having infinite length, i.e., an infinite number of periods. The IOSLM makes use of gratings having only 10-15 periods. This finite length has three serious effects on grating performance. First, the finite height gives rise to diffractive spreading in the diffracted beam. Second, the light impinges onto the grating (whether a SAW or an electrooptic segment) along one side as well as across the front edge of a grating, and exits along both sides as well as across the back face. Third, only a fraction of the light entering the grating can possibly experience the full depth of the grating; the effective efficiency of the grating is thereby reduced. In this section we derive a simple model for estimating this efficiency reduction.

Our model is based on a combination of geometric optics and Kogelnik's[8] couple-wave theory for gratings of infinite extent. Referring to Fig. (2-5), we can see that light rays that enter the front face of the grating (x=0) at z-coordinates in the range $0 \leq z_o \leq z_c$ can experience the full depth, d, of the grating. Rays that pass x=0 in the region $-d \tan\theta \leq z_o \leq 0$ will enter the grating along the bottom edge and exit along the right face (x = d). Since a ray passing x = 0 at z-coordinate z_o traces a line of equation

$$z = z_o + x\tan\theta, \tag{2-31}$$

this ray will enter the grating at z = 0 and x-coordinate

$$x = -z_o \cot\theta. \tag{2-32}$$

Similarly, rays entering the front face in the range of z_o values $z_c = \ell - d\tan\theta \leq z_o \leq \ell$ will exit along the top face at $z = \ell$ with

$$x = (\ell - z_o)\cot\theta \tag{2-33}$$

Thus the effective grating depth for these three regions is (recall that the grating depth is measured along the x-axis)

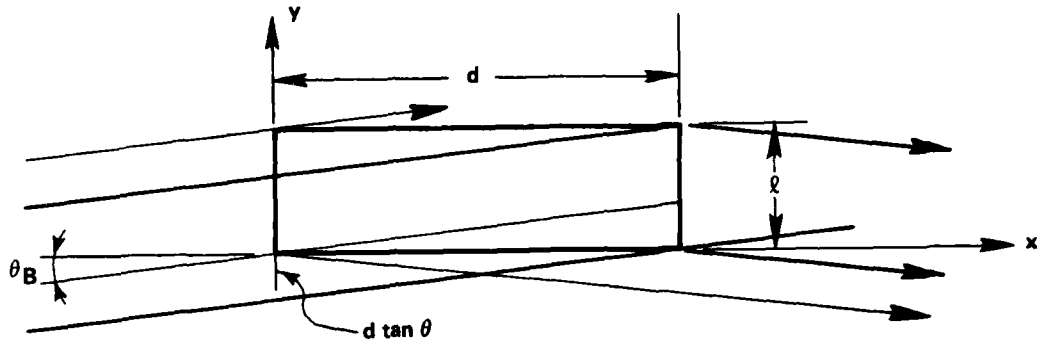

Figure 2-5. An isolated grating segment showing light ray entry along the front face and along the bottom edge, and indicating the notation used.

$$d_{eff} = d - z_o \cot\theta \qquad \text{if } -d\tan\theta \leq z_o \leq 0$$

$$= d \qquad \text{if } 0 \leq z_o \leq \ell - d\tan\theta$$

$$= (\ell - z_o)\cot\theta \qquad \text{if } \ell - d\tan\theta \leq z_o \leq \ell \qquad (2\text{-}34)$$

We now invoke Kogelnik's theory, applying it to rays, in the form

$$\eta(d_{eff}) = \sin^2(\Gamma\, d_{eff}), \qquad (2\text{-}35)$$

where

$$\Gamma = \pi\Delta n/\lambda_o \cos\theta_B \quad . \qquad (2\text{-}36)$$

We calculate an "average" efficiency for the grating segment using

$$\eta_{ave} = \int_{-d\tan\theta}^{\ell} \eta(d_{eff})dz_o/(\ell + d\tan\theta)$$

$$= [\ell\sin^2\Gamma d + d\tan\theta(\cos^2\Gamma d - \frac{\sin 2\Gamma d}{2\Gamma d})]/(\ell + d\tan\theta) \qquad (2\text{-}37)$$

It should be noted that we have assumed here that $\ell \geq d\tan\theta$, because if $\ell < d\tan\theta$, then no ray can traverse the full depth and the depth in excess of $\ell \cot\theta$ is ineffective.

For the case where $\sin^2\Gamma d = 1$, we find

$$\eta_{ave} = \frac{\ell}{\ell + d\tan\theta} \qquad (\eta_{max} = 1) \qquad (2\text{-}38)$$

For comparison, we note that for our 1-SAW correlator, $\Lambda = 13.3$ μm, $d = 2.0$ mm, and $\ell = 15\ \Lambda$. Thus, for $\lambda_o = .633$ μm in $LiNbO_3$ ($n = 2.2$), we find

$$\eta_{ave} = 0.90 \qquad (\eta_{max} = 1) \qquad (2\text{-}39)$$

For the 2-SAW correlator, $\Lambda = 8.41$ μm, $\ell = 13\ \Lambda$, and $d = 2.0$ mm, so

$$\eta_{ave} = 0.76 \qquad (\eta_{max} = 1) \qquad (2\text{-}40)$$

The reduced efficiency in the IOSLM leads to errors in the correlation, because the IOSLM will send light into both output beams if its efficiency is lowered from 100%.

3. FEASIBILITY DEMONSTRATION

The initial effort on the project was directed at demonstrating the feasibility of the use of grating arrays as IOSLMs in a correlator. For this purpose, it was not necessary to have a programmable array. For the input signal, we used a SAW, modulated by a digital word generator in an on-off fashion. The region of the SAW was adjacent to a region containing a photoresist grating, masked to produce grating segments of the same length as the SAW segments produced by the word generator; this formed a nonprogrammable IOSLM. The period of these grating segments was chosen to provide a good signal isolation, and only the 1-1 coincidences were detected. Thus, the device did not produce a true correlation.

The behavior of the fixed filters was investigated by looking at light diffracted by both the fixed grating and a digitally modulated SAW using the arrangement shown in Fig. 3-1. The intensity of the doubly diffracted light, plotted as a function of time, is a representation of the partial correlation of the two grating patterns. The results of this work are summarized in Appendix 1 which is a reprint of a paper published in Optics Communications.

During this phase of the program we attempted to investigate the minimum bit size which could be used before encountering degradation in the quality of the correlation signal due to diffraction effects, or equivalently, due to spectral spread in the SAW. To investigate this limit the following simple experiment was performed. A long grating with $\Lambda = 6.3$ μm and $d = 2$ mm was fabricated in place of the segmented grating shown in Fig. 3-1. The acceptance angle of this grating is $\Delta\theta_B = \Lambda/d = 3.15$ mrad. The doubly diffracted signal amplitude was then measured as a function of Δt, the SAW pulse duration. For acoustic pulse lengths shorter than the limiting optical aperture of the system a linear relationship between Δt and peak signal amplitude is expected. Diffraction effects are not expected until the pulse length approaches 100 μm (about 30 nsec), and not even then if near-field conditions obtain. As can be seen in Fig. 3-2 our results show the expected linearity down to 50 nsec pulse durations. Unfortunately, low signal levels and difficulties in producing square r.f. pulses prevented us from taking usable data for shorter pulses.

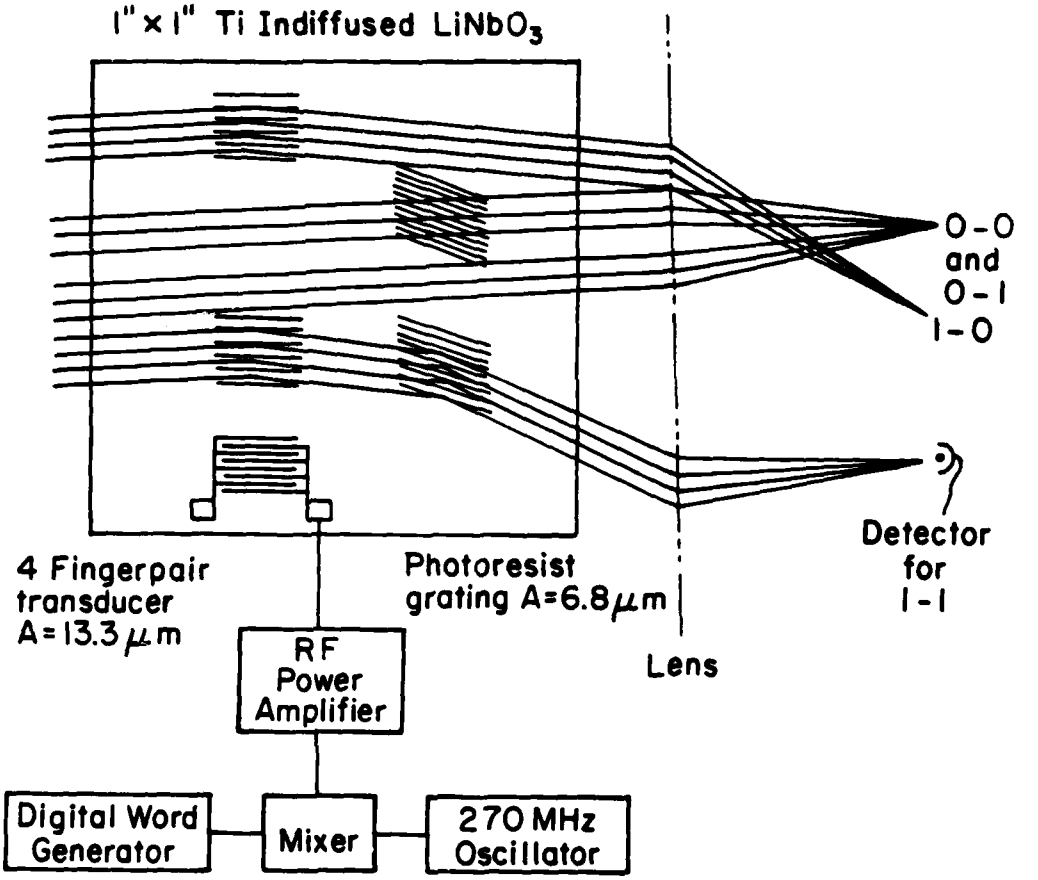

Figure 3-1. Schematic layout for the feasibility experiment using masked photoresist gratings for the "filter"

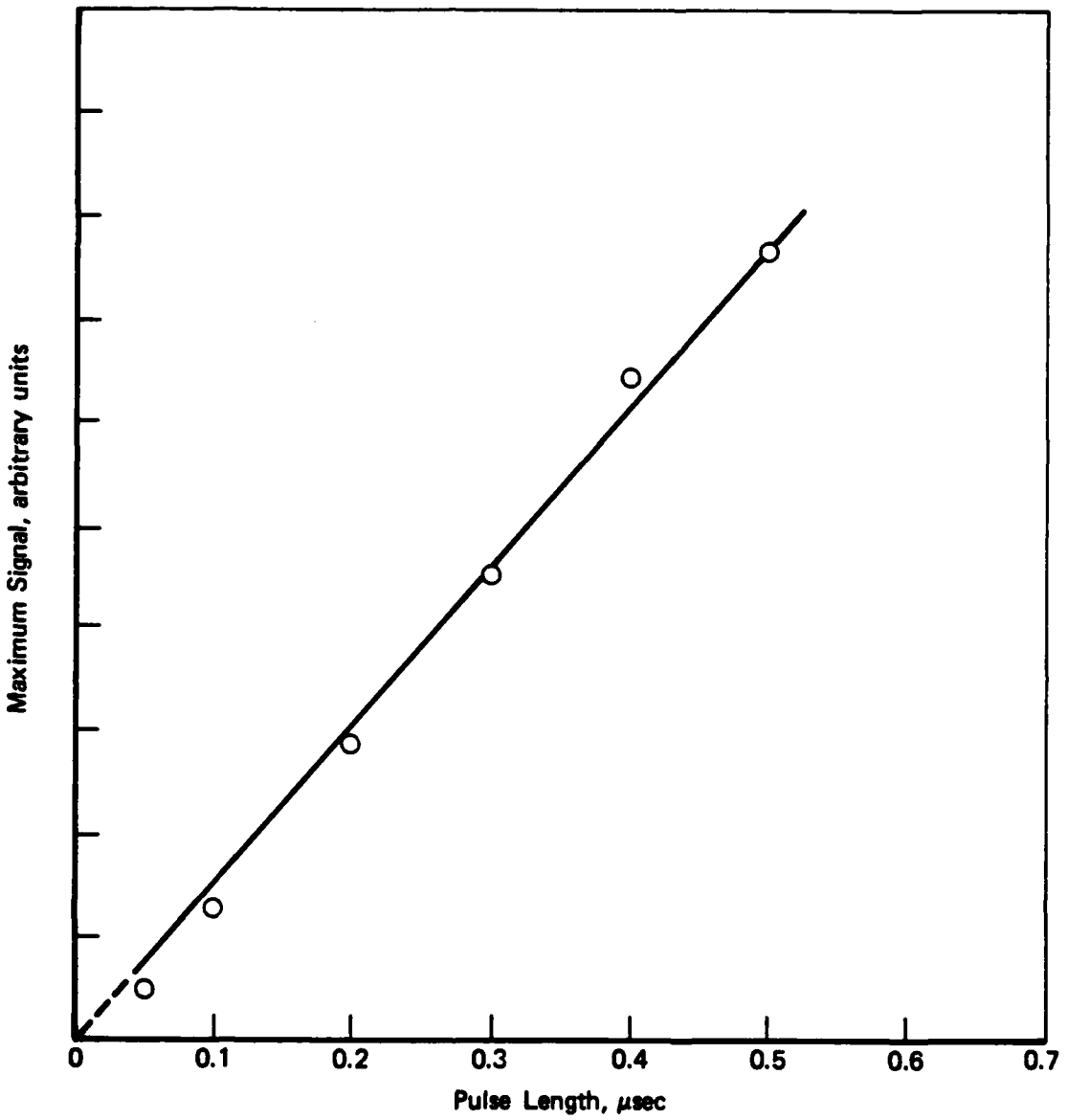

Figure 3-2. Graph of signal amplitude versus pulse length for the twice-diffracted beam. Approximate linearity down to pulse lengths of 50 nsec is demonstrated

4. ONE-SAW CORRELATOR

The basic considerations in designing an electrooptic array of gratings are choice of period to match that of the SAW, choice of number of periods per channel, which must also, for the design of Appendix 1, match that of the SAW, and choice of number of channels.

We chose 32 channels for the first programmable device in order to demonstrate a non-trivial correlator while at the same time keeping the mask fabrication and the connection problems at an easily manageable level. A grating period of 13.3 μm requires line widths of 3.3 μm in the interdigital structures (SAW transducer and the IOSLM itself), which keeps the photolithography fairly simple. For lithium niobate (LNO) substrates, this period corresponds to a SAW frequency of 236 MHz, providing good coupling at a fairly low frequency. A choice of 15 periods/channel gives a width for one channel, or bit, of 200 μm, making optical diffraction effects negligible. The acoustic velocity in LNO is 3.5 μm-GHz, so this bit length corresponds to a data rate of 17.5 Mb/sec, a modest but usable value.

The remaining feature to choose is the grating depth. This parameter impacts upon the diffraction efficiency for a fixed operating voltage or the operating voltage for fixed (usually maximum attainable) diffraction efficiency. The choice of 2.0 mm allowed maximum diffraction efficiency of about 95% to be obtained with a voltage of 4.0 volts when the IOSLM is deposited directly on the bare waveguide surface. It is usually desirable to use a buffer layer of glass between the waveguide surface and the electrodes in order to reduce both the losses and the scattering found when the electrodes are deposited directly upon the bare waveguide surface. Such glass layers tend to increase the voltage required for maximum diffraction efficiency. In our case, the voltage increased to 10 volts.

The performance of the programmable IOSLM in a correlator is discussed in detail in Appendix 2. Fig. 4 of that Appendix shows both the computed and the observed autocorrelation of a specific 32-bit word. It can be seen that the observed response is very much as expected, but that both curves are asymmetric. This asymmetry is due to a bias inserted by the particular configuration used (Fig. 1, Appendix 2). In a later section, we discuss an improved design that overcomes this problem.

In Fig. 4-1 we show an additional response curve for the correlator. In this case several bit sequences corresponding to the word programmed into the IOSLM have been immersed in a series of pseudorandom words in the signal applied to the SAW modulator. It can be seen that the correlation peak is clearly visible above the surrounding noise.

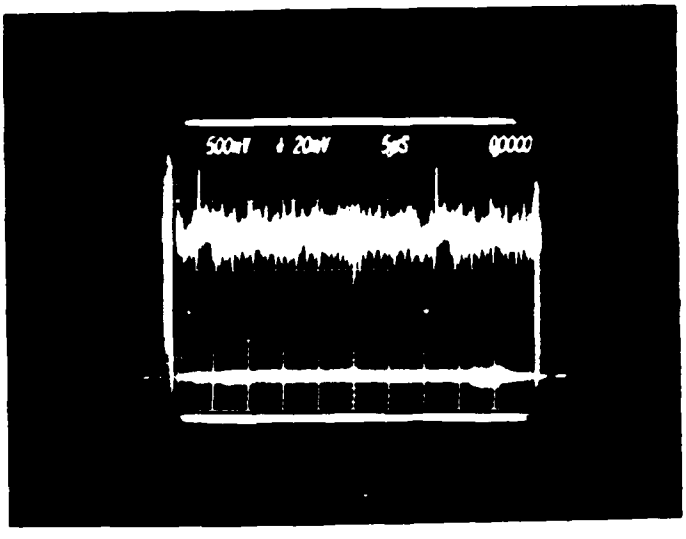

Figure 4-1. Correlator response to signal buried in noise.

5. TWO-SAW CORRELATOR

DESIGN

Geometric Layout

The reason for using two surface acoustic waves at different frequencies in the correlator is to prevent light from being diffracted by the electrooptic grating unless it has first been diffracted by a surface acoustic wave. This eliminates the contamination of the correlation signal due to diffraction by the electrooptic grating of light that is undiffracted by the surface acoustic waves (and light which is diffracted from the electrooptic grating in the absence of the surface acoustic waves). The two-SAW design accomplishes this purpose. The geometric arrangement is such that light diffracted from the low frequency SAW impinges on the electrooptic grating at the Bragg angle below the grating axis while light diffracted from the high frequency SAW impinges upon the IOSLM at the Bragg angle above the axis of the grating. Here the axis of the grating is defined to be the direction parallel to the grating fingers. The angular relationships relative to the IOSLM are shown in Fig. 5-1. The figure is highly schematic in that the surface acoustic waves are shown as collinear. In fact each SAW must be inclined relative to the incident light at its own Bragg angle and the IOSLM itself must also be inclined so as to present Bragg angles to the rays from the two SAWs. However Fig. 5-1 does show the correct geometric relationships of the output beams and illustrates all four cases that need to be correlated, that is two zeros, a zero and a one, a one and a zero, and two ones.

The diagram in Fig. 5-2 illustrates the actual geometric arrangement used in the two-SAW correlator. The center lines of the 2 SAWs and of the IOSLM are illustrated. It is important that a ray that addresses the device as shown should encounter the low-frequency SAW before it encounters the high-frequency SAW. This ensures that light diffracted from a particular ray by the high-frequency SAW and light diffracted from the same ray by the low-frequency SAW have a crossing point, that is, a caustic. It is a simple matter to show that the locus of such caustics is a straight line which passes through the intersection point of the two SAW center lines. We place the IOSLM along this

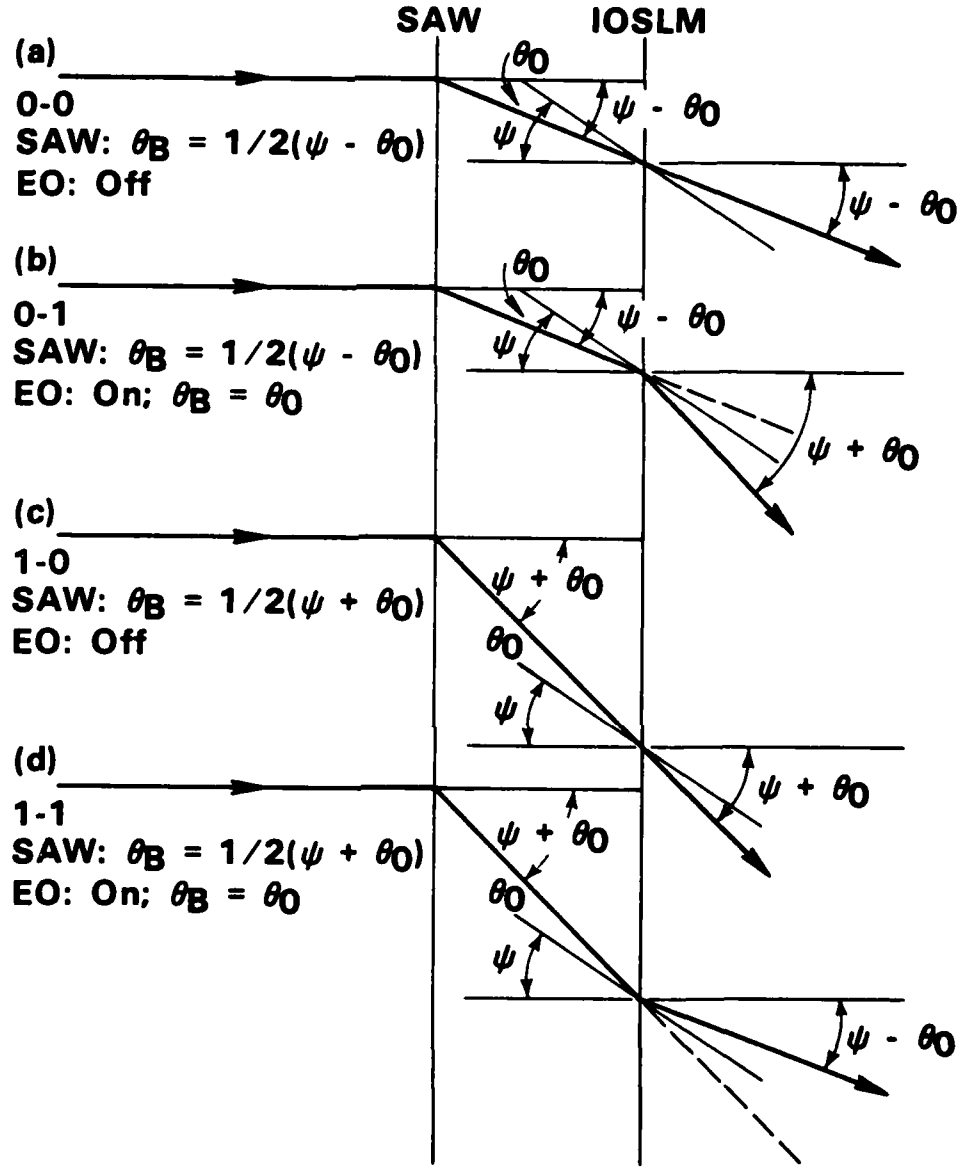

Figure 5-1. Angular relationships for the 2-SAW correlator for the four basic bit combinations (0-0, 0-1, 1-0, 1-1). The two SAW's are shown as collinear for simplicity, and the IOSLM is shown as parallel to the SAW axes, but having fingers slanted by the angle 4. In the actual design, the two SAW and the IOSLM axes are tilted relative to one another and the IOSLM fingers are unslanted

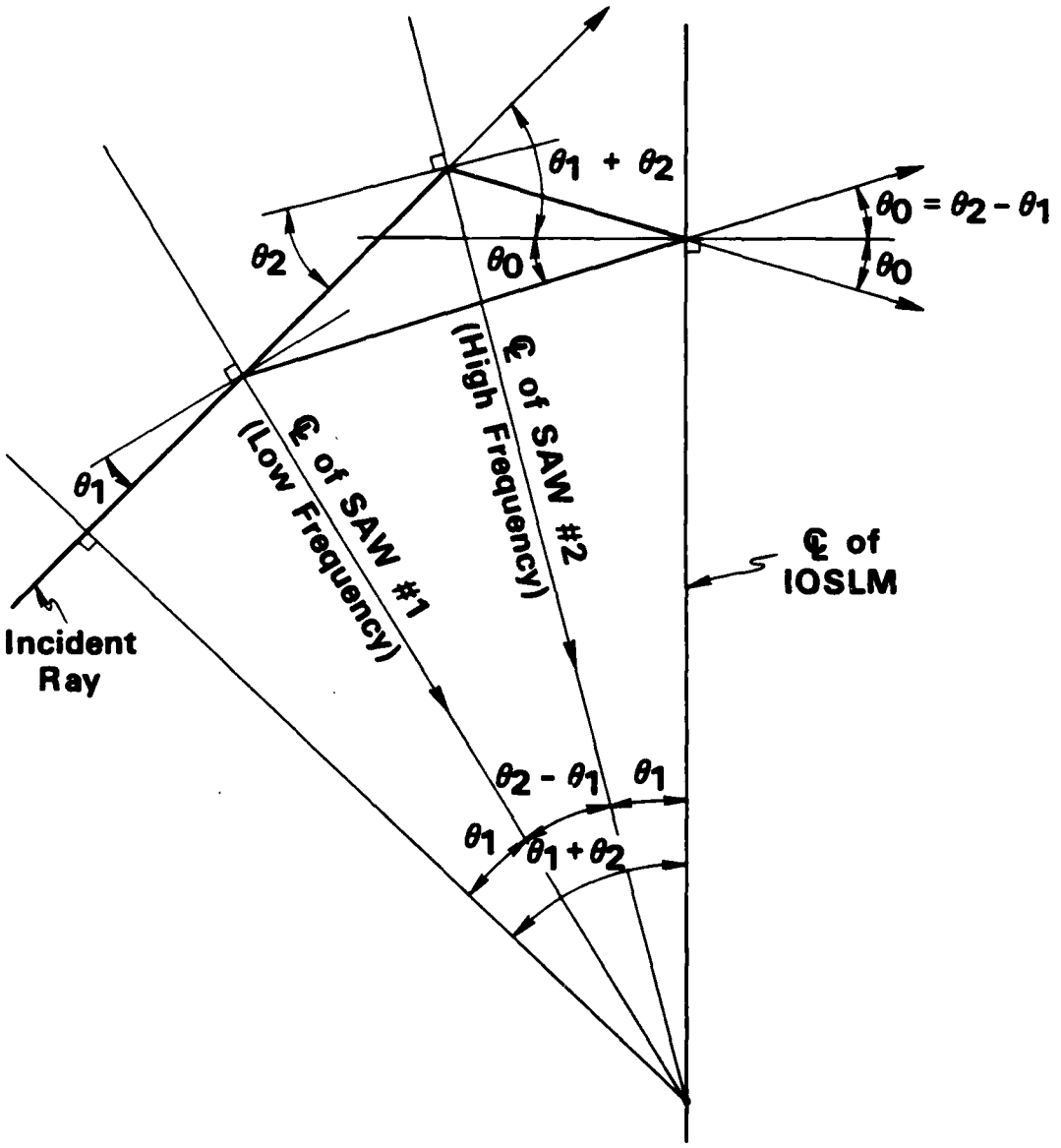

Figure 5-2. Layout geometry for the 2-SAW correlator, showing angular relationships. The IOSLM is placed along the caustic generated by the two SAW's. Angles are given for the small-angle approximation; only the SAW and IOSLM axes are shown

line of caustics so that light diffracted from a particular incident ray passes through the same point of the IOSLM regardless of which SAW causes the diffraction. This arrangement fixes all of the angular relationships. The angles indicated in Fig. 5-2 are not exact but are nonetheless quite precise approximations. The location of the crossing point of the two SAWs and the IOSLM is not fixed by any criterion that we have chosen so far. There are a number of factors that are involved in the choice of the location of this intersection point. First, it should be noted that it is desirable that surface acoustic wave transducers have counter transducers (that is, transducers of the same center frequency placed along the same center line opposite to the generating SAW transducers) in order that insertion loss and other characteristics of the surface acoustic waves themselves can be more easily monitored. These counter transducers must be placed far enough from the intersection point that they can be positioned without physically interfering with one another. Second, the generating transducers must be placed far enough from the counter transducers to accommodate the full width of the optical beam (with perhaps a few millimeters clearance on each side for ease of experimentation). Third, since the two surface acoustic waves travel in distinct directions relative to the incident light beam, the synchronization or interleaving of the two bits streams corresponding to zeros and ones of the data stream will slowly be degraded. This is not a large effect over the width of typical optical beams that are used in these correlators, because of the small angles involved. This dephasing effect might typically amount to about one-tenth of a bit across the width of the optical beam. However, even this small effect can be minimized by choosing the location of the generating SAW transducers so that the two bit streams are precisely synchronized at the center of the optical beam.

The operation of this two-SAW correlator is illustrated schematically in Figs. 5-3 and 5-4, which show the operation of the device at two different time epochs. It should be observed here that, although we have always indicated that the light beam encounters the surface acoustic wave segments before it encounters the IOSLM, in fact it is irrelevant in which direction the light passes through the device. If the light beam encounters the IOSLM first, then, of course, light is diffracted from this structure whether or not there are SAW segments present. The two SAW streams now act simply to select from the diffracted beams of the static IOSLM those components that are relevant to the

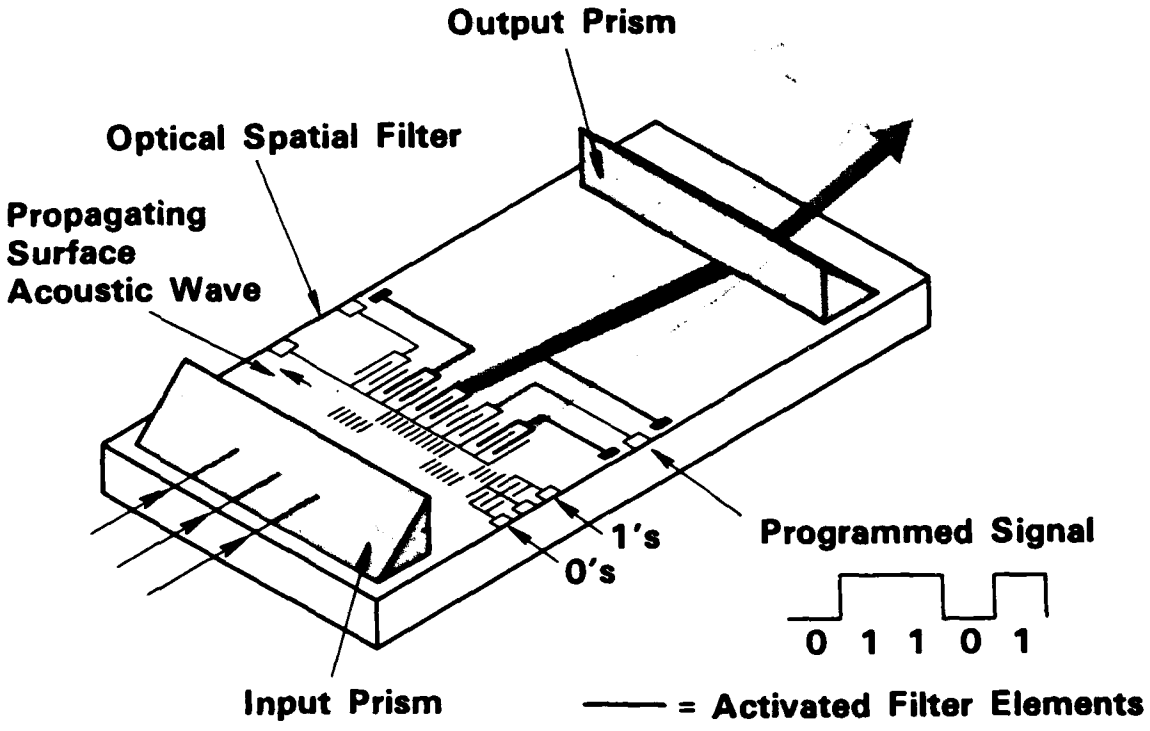

Figure 5-3. Illustration of a 2-SAW, 5-bit correlator in operation at the N-1st (N-1 = 4) time epoch. The autocorrelation of the word 01101 is shown. Correlation (C) terms (0-0 and 1-1) are deflected downward in the picture, while anticorrelation (A) terms (1-0 and 0-1) are deflected upwards. The overlap region here covers four segments of the possible five in the IOSLM. Here, C = 1 and A = 3 (in arbitrary intensity units).

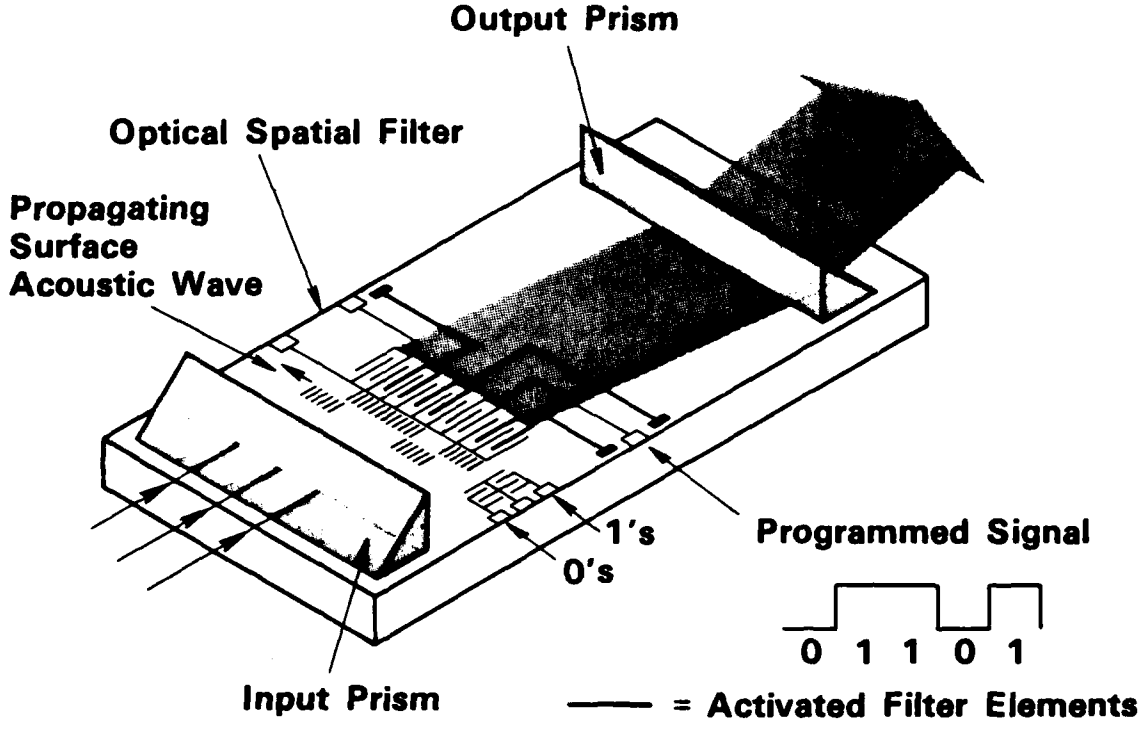

Figure 5-4. Illustration of a 2-SAW, 5-bit correlator in operation at the N^{th} (N = 5) time epoch. This is the completely overlapped case and C = 5, A = 0.

correlation for the current time epoch. Those relevant components, and only those components, are diffracted into the output direction; this output beam proceeds along the same line that the input beam traced when the SAWs were encountered first.

Limitations and Tradeoffs of the Device

There are a number of characteristics and features of the two-SAW correlator which produce limitations in the operation of the device. Some of these limitations are imposed by facilities, fundamental physical considerations, or by materials considerations. Others are the result of simple engineering choices. Examples of the former type of limitation are attainable photolithographic line width, diffractive spreading of the acoustic or the optical beam, and the choice of lithium niobate as a substrate in our systems. Examples of the latter type of limitation include the bit size (that is the physical length of a bit), the data rate of the correlator, and the length of a word in the correlator. Regardless of the source of the limitations they are not independent. Generally two or more such limitations will be interrelated in such a way that a tradeoff is possible. In this section we will discuss some of these general types of limitations and the interrelationships among them which lead to engineering tradeoffs. This discussion will lead us to a rather simple design procedure for the correlator which incorporates many of the interrelationships among the parameters of the design. Following this discussion we will describe the geometry used and the reasons for choosing it.

Photolithography

Our current photolithographic facilities make use of hard-contact printing. Experience has shown us that, while we can produce line widths as small as .9 μm, a more practical limitation is about 1 μm. Even line widths of 1 μm are not routinely reproducible. This is especially true in the electro-optic grating array region of the pattern where the finger lengths are on the order of 2 mm long, so that 1 μm finger widths lead to aspect ratios of about 2000 to 1. In addition there are an extraordinarily large number of such fingers required in one of these grating arrays—for example the current mask

uses 13 finger pairs per bit and 32 bits per correlated word, leading to a total of 832 fingers. Since the grating period is 4 times the minimum finger width, the preceding considerations would tend to limit us to a minimum period of 4 μm. Although photolithographic yield considerations—that is the number of attempts needed to produce a usable pattern—would lead us to choose even larger periods, examination of the relationship among the periods of the two surface acoustic waves and that of the electrooptic grating lead us to accept a 4 μm period as a design specification for the high-frequency SAW transducer, and to plan for approximately 8 μm periods for the low-frequency SAW transducer and for the very demanding electrooptic grating array.

Diffraction

When a light beam encounters a grating segment of finite height, there are two diffraction effects that are important to us. First, the presence of the modulation that comprises the grating itself produces a diffracted beam, angularly separated from the incident beam by twice the Bragg angle. Second, the finite height of the grating segment causes a diffractive spreading of both the incident and the diffracted beams. It is this second effect that we are interested in here. It will be seen later that inefficiency of the electro-optic grating segments is solely responsible for the error signals in the two-SAW correlator. If the diffracted beam from one of the surface acoustic wave segments suffers a sufficiently large spread (due to diffractive effects) to take part of the beam out of Bragg incidence, then this effect will appear as an inefficiency of the electrooptic grating. This leads us to a relationship between the segment height, h, and the electrooptic grating depth, d:

$$h >> (\lambda/\Lambda)d \qquad (5\text{-}1)$$

here λ is the optical wavelength in the medium, λ_o/n, where n is the index of refraction of the medium; and Λ is the period of the electrooptic grating array. For operation in lithium niobate where $n = 2.2$, using $\lambda_o = .633$ μm, $\Lambda = 8$ μm, and $d = 2$ mm, leads to the requirement that h should be much larger than 72 μm. This interim may be too severe for situations (like the one here)

where the IOSLM is in the undeveloped near field of the light distribution. It should be noted that this criterion is in conflict with the desire for high data rates because the product of the data rate and bit length is the surface acoustic wave velocity, a material parameter.

SAW Bandwidth

The time required to switch the surface acoustic wave on or off is approximately equal to the reciprocal of the bandwidth:

$$\tau = 1/B \tag{5-2}$$

where τ is the switching time and B the transducer bandwidth. For most faithful operation, this time must be very short compared to the duration of one bit, that is, compared to the reciprocal of the data rate. Thus we have,

$$R << B, \tag{5-3}$$

where R is the data rate. Now the bandwidth of a surface acoustic wave transducer is approximately equal to the center frequency of the transducer divided by the number of finger pairs in the transducer. Since the frequencies of the surface acoustic waves of the correlator are fixed, one would ordinarily be able to use a large number of finger pairs, thereby obtaining a high transduction efficiency to surface acoustic waves, high acoustic amplitude, and thereby high acoustic diffraction efficiency. The preceding discussion tells, us, however, that we need high bandwidths in order to get high data rates. Since the bandwidth is proportional to the frequency, this criterion would tend to favor the use of high SAW frequencies. This choice would conflict with the unalterable photolithographic limitation on the minimum period that can be used. In the actual mask design we chose a modest bandwidth of about 25% of the center frequency for the low frequency SAW. Since the high frequency SAW was chosen to have a frequency roughly twice that of the low frequency SAW, this meant that we could use an 8 finger pair transducer for the high frequency SAW, thereby increasing the transduction efficiency. This is important because the acoustooptic interaction tends to fall off rapidly for high frequencies. By using this slight freedom we were able to partially compensate for this fall-off.

Grating Segment Width vs Length

We discussed above the relationship between segment height and the depth of the electrooptic grating. Here we discuss a geometric restriction on the segment height versus segment depth which applies to both the SAW segments and the electrooptic segments. This restriction is placed by the fact that the light is not incident on any of the grating segments parallel to the grating fringes; rather it must be incident at the Bragg angle. This means that light is incident upon an isolated segment both on the front and on the side of the grating segment. Of the light rays encountering the segment, only those that enter along a certain fraction of the front edge of the segment can encounter the full grating depth. Light rays which enter along the sides or outside of the special region along the front encounter effectively a shallower grating and therefore a less efficient grating. (A simple model for the fall-off in diffraction efficiency is discussed in Appendix 1). This immediately impacts the light distribution in the diffracted beam, causing it to taper off at the edges. Thus the effective aperture of the diffracted beam is reduced and it suffers more from spreading effects. If the grating segment is not isolated then part of the light that is not diffracted by its neighbor will be diffracted by the segment or vice versa. Incomplete diffraction of the light entering a portion of the front of a grating segment allows some of this light to leak into the side of the neighboring grating segment, thereby leading to crosstalk among the channels. This effect is minimized by shortening the grating depth or by maximizing the grating height. Shortening the grating depth reduces the efficiency, degrades the S/N ratio, and in the case of the electrooptic grating, increases the error rate. Increasing the height of the grating segment reduces the data rate that can be attained.

Selectivity

If the two-SAW correlator design is to function properly, then the incident light beam must not be diffracted by the electrooptic grating unless it is first diffracted by a surface acoustic wave segment. The expression given in Section 2 for the diffraction efficiency of a grating shows that as the angle of incidence onto a Bragg grating is moved away from Bragg incidence, the efficiency oscillates, reaching zero at an equally-spaced series of angles.

It is a straightforward matter to solve the equations for the diffraction efficiency to determine the location of these zeros. This was carried out in Section 2, where also is a table showing the values of the grating depth required, under the assumption that the electrooptic grating has 100% diffraction efficiency, to obtain incidence at a zero of the diffraction efficiency for the actual geometric layout used in the current correlator mask. The actual value of grating depth used in the correlator mask is 2 mm and corresponds to $\tau = 9$. Finally, it was also pointed out in Section 2 that the required index modulation is a function of the grating depth. This dependence of grating modulation on grating depth comes about because of the assumption that the grating efficiency be 100%. For the parameters upon which the actual mask design was made, this leads to a calculated voltage of 3.2 volts to produce the required index modulation.

Optical Beam Width

The required optical beam width is the product of the number of bits in the correlated word and the length of a single bit. Since we have earlier commented that the product of the data rate times the length of one bit is the surface acoustic wave velocity, we can eliminate the bit length and determine that the required optical beam width is the number of bits times acoustic velocity divided by the data rate. This last form is given here because it is usually more desirable to design to the data rate than to design to the bit length.

We have discussed here the principal relationships among the design parameters that are imposed by various fabrication and operational limitations of the correlator. In the fielded device, this list would certainly be far longer. For research purposes, the list is sufficiently long to reassure us that we have considered most of the effects which will affect device operation. These considerations have led us to a design procedure which we will describe in the next section.

Design Procedure

A simple design procedure has been set up for the two SAW correlator. After considering the listed constraints and tradeoffs of the previous section, we have chosen the following basic assumptions:

(1) The data rate, R(G-bits/sec), should be an input parameter, i.e., should be specified at the start of the design procedure.

(2) The high frequency SAW should have periods no smaller than 4 μm.

(3) The low frequency SAW should have approximately the same period as the IOSLM.

(4) The IOSLM must have an integral or a half integral number of finger pairs per bit.

Item 1 enables us to design to a data rate; Item 2 is simply a statement of our current photolithographic limitations; Item 3 is a result of a design arrangement. The Bragg angles of the SAWs in the IOSLM satisfy $\theta_{eo} = \theta_2 - \theta_1$, where θ_{eo}, θ_2, and θ_1 are the Bragg angles of the electrooptic grating and the high- and low-frequency SAW's. In terms of the grating periods this becomes $1/\Lambda_{eo} = 1/\Lambda_2 - 1/\Lambda_1$. From this relationship, we can see that once the period of the high frequency SAW, Λ_2, is chosen, the period of the electrooptic grating and the low frequency SAW have a fixed relation. Increasing one requires that the other be decreased. For photolithographic ease it therefore seems most reasonable to chose them approximately equal. Item 4 is simply a practical matter: only integral or half integral numbers of finger pairs per bit are possible without periodic disruptions of the finger pattern.

Using these design criteria, it is a simple matter to generate a suitable design for the two-SAW correlator once some elementary choices have been made. The remainder of this section illustrates the design of the 2-SAW correlator that was actually implemented.

For LNO and a light wavelength of 0.6328 μm, the high-frequency SAW must have

$$f_2 < V_a/4.0 = 0.875 \text{ GHz} \qquad (5\text{-}4)$$

because of item (2). Let us adopt this maximum value for f_2. For a specified data rate, R, the length of one bit will be

$$\ell = V_a/R \tag{5-5}$$

so the number of periods/bit will be

$$N = \ell/\Lambda = f/R \tag{5-6}$$

For the IOSLM, then, following specification (4), we find the number of finger pairs/bit for the electrooptic grating

$$N_{eo} = \text{Int}(f_2/2R) \tag{5-7}$$

for integer N_{eo}, or

$$N_{eo} = \text{Int}(f_2/R)/2 \tag{5-8}$$

for half-integer N_{eo}. For a 32 Mb/sec data rate (0.32 Gb/sec) and f_2 = .875 GHz, these formulas give 13 and 13.5, respectively, so by Eq. (5-6), f_{eo} will be 0.416 GHz or 0.432 GHz, respectively, and f_1 will be 0.459 GHz or 0.443 GHz, respectively. These design features are summarized in Table II.

Finally, there is one other feature that deserves mention. The acoustic waves undergo a diffractional spread by an amount determined by the acoustic aperture of the transducers, according to the usual formula:

$$\alpha = \Lambda/W_a \tag{5-9}$$

where α is the spread angle and W_a is the acoustic aperture. It is desirable to choose the ratio of the two acoustic apertures so that the two SAWs undergo the same angular spread, so that whatever diffractional degradation occurs will occur to both SAWs equally. This requires that

$$\Lambda_1/W_{a1} = \Lambda_2/W_{a2} \tag{5-10}$$

TABLE II. 32 Mb/Sec CORRELATOR DESIGN FIGURES

Item, Symbol (Units)	Values: Integer # Periods/bit	Values: Half-Integer # Periods/bit
Low-Frequency Transducers		
Frequency, f_1 (MHZ)	459	443[a]
Period, Λ, (μm)	7.625[a]	7.901[a]
Aperture, W_{a1}(mm) T1[b]	1.0	1.0
T2	0.9	0.9
# Finger Pairs[c]	4	4
Bragg Angle @.633 μm, θ_1(rad)	0.0189	0.0182
High-Frequency Transducers		
Frequency, f_2 (MHZ)	875	875
Period, Λ_2, (μm)	4.0	4.0
Aperture, W_{a2} (mm) T1[b]	0.50	0.50
T2	0.45	0.45
# Finger Pairs	8	8
Bragg Angle @.633 μm, θ_2 (rad)	0.0359	0.0359
Electrooptic Grating		
Equivalent Frequency f_{ep}, (MHZ)[d]	416	432
Period, Λ_{eo} (μm)	8.413	8.102[a]
Depth, d(mm)	2.0	2.0
No. Periods/bit	13.0	13.5
Bit length, (μm)	109.4	109.4
Bragg Angle θ_{eo} (rad)	0.0171	0.0178

TABLE II. (Continued)

(Footnotes)

(a) These values are different from those reported earlier; the earlier results contained a computational error.

(b) Each SAW launching transducer has a counter transducer for measurement of losses. The counter transducers have slightly smaller apertures.

(c) Number of finger pairs for each transducer. The high-frequency transducers were given more finger pairs to increase the transduction efficiency.

(d) "Equivalent" frequency is calculated as $f_{eo} = v_a / \Lambda_{eo}$.

In the design of Table II, then, we will have

$$W_{a2}/W_{a1} = 0.475 \text{ or } 0.469 \qquad (5\text{-}11)$$

for the two cases discussed.

On the basis of this design, the mask of Fig. 5-5 was designed.

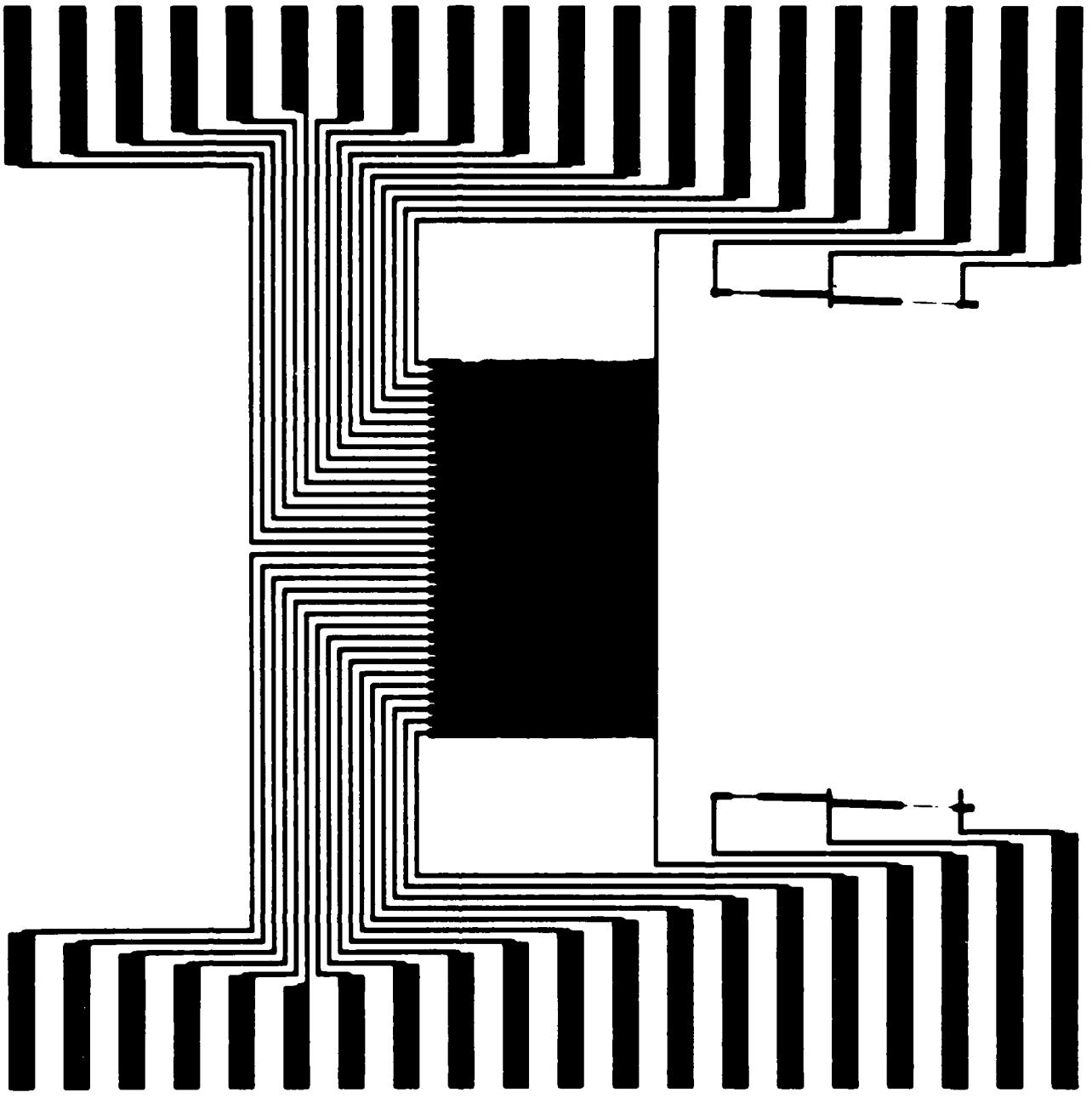

Figure 5-5. Metallization pattern mask.

CHARACTERIZATION

Computer Simulation

In the early stages of this work, it became clear to us that it would be very useful to have a computer code which would simulate the operation of the various correlators. One need calculate only a very few correlations of 32 bit binary sequences in order to understand the desirability of having this very tedious calculation carried out by the computer. Hence, early in the work on the single SAW correlator a primitive computer code was developed which would calculate the intensities of both the correlation and the anticorrelation signals from the device. During the course of the project, these codes have been altered many times to introduce new features or new conveniences. However, the basic operation of the codes has always been the same.

In the following description of the code, we will always refer to the binary sequence contained in the SAW grating segments as the signal word, and the binary sequence of the activated segments in the IOSLM as the filter word. The simulation of the correlator output intensities proceeds in two steps. First, quantities that we will call "elementary correlations" are calculated. An elementary correlation of two 32 bit binary words is an array of 63 numbers, calculated as the sum of the coincidences of ones in the two words for the 63 discrete positions of the two words relative to one another that contain at least one bit of overlap. An entry in one of these arrays can have an integer value in the range zero through thirty-two. Four elementary correlations are calculated using the signal and the filter word. These four correlations are

(a) The signal word correlated with the filter word, denoted SF.

(b) The complement of the signal word correlated with the complement of the filter word, denoted S'F'.

(c) The signal word correlated with the complement of the filter word, denoted SF'.

(d) The complement of the signal word correlated with the filter word, denoted S'F.

These four elementary correlations can be used to construct the intensity peak at the 63 instants of time at which the overlapping parts of the SAW and the IOSLM grating segments are perfectly aligned.

Having the four elementary types of correlations for the signal and filter words, it is a simple matter to construct the expected output intensities in the two beams (that is in the correlation and anticorrelation beams). First, we note that the correlation beam receives contributions any time the signal and the filter word both contain a one or both contain a zero, while the anticorrelation beam receives a contribution whenever one of them contains a one and the other contains a zero. Therefore, what ought to appear in the correlation beam is a sum over the SF and S'F' elementary correlations weighted by the diffraction efficiency of the appropriate SAW or IOSLM segments. Similarly, what ought to appear in the anticorrelation beam is a sum over the contributions from the S'F and the SF' elementary correlations, again weighted by the appropriate SAW or IOSLM efficiencies. We should recall here that our coding for a "zero" in the signal word is a grating segment in the low frequency SAW, while the coding for a "one" in the signal word is a grating segment in the high frequency SAW. In the IOSLM, however, the coding for a "one" is an activated segment while the coding for a "zero" is an unactivated segment. The IOSLM is effective in diffracting light only if it has first been diffracted by some SAW segment. Thus, while imperfect diffraction from a SAW segment may affect the signal to noise ratio or, if the two SAWs diffract with unequal efficiencies, may contribute to some distortion of the correlation waveform, imperfect diffraction in the SAWs can never give erroneous contributions to the correlation or the anticorrelation beams. On the other hand, imperfect diffraction by the IOSLM means that an activated segment will send contributions into both beams, leading to erroneous contributions in one of the beams. IOSLM segments which are coded for zeros, that is, unactivated, do not generate any errors. For an activated IOSLM segment, the error contribution arises from the transmitted beam, so that a 100% diffraction efficiency in the segment will always eliminate the error term.

The actual construction of the output intensities proceeds as follows: for each of the sixty-three instants of time at which the correlation or the

anticorrelation is to be constructed, the correlation and the anticorrelation intensities are calculated as

$$I_C(i) = \eta_H\eta_F\ SF(i) + \eta_L\ S'F'(i)$$

$$+ \eta_L(1 - \eta_F)\ S'F(i) \qquad (1 \leq i \leq 63) \qquad (5\text{-}12)$$

$$I_A(i) = \eta_L\eta_F\ S'F(i) + \eta_H\ SF'(i)$$

$$+ \eta_H(1 - \eta_F)\ SF(i) \qquad (1 \leq i \leq 63) \qquad (5\text{-}13)$$

In these equations, the index i refers to i^{th} instant of time; η_L and η_H are the diffraction efficiencies for the low- and the high-frequency SAWs, respectively; and η_F is the diffraction efficiency for the IOSLM. Also, the last term in each equation is the error term; it is seen to be proportional to 1 minus the efficiency of the IOSLM, i.e., it vanishes when the IOSLM has 100% efficiency. On the other hand any effect that reduces the apparent efficiency of the IOSLM will lead to increased error terms. As we saw earlier, one such effect is the finite height of the SAW and the IOSLM grating segments.

The bulk of the actual computer code is, in fact, associated with entering data into the code, displaying or printing the elementary correlations or the final output intensities, plotting these correlations or intenstities, and handling the data in such a way as to attain pleasing displays or plots. But this is normal in computer codes. It was convenient to implement these codes (in a combination of BASIC for the bulk of the code, and assembly language for the calculation of the elementary correlations) on a small microcomputer (TRS80 - Model 1). This allowed the program to be fully interactive so that it can be used both for the calculation of correlation and anticorrelation curves for various binary sequences of interest, and for "hands on" simulated experimentation to familiarize researchers with the correlation output from particular sequences and the variations in correlation resulting from specific changes in the words that are being correlated. These codes have proved very useful throughout the program.

Experimentation

Fabrication

The waveguide is fabricated by depositing 175 Å of titanium on the $LiNbO_3$ surface by e-beam evaporation. The waveguide then indiffused for 2-1/2 hours at 1000°C in a O_2/H_2O atmosphere running at 5 SCFH. The oxygen bubbled through water held at 95°C.

The buffer layer is composed of 1000 Å of Corning 7059 glass r.f. sputtered onto the waveguide surface. The sample is then annealed at 650°C in flowing argon to permit the electric field produced by the IOSLM to reach the waveguide layer. The buffer layer prevents diffraction from the aluminum fingers of the grating when no voltage is applied.

The correlator pattern is fabricated on the waveguide and buffer layer surface by depositing 1000 Å of aluminum by thermal evaporation from a tungsten boat. The sample is then coated with 5000 Å of positive photoresist and baked at 85°C for 1/2 hour. The sample is now exposed to 28.5 mJ of ultraviolet light with the mask in place. After developing the pattern for 20 seconds, the unwanted aluminum regions are etched away in an acid etch for 2-3 minutes to form the final correlator metallization pattern.

Assembly

The IOSLM is connected to the copper leads on the PC board via a "zebra" connector, which is composed of a silicon-type material with a conductive material imbedded in the silicon to form the contact leads. The silicon strip is laid down around the IOSLM leads and the copper PC board leads and pressure is applied to form the desired contacts. The zebra connectors are commonly used in LCD technology to form the connection between liquid crystals and the electronics. We chose to use the zebras in this device rather than making the connections using separate copper wires and silver conductive paste because of the simplicity of the method.

The zebra connectors work well for our application of the IOSLM because the desired word is loaded into the IOSLM (via the data-word generator and shift register) and remains there for an indefinite period of time. The

rate that words in the IOSLM can be changed, however, is limited by the resistance of the zebra conductive elements, typically about 5KΩ. The capacitors for one bit of the IOSLM (13 finger pairs), including the zebras and copper leads, is typically 16 pF. The rise time for a long pulse would be $t_r = 2.2$ RC or about 176 nsec. Figure 5-6 shows the typical pulse response of the system. The top trace (Fig. 5-6 (a)) is the output pulse from the data-word generator and the bottom trace is the pulse form at the copper lead just before the zebra. The bottom trace (Fig. 5-6 (b)) shows the pulse form at the aluminum lead of the IOSLM just after it has passed through the zebra connector. The pulse shows a rise time of about 180 nsec, as predicted. Thus, the zebras limit the switching rate of the IOSLM to about $(2 \times 196 \text{ nsec})^{-1} = 2.8$ MHz. For our application this is irrelevant, but to switch words at a rate faster than 2.8 MHz, would require making the connections using some other connection method. In order to drive the SAW transducers at a rate of 32 MHz, we wired the r.f. electronics directly to the aluminum leads with a coaxial cable and silver paint, thus bypassing the zebra connectors.

Experimental Arrangement

Figure 5-7 shows a diagram of the experimental setup for the two-SAW programmable correlator. A spatially-filtered, collimated, He-Ne laser beam is truncated by a 3.5 mm aperture. The input beam enters the 1" x 1" $LiNbO_3$:Ti waveguide via a rutile input coupling prism. It first encounters the low frequency SAW transducer, then the high frequency SAW transducer, and finally the IOSLM. It then exits the waveguide via the output coupling prism. The correlation signal is focused by a lens onto photodetector A. The "anticorrelation" is focused by another lens onto photodetector B and the straight-through beam is blocked by a beam stop. The outputs from detectors A and B are connected to a dual trace differential amplifier on the oscilloscope where the signals are analyzed.

Included in the figure are the electronics used to drive the correlator. The digital word generator produces a 32 bit digital word through the output A. This word passes into the data shift register and is subsequently loaded into the IOSLM. The same digital word is mixed with the 459 MHz r.f. oscillator,

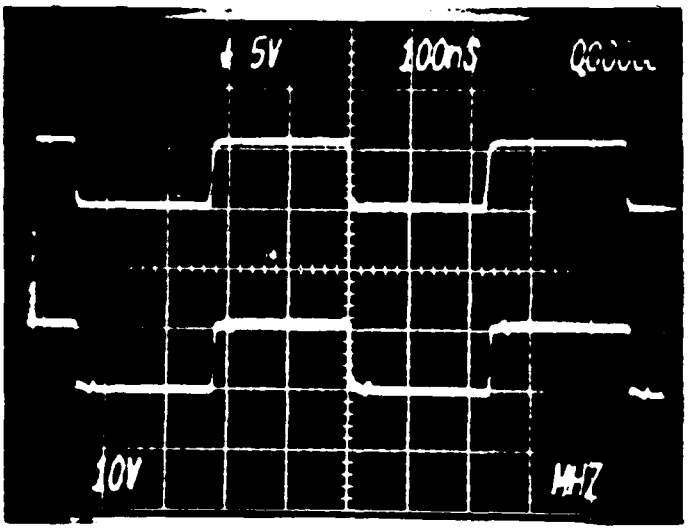

(a)

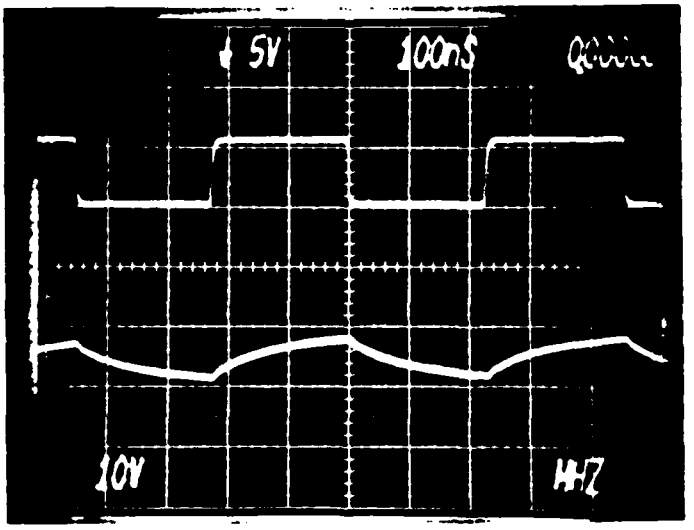

(b)

Figure 5-6. Effect of the zebra connector resistance on the pulse response of the system.

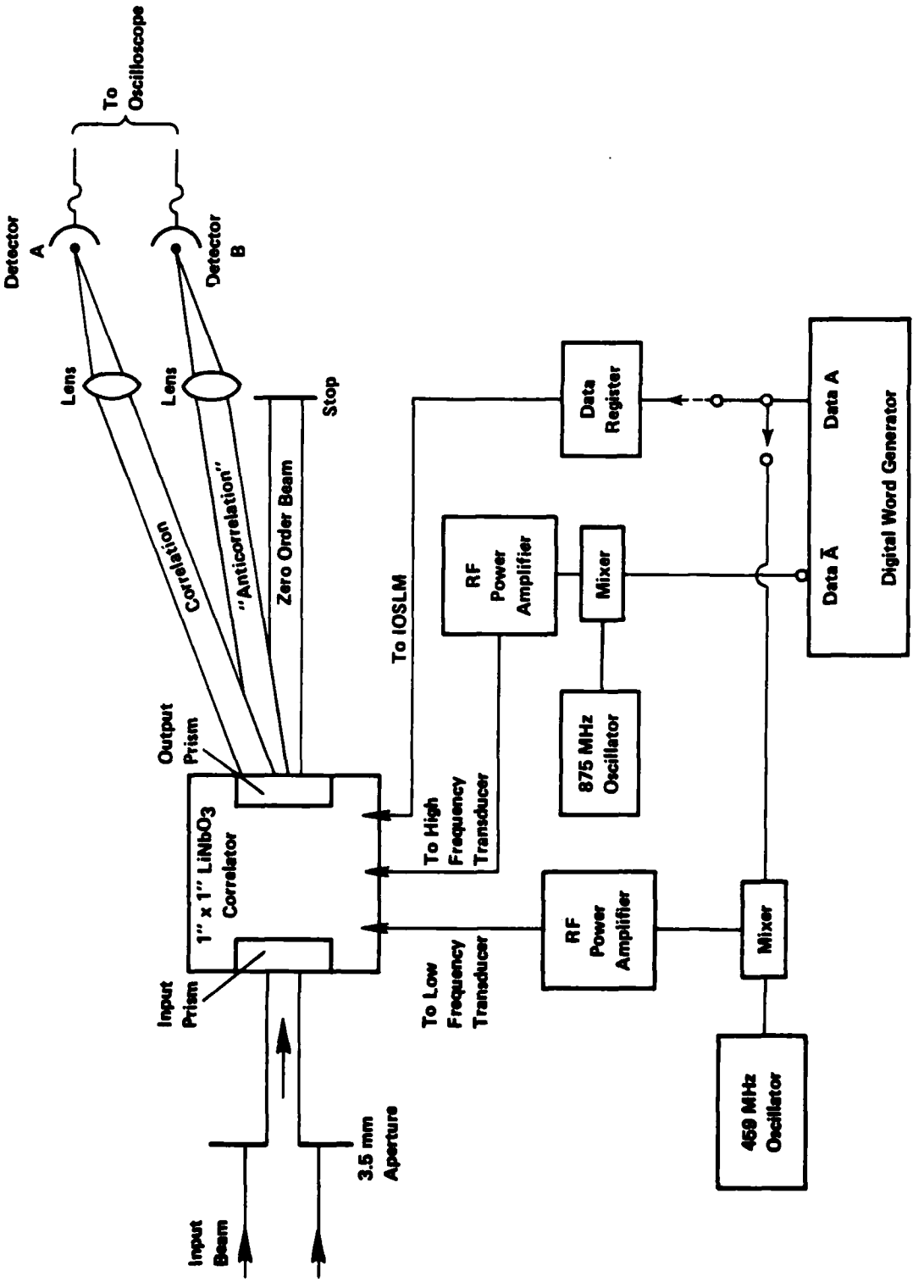

Figure 5-7. Experimental setup for the two-SAW correlator

amplified with an r.f. power amplifier, and connected to the low-frequency SAW transucer. The ones-complement of the 32-bit digital word is produced at out-out $\overline{A}$ and is mixed with the 875 MHz r.f. oscillator, amplified by another r.f. power amplifier, and connected to the high-frequency SAW transducer. (This is not the connection scheme proposed in Appendix 2). It was originally planned that (for autocorrelations) the digital word loaded into the IOSLM would also be passed to the high-frequency SAW, while its ones-comp'ement would be run through the low-frequency SAW. Because of photolithographic problems in reproducing the high-frequency SAW transducer, the two-SAW correlator was first tested using only the low-frequency transducer. Thus, the digital word loaded into the IOSLM was also passed to the low-frequency transducer. When the photolithographic problems were solved and the high-frequency SAW transducer was correctly replicated, the one's complement word was simply passed to the high-frequency SAW transducer. The net effect of this is to interchange the locations of the correlation and "anticorrelation" beams.

Results

Diffraction Efficiency

Figure 5-8 shows a graph of the diffraction efficiency (normalized to 500 mW dissipated r.f. power) versus frequency for the low frequency SAW transducer. This transducer is a 4-finger-pair transducer with a period of $\Lambda = 7.63$ μm. Its designed center frequency is $f_o = 459$ MHz. The bandwidth of the transducer should be 115 MHz. The graph shows that a peak of 78% diffraction efficiency was reached for 500 mW dissipated r.f. power at about 435 MHz, slightly lower than the design of 459 MHz. No attempt was made to impedance-match the r.f. electronics to the SAW transducer, and this is probably the cause of the frequency shift. The bandwidth at the half-power point was measured to be 117 MHz, very close to the design bandwidth of 115 MHz.

Figure 5-9 shows a graph of the diffraction efficiency (normalized to 500 mW dissipated r.f. power) versus frequency for the high-frequency SAW transducer. This transducer is an 8-finger-pair transducer with a period of $\Lambda = 4.0$ μm. Its designed center frequency if $f_o = 875$ MHz. The bandwidth of the transducer should be 109 MHz. The graph shows a peak of 34% diffraction

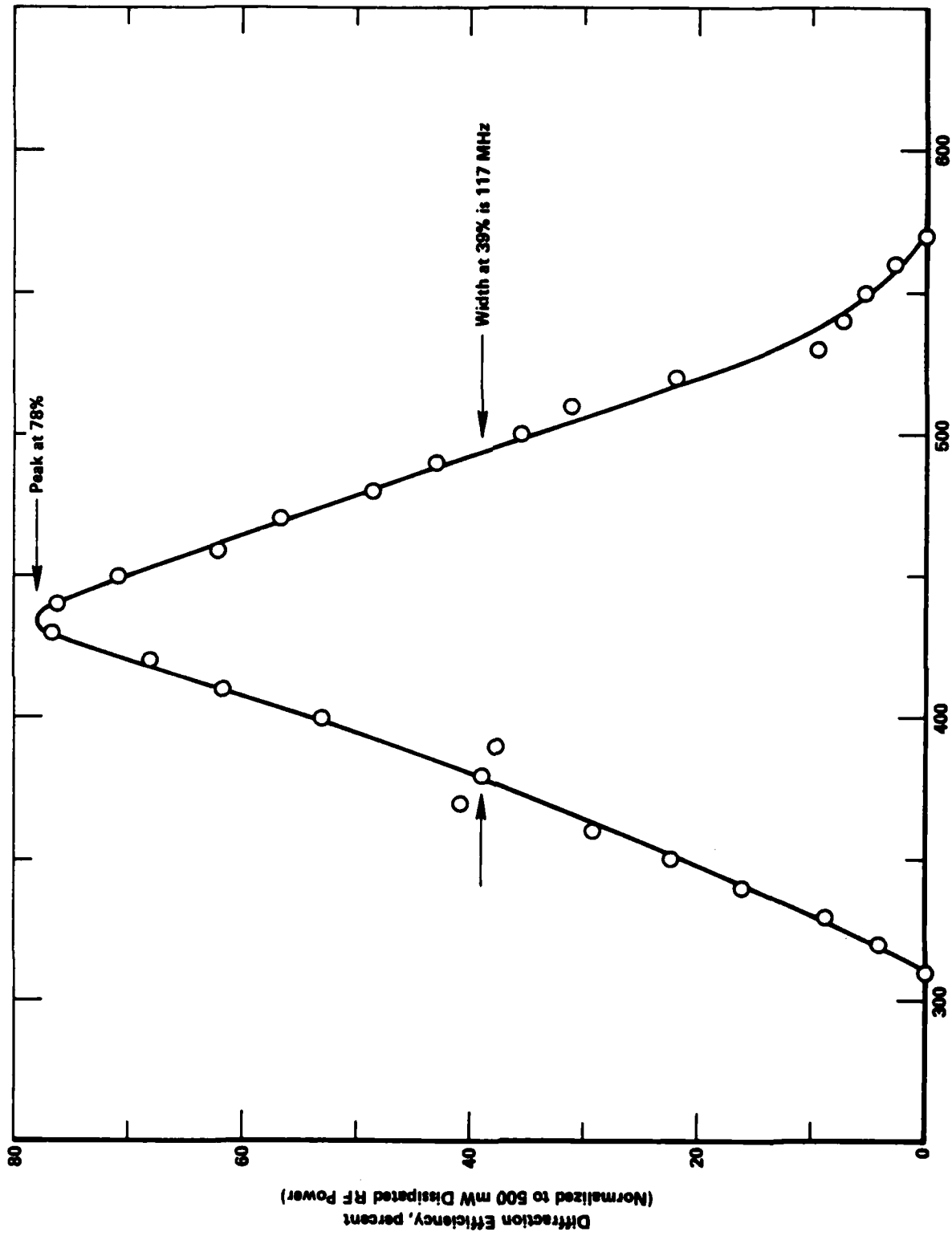

Figure 5-8. Diffraction efficiency versus frequency for the low-frequency SAW transducer.

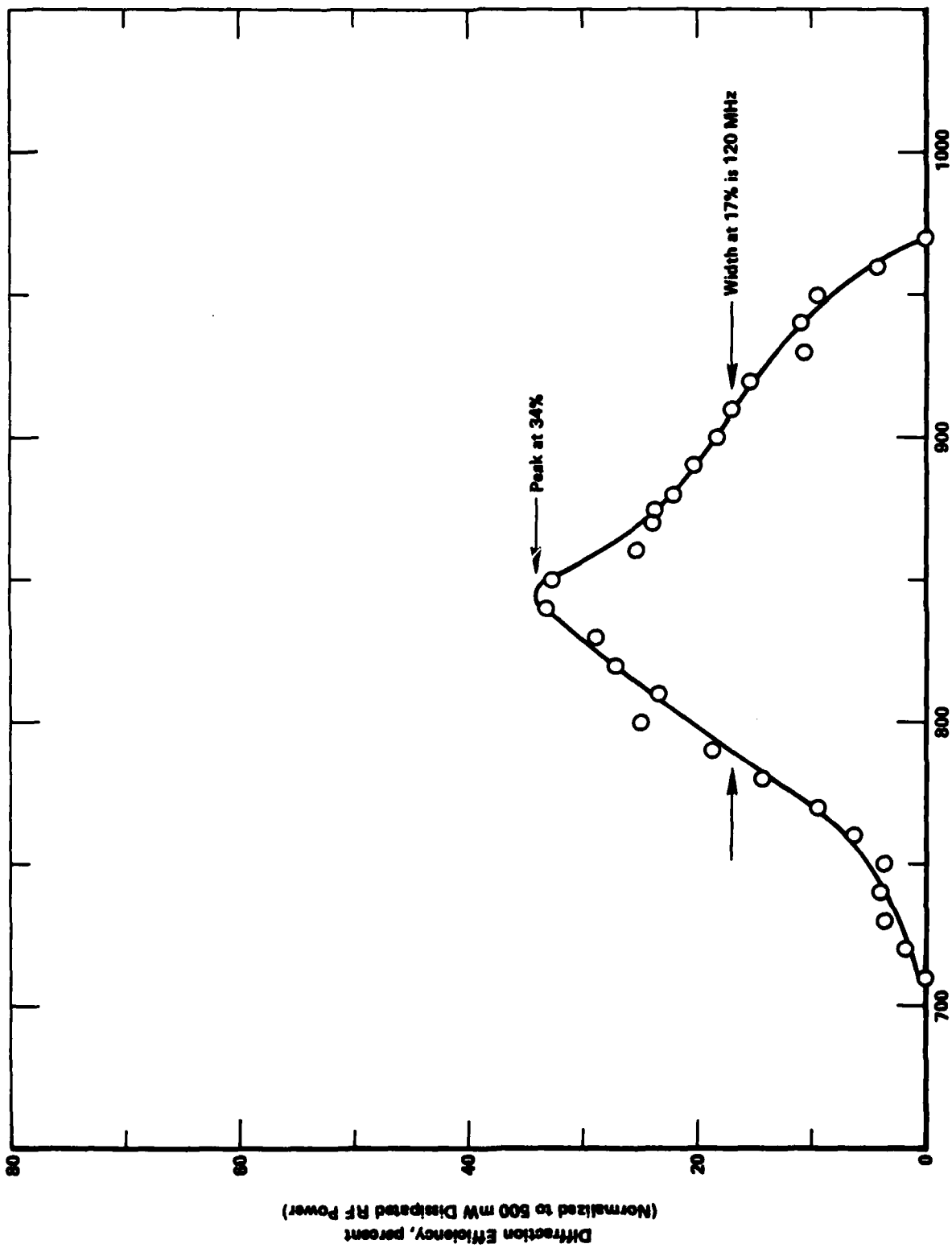

Figure 5-9. Diffraction efficiency versus frequency for the high frequency SAW transducer.

efficiency for 500 mW dissipated r.f. power at about 845 MHz. Again, no attempt was made to impedance match the circuit and the bandwidth of 120 MHz is not much different from the design value.

The IOSLM for the two-SAW correlator had the same diffraction-efficiency-versus voltage curve as the earlier one-SAW device. A diffraction efficiency of nearly 100% was obtained for an input voltage of 10 volts. It was noted that for buffer layers thinner than 1000 Å, maximum diffraction efficiency is reached at lower input voltages. An example is a sample waveguide with a buffer layer of 500 Å sputtered on its surface. The sample was then annealed at 650°C for one-half hour in flowing argon. An IOSLM was deposited on its surface whose maximum diffraction efficiency occurred at an input voltage of 8 volts. A minimum occurred at 16 volts and the next maximum occurred at 24 volts.

An additional measurement was performed on this sample to check that if a number of channels were turned on in parallel, the same amount of light was diffracted as would be if each channel was energized singly and then summed together. The data are presented in Tables III and IV. The variance in diffracted power from channel to channel appears to be due to the problem of obtaining uniform contact with the zebra connectors. Otherwise, the data seem to show that if the channels are combined in parallel, they diffract the same amount of light that they would if they were energized singly and then summed together.

Correlator Performance

Figure 5-10 shows the calculated intensity-versus-time function and the experimental result obtained for the correlation of the digital 32-bit word in the lower trace of the inset. Figure 5-11 shows the calculated and experimentally obtained results for the "autocorrelation" of the same digital word. Both results follow the predicted functions very closely.

Response to Simple Test Words. Figure 5-12 shows the correlator response to the simple test word of 16 "ones" and 16 "zeros" with only the low-frequency SAW energized. The top photograph shows the correlation and the "anticorrelation" signals. When these are subtracted with the

Table III. Diffraction Efficiency Measurements on Individually Activated Grating Segments

Channel No.	Diffracted Power, nW
10	2.15
11	1.96
12	1.99
13	2.40
14	2.46
15	2.87
16	2.38

Table IV. Diffraction Efficiency Measurements on Combinations of Grating Segments

Channel No.	Measured Power, nW(a)	Calculated Power nW(b)
15, 16	4.79	5.25
14, 15, 16	7.22	7.71
13, 14, 15, 16	9.73	10.11
12, 13, 14, 15, 16	11.92	12.10
11, 12, 13, 14, 15, 16	14.23	14.06
11, 13, 15	7.28	7.23
10, 13, 16	7.03	6.93

(a) Power measured in diffracted beam from the indicated segment combinations.

(b) Calculated as the sum of values from Table III for the segments listed.

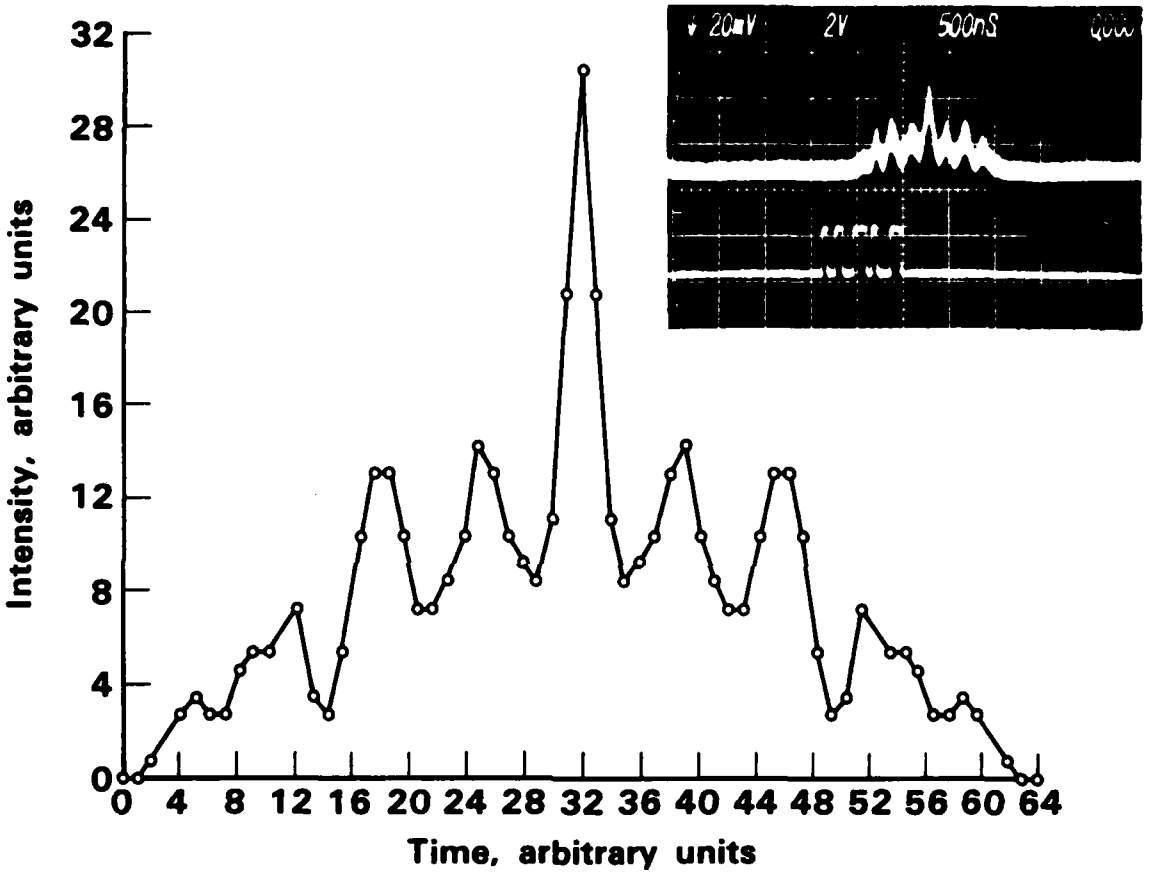

Figure 5-10. Correlation Function

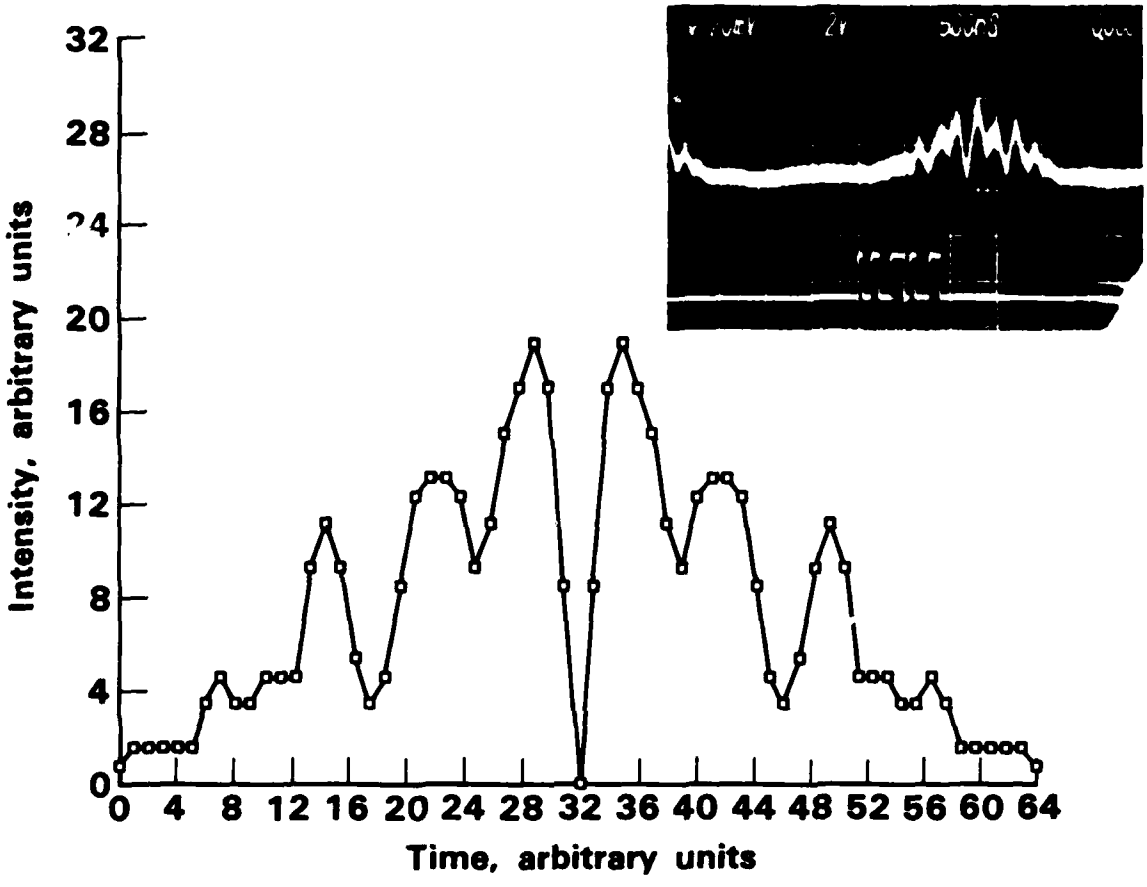

Figure 5-11. Anti-Correlation Function

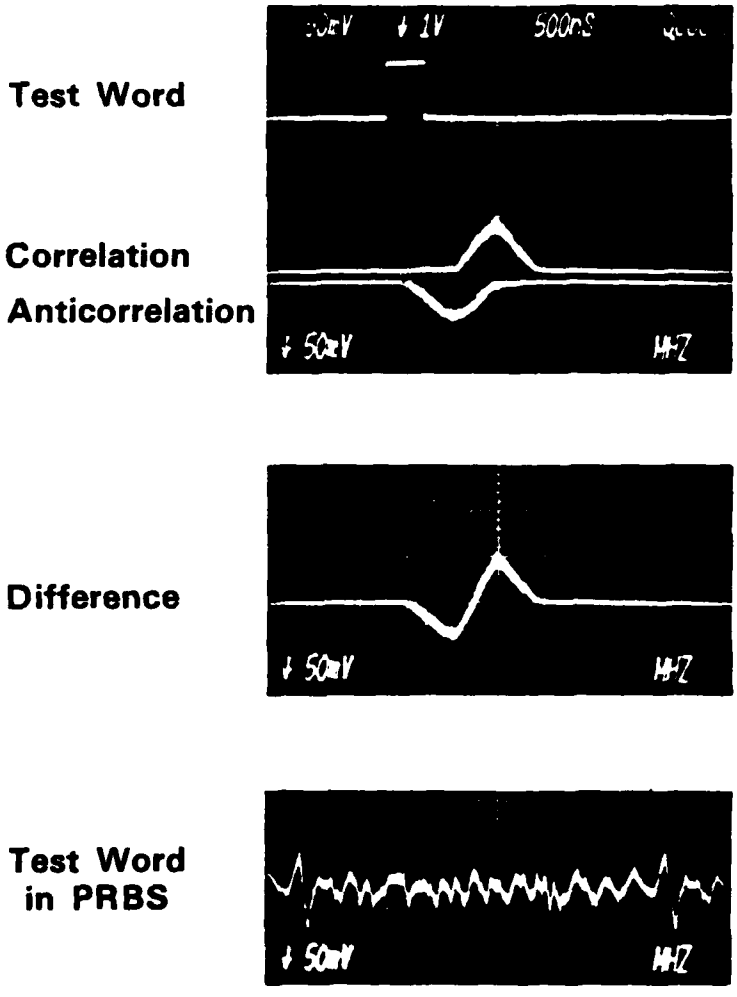

Figure 5-12. Correlator Output (Low-Frequency SAW)

differential amplifier on the oscilloscope, the difference shown in the middle photograph results. The test word was then buried twice in a pseudorandom binary sequence (PRBS) giving the bottom photograph. The peaks in the signal show where the test words were buried.

Figure 5-13 shows the correlator response to the 32-bit digital word listed at the top of the figure. The top photograph is with the low-frequency SAW energized above; the middle photograph shows the result when high-frequency SAW is energized alone; and the bottom photograph shows the correlator output with both SAWs energized. Figure 5-14 shows the difference (the correlation minus the "anticorrelation") for the same test word. The bottom photograph shows that the test word is easily recognized when buried (twice) in the PRBS.

Response to Complex Test Word. The correlator output for a complex word is shown in Figures 5-15 and 5-16. Figure 5-15 shows the correlation and "anticorrelation" response (for the low, high, and both SAW frequencies) to the test word listed at the top of the figure. Figure 5-16 shows the difference function for the same test word. Again, the complex test word is easily recognized when buried in a PRBS.

Response to "Picket Fence" Word. A simple "picket fence" test word (alternating ones and zeros) was input into the correlator with increasing frequency to test the speed response of the system. Figure 5-17 shows the correlator response to a 60 nsec picket fence (60 nsec on, 60 nsec off). The correlation and "anticorrelation" outputs are shown (for the low, high, and both SAW frequencies). Figure 5-18 shows the difference (the correlation minus the "anticorrelation") for the 60 nsec picket fence.

Figure 5-19 shows the correlator's response to a 150 nsec picket fence and a 30 nsec picket fence, the top photographs showing the correlation and the "anticorrelation" (for the low frequency SAW only) and the bottom photographs showing the difference. It can be seen that reducing the pulse width from 150 nsec to 60 nsec to 30 nsec causes the nulls in the correlation signal (which theoretically should return to the baseline) to begin to rise off the baseline so the frequency of the picket fence is increased. A number of factors combine to produce this effect: diffraction spread from the single bits of the SAWs and the electrooptic grating, time response of the photodetectors, and reduced diffraction efficiencies of the low- and high- frequency SAW transducers and the IOSLM. The last factor was found to be the most significant one

Low Frequency SAW

Correlation

Anticorrelation

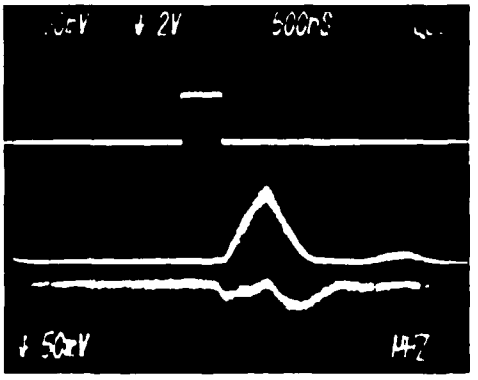

High Frequency SAW

Correlation

Anticorrelation

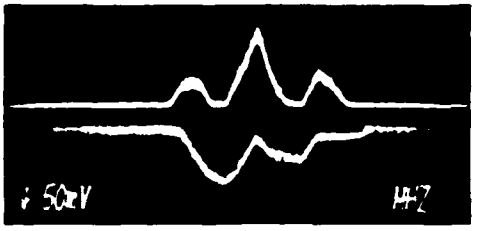

Both SAW Frequencies

Correlation

Anticorrelation

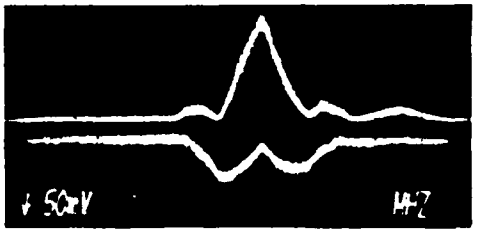

Figure 5-13. Correlator Output. Autocorrelation of: 00000111111111111111100000000000.

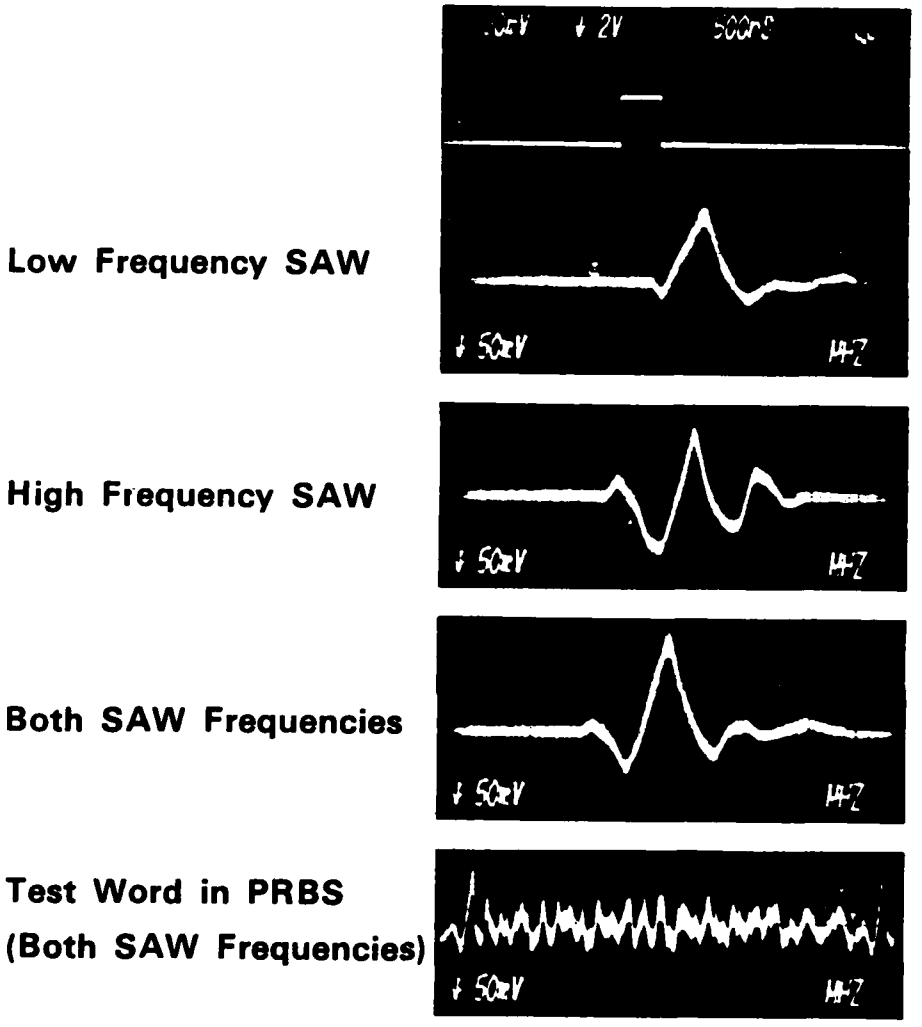

Figure 5-14. Correlator Output. Autocorrelation of: 00000111111111111111100000000000.

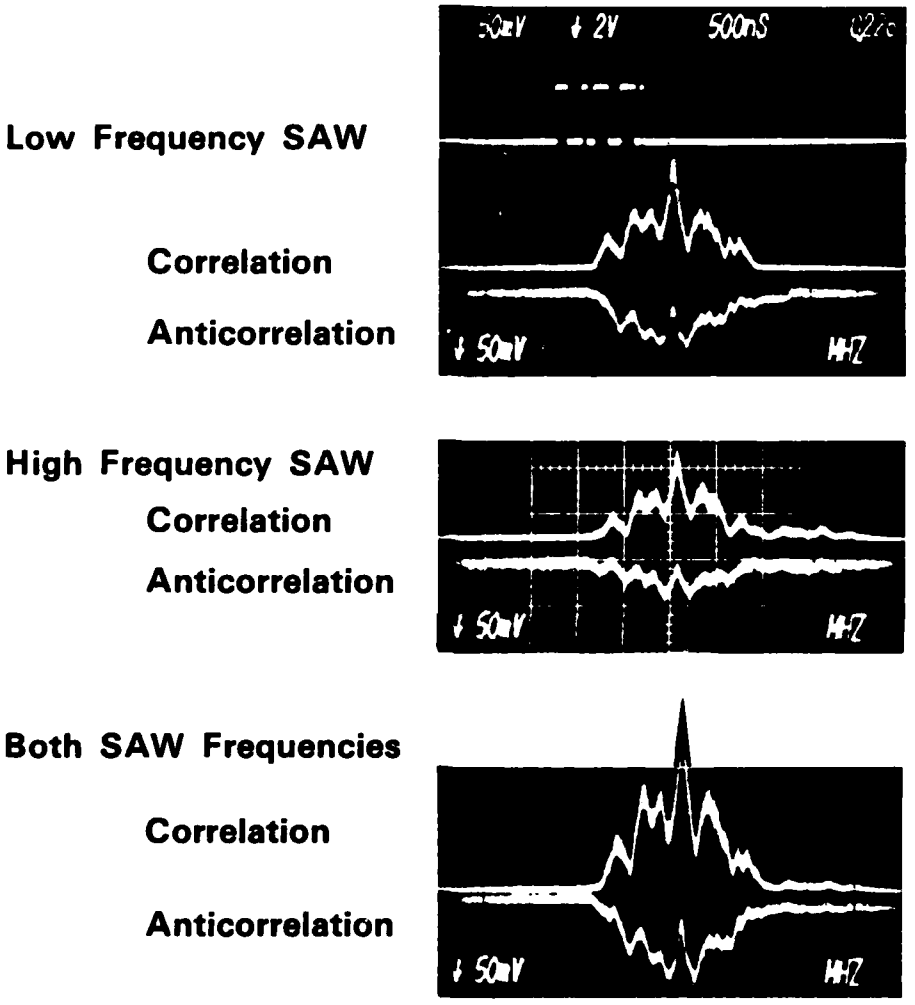

Figure 5-15. Correlator Output. Autocorrelation of 00100111110000111110011000001111.

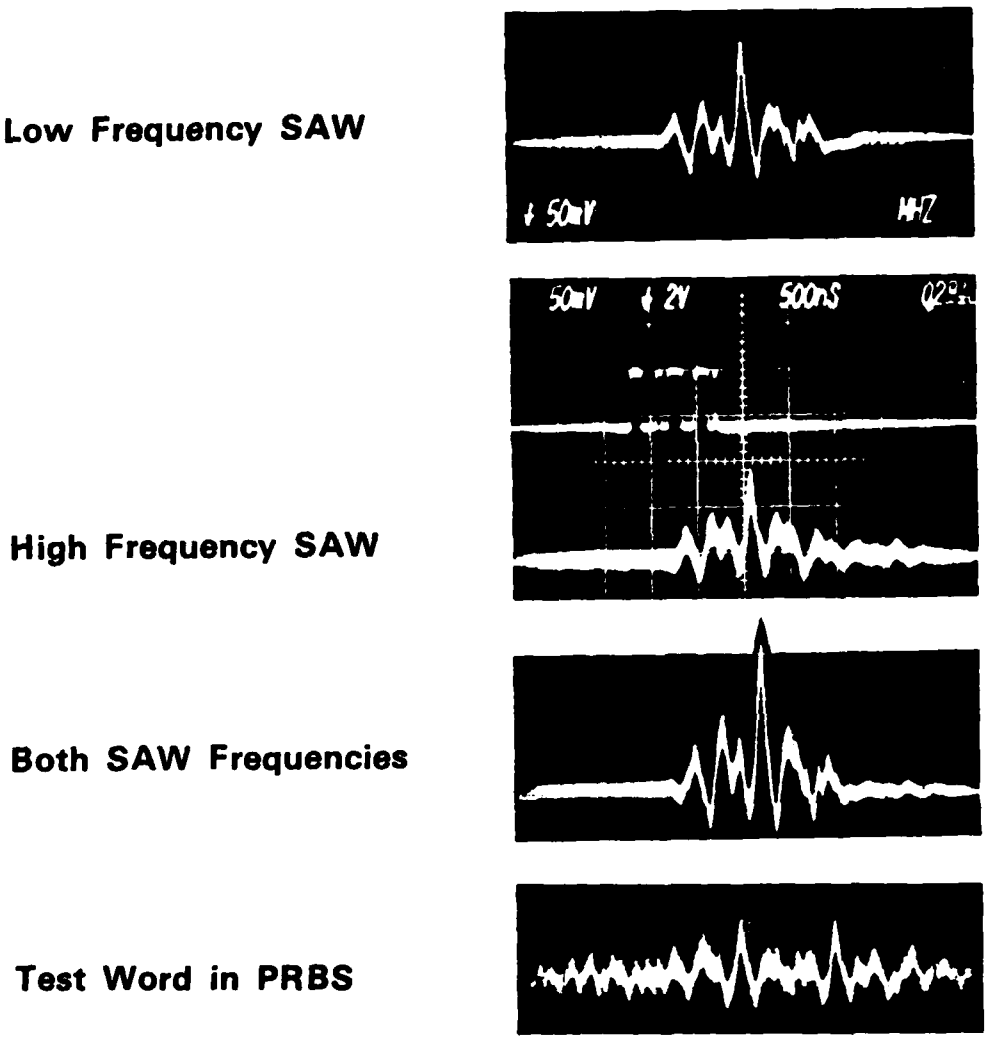

Figure 5-16. Correlator Output. Autocorrelation of 00100111110000111110011000001111.

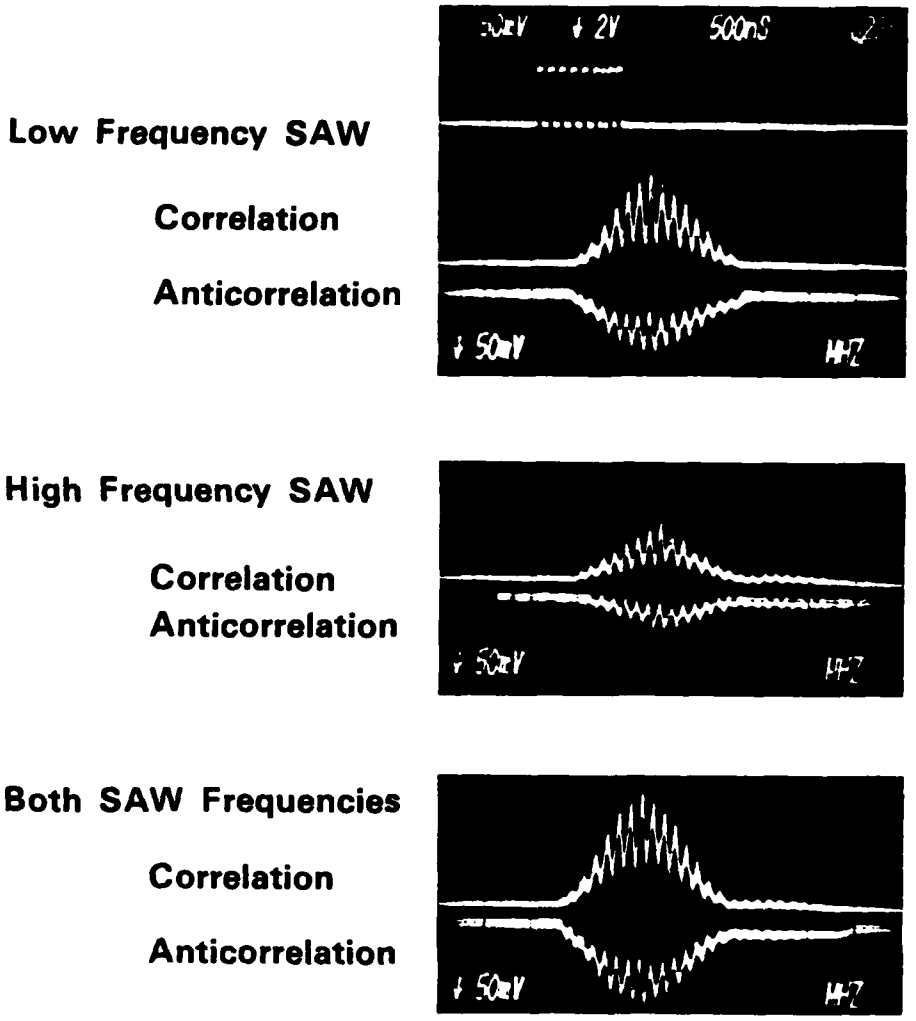

Figure 5-17. Correlator Output (60 nsec Picket Fence).

Low Frequency SAW

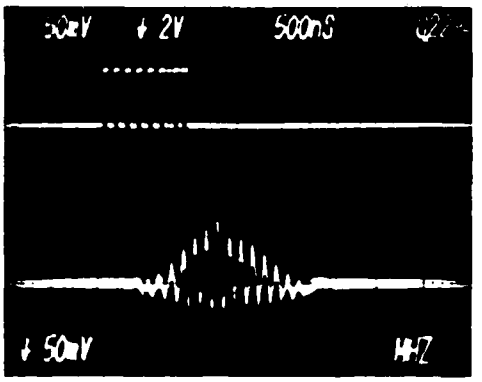

High Frequency SAW

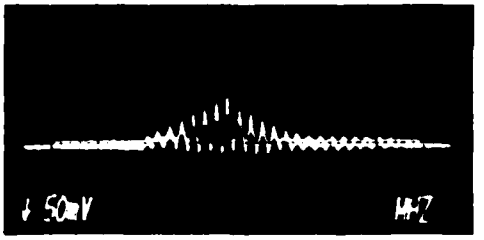

Both SAW Frequencies

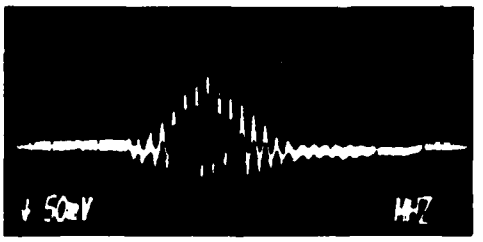

Figure 5-18. Correlator Output (60 nsec Picket Fence).

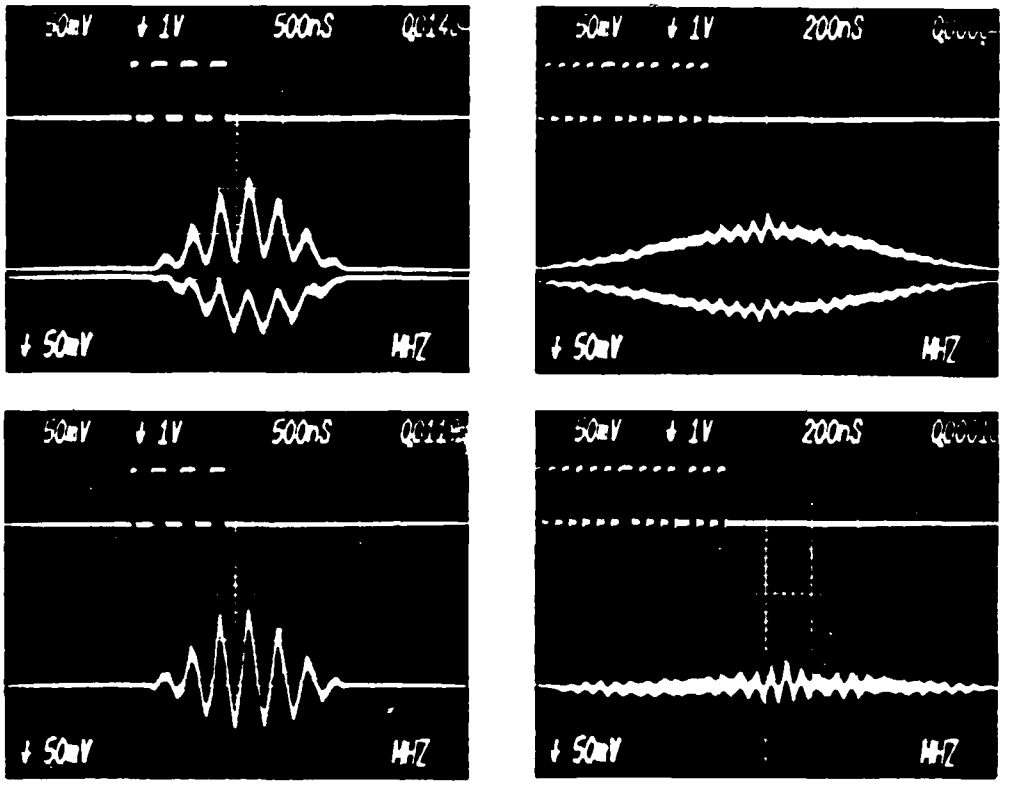

Figure 5-19. Autocorrelation of Picket Fence (Low-Frequency SAW).

contributing to the problem. It could be partially corrected by designing the SAW transducers for a higher diffraction efficiency, while still maintaining the bandwidth needed for the system.

6. OTHER IOCs EMPLOYING GRATING ARRAYS

In addition to the space-integrating correlator, there are a number of other uses which can be made of the integrated optical spatial light modulator or of variations on this basic grating array structure. The applications are by-and-large computational; however the first application which we discuss is the use of an IOSLM as a character generator.

The basic geometry for the character generator is shown in Fig. 6-1. The IOSLM would be driven by circuitry which would generate the appropriate signals for synthesizing characters. The output of the IOSLM would be scanned across an appropriate photoreceptor by a rotating mirror and would generate an entire line of characters at each pass. For the present 32-element device this could result in a writing speed which was 32 times the writing speed of current document generation machines or conversely a much slower rotating mirror could be used thereby eliminating a severe mechanical problem in these machines. Fig. 6-2 shows the imaged IOSLM output when alternate bits are turned on. The zero order is shown on the right and the first order, which would be used as the writing light, is shown on the left. As can be seen there are 16 clearly resolved spots. If all 32 elements were energized the 32 beams would merge and a solid line could be produced. The device is thus well suited for alphanumeric character generation.

SIGNAL-PROCESSING CONFIGURATIONS

The one-SAW correlator described in Section 4 is easily used as a parallel-to-serial converter. This is done by entering a word in parallel onto the IOSLM and energizing the SAW transducer with a single pulse whose width is no greater than the width of a single IOSLM window. The output of the correlator then presents serially in time the modulation pattern introduced spatially on the incident light beam. An example of such an output is shown in Fig. 6-3.

Another important operation in signal processing or communications is time division multiplexing. At the top fo Fig. 6-4 the usual time division multiplexing scheme is depicted. Here three signals from three channels are interleaved into a single fixed stream. Notice that each of the individual

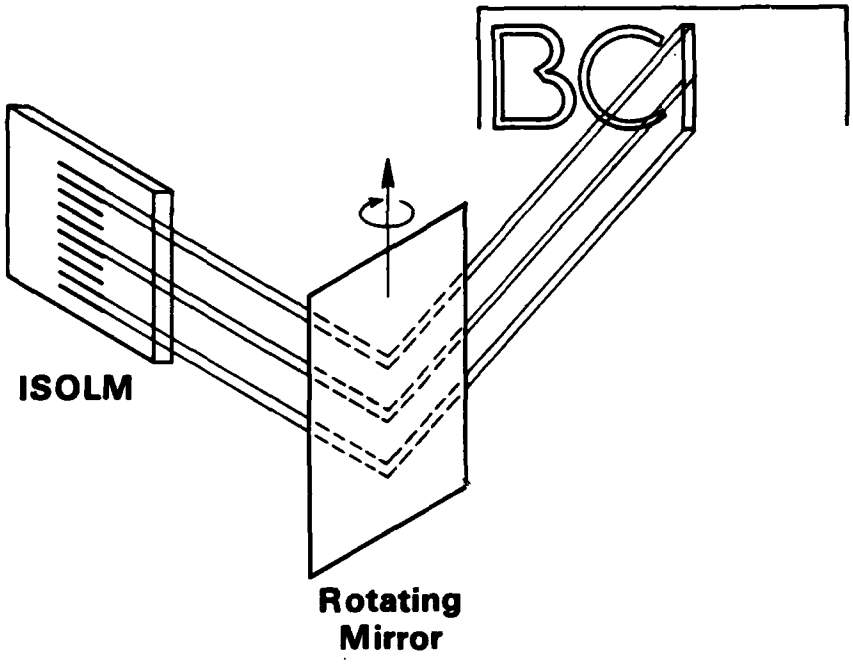

Figure 6-1. A schematic indicating the manner in which an IOSLM can be used as part of a character-generation system.

Figure 6-2. The output pattern of a 32-element IOSLM with alternate bits energized such as to produce maximum diffraction efficiency. The first order pattern appears on the left and the zero order on the right.

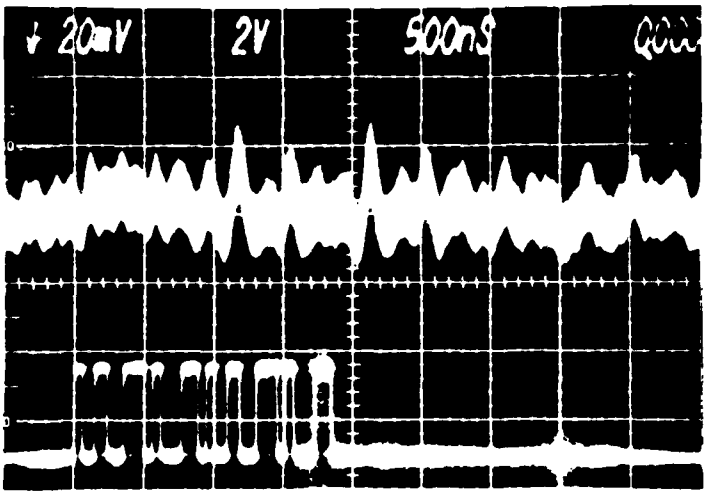

(a) Correlation Over Background Noise

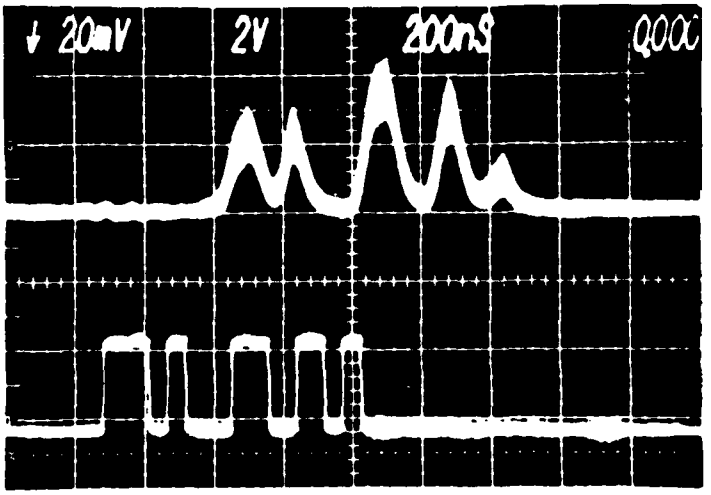

(b) Parallel to Serial Conversion

Figure 6-3. An oscilloscope trace showing in the bottom of the bit pattern applied to the IOSLM and in the top the optical output of the device when interrogated with a single SAW pulse. This illustrates the parallel to serial conversion operation.

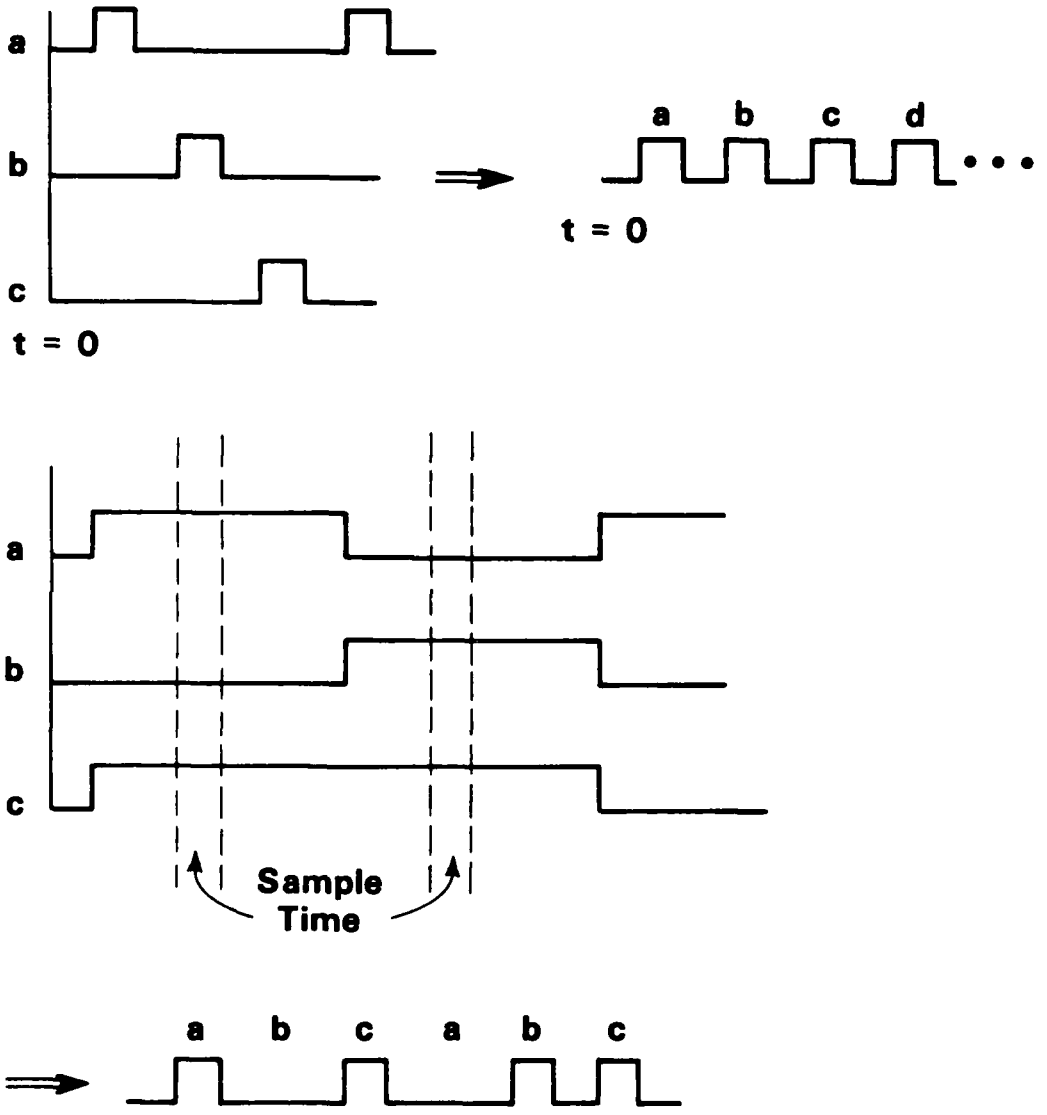

Figure 6-4. The top part of the figure illustrates conventional time-division multiplexing scheme. The second part of the figure illustrates the strobe-multiplexing concept described in the text. The advantage of the latter approach is that the individual input channels do not have to produce the short pulses characteristic of the multiplexed data stream.

streams contains bit lengths which are identical to those which appear in the multiplexed bit stream. This means that each of the signal generators which create the three original data streams must be capable of generating pulses which are as short as those of the final multiplex stream. In the middle of the figure we show another approach to time division multiplexing in which each of the original input signals can be run at a slow data rate and the pattern is repetitively strobed to create a multiplexed signal.

A device for performing this strobe function is shown in Fig. 6-5. The figure shows a $LiNbO_3$ waveguide with an IOSLM structure and coupling horns which take the output of each of the IOSLM channels and couple it to a fiber. The fibers are in alignment grooves on a silicon substrate which completes the flip-chip arrangement. Each of the IOSLM segments is run by one of the low speed input signals. When the IOSLM is loaded, a short pulse of light irradiates it uniformly. Because of the unequal lengths of the fibers the pulse from each successive segment of the IOSLM arrives at the detector or the transmitting fiber in the proper multiplexed sequence. Such an arrangement allows a good deal of flexibility in the choice of data rates and drive circuitry and places no severe speed requirements on any of the electronic components.

COMPUTATIONAL GEOMETRIES

Subtraction

The diffraction efficiency of an electrooptic grating is a function of the difference in the voltages applied to the two electrodes. Therefore as shown in Fig. 6-6 it is possible to perform a simple subtraction operation simply by applying two voltages, one to each side of the grating structure. Of course the diffraction efficiency is not linearly proportional to the difference which places some limitations on this device.

An advantage of using optical techniques to perform computational functions is that in many cases a sum can be performed very simply by using a lens to collect a number of outputs and cause them to be incident upon a single detector. The use of such an arrangement to perform vector subtraction is shown in Fig. 6-7. The subtraction is performed simply by introducing the components of the vector A on the left side of the electrode structure and the

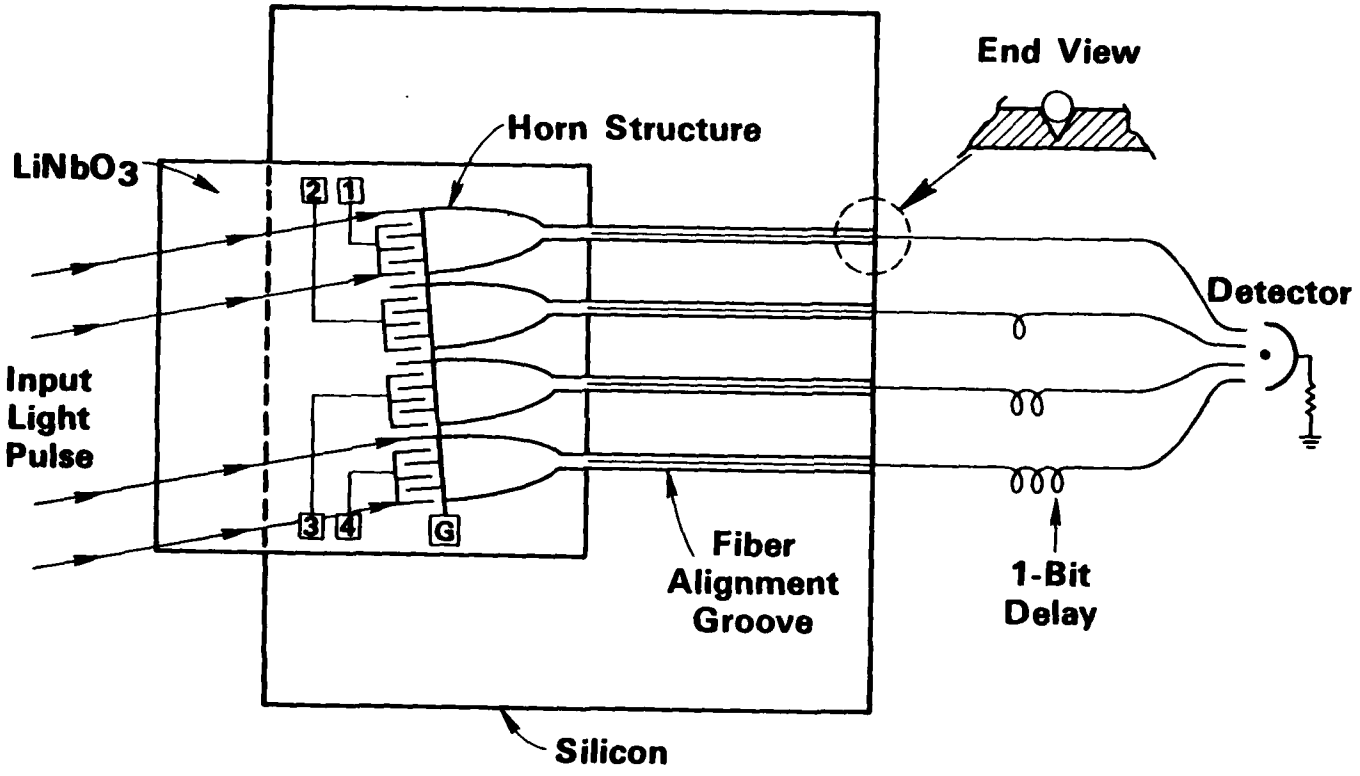

Figure 6-5. A schematic of a flip-chip integrated optical approach to the design of a 4-channel multiplexer using fiber-optic delay lines.

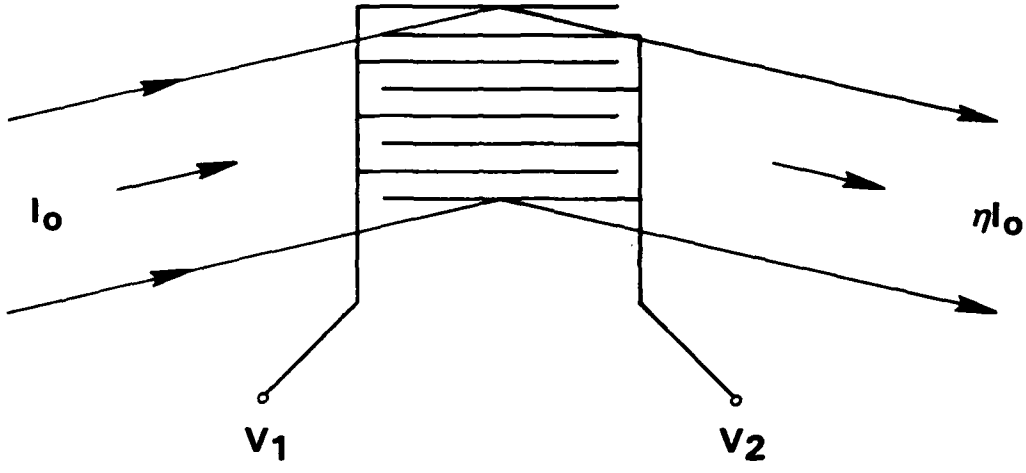

$$\eta = \sin^2 [a(V_1 - V_2)]$$

DIGITAL Exclusive OR

ANALOG Subtraction

Figure 6-6. A simple electrooptic grating structure used to generate the signal which is proportional to the difference of two voltages. If V_1 and V_2 can only have the values 0 or V then this device generates the digital exclusive-OR operation.

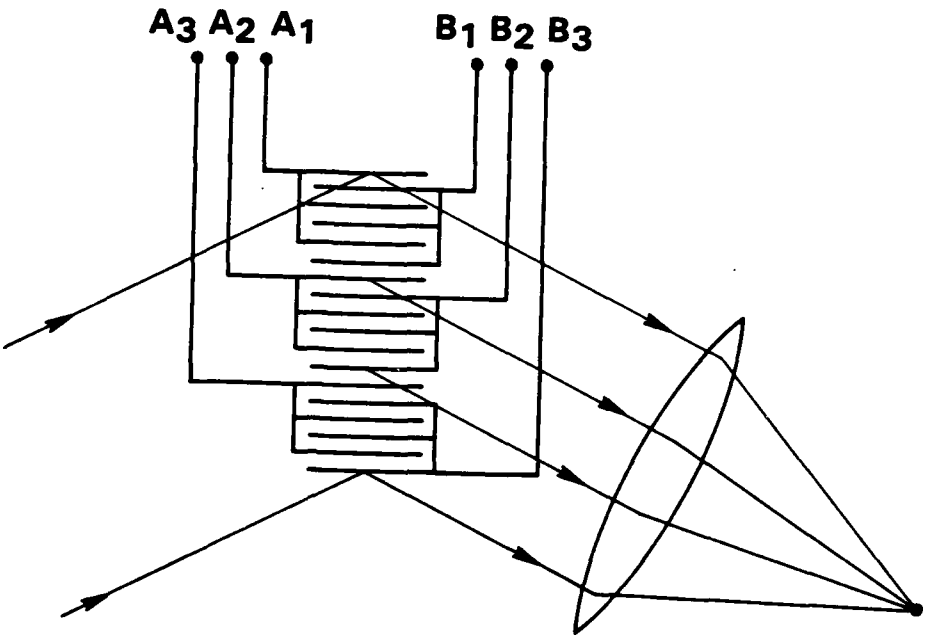

$$I = \Sigma I_i = \Sigma a^2(A_i - B_i)2$$

Figure 6-7. A linear array of subtraction units (such as that shown in Figure 6.6) whose output is summed by a single lens and which can be used to perform vector substration.

corresponding components of the vector B on the right side of the structure. The electrode pattern for such a vector subtractor or parallel comparator is shown in Fig. 6-8. A device of this structure having the same electrode dimensions as the IOSLM described in Section 4 was fabricated on a 1" square $LiNbO_3$:Ti waveguide. Preliminary investigations indicated that the device behaved as expected although great care must be taken to ensure that the prism-coupled light beam is quite uniform if the device is to operate properly.

Multiplication

The herringbone structure shown in Fig. 6-9 is designed so that light which is diffracted from the left-hand grating will be incident on the right-hand grating at its Bragg angle. The output intensity of the structure is therefore proportional to the product of the diffraction efficiencies of the two gratings. Since the spine of the structure is grounded the first diffraction efficiency η_1 is proportional to the voltage A and η_2 is proportional to B. The output of the device is therefore proportional to the product of the two voltages.

As shown in Fig. 6-10 a lens can be used to sum the outputs of a series of herringbone grating structures. Therefore in a manner analogous to the subtraction operation shown in Fig. 6-7 it is possible to perform vector multiplication.

The operation of matrix-vector multiplication is important in many areas. A variety of optical techniques have been suggested which are capable of high-speed matrix multiplication. In some of these devices the matrix values are stored on a mask which must be physically inserted into the optical system. Changing matrices is therefore an intrinsically slow operation. A modification of the vector-multiplication structure shown in Fig. 6-10 can be used to construct a matrix-vector multiplication IOC in which both the vector and the matrix components can be altered at high speeds by the use of electrical signals. A schematic of this IOC is shown in Fig. 6-11. The figure shows an IOC for the multiplication of a 3-dimensional vector by a 3 x 3 matrix. Detailed design studies show that a 16-dimensional device can be fabricated on a 1" square substrate.

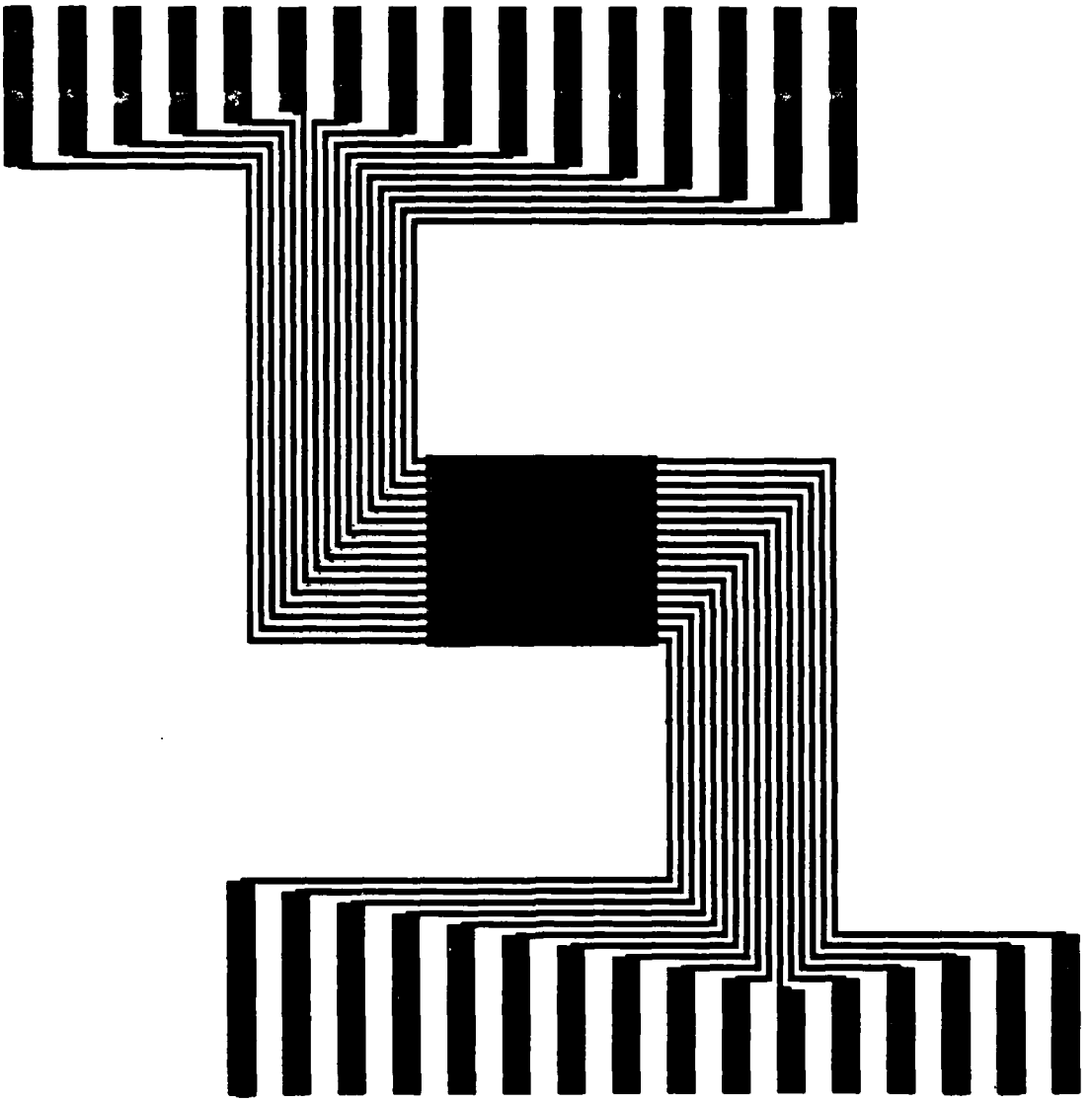

Figure 6-8. The metallization pattern for an IOC for performing vector subtraction or data-set comparison.

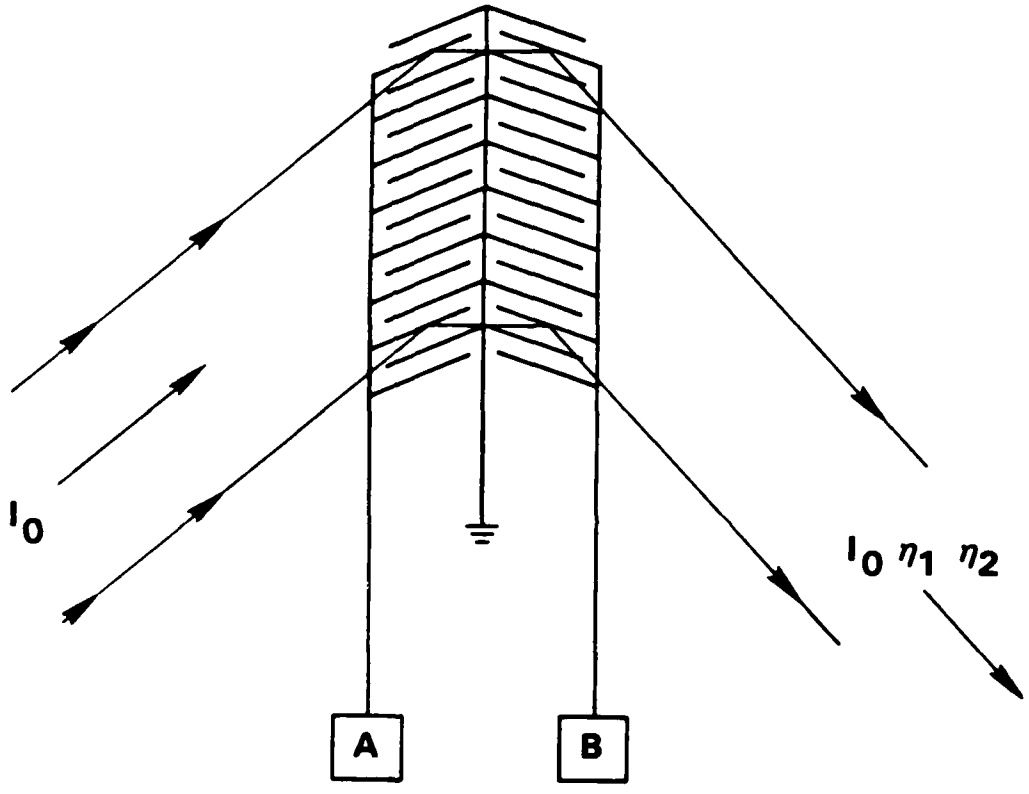

Figure 6-9. A herringbone electrode structure for performing multiplication. Note that the spine of the structure is grounded and that the output light intensity is proportional to the product of the two diffraction efficiencies, η_1 and η_2.

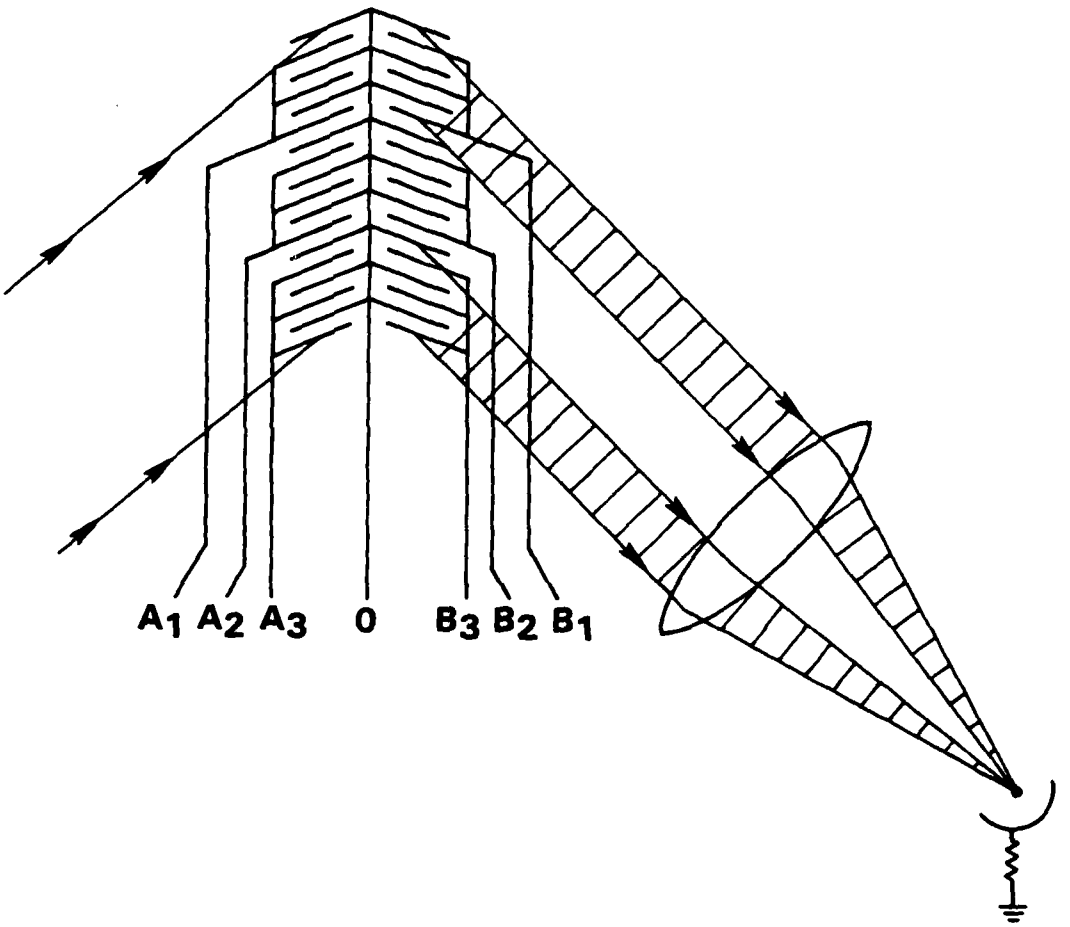

Figure 6-10. The extension of the simple multiplication device to one capable of performing vector multiplication.

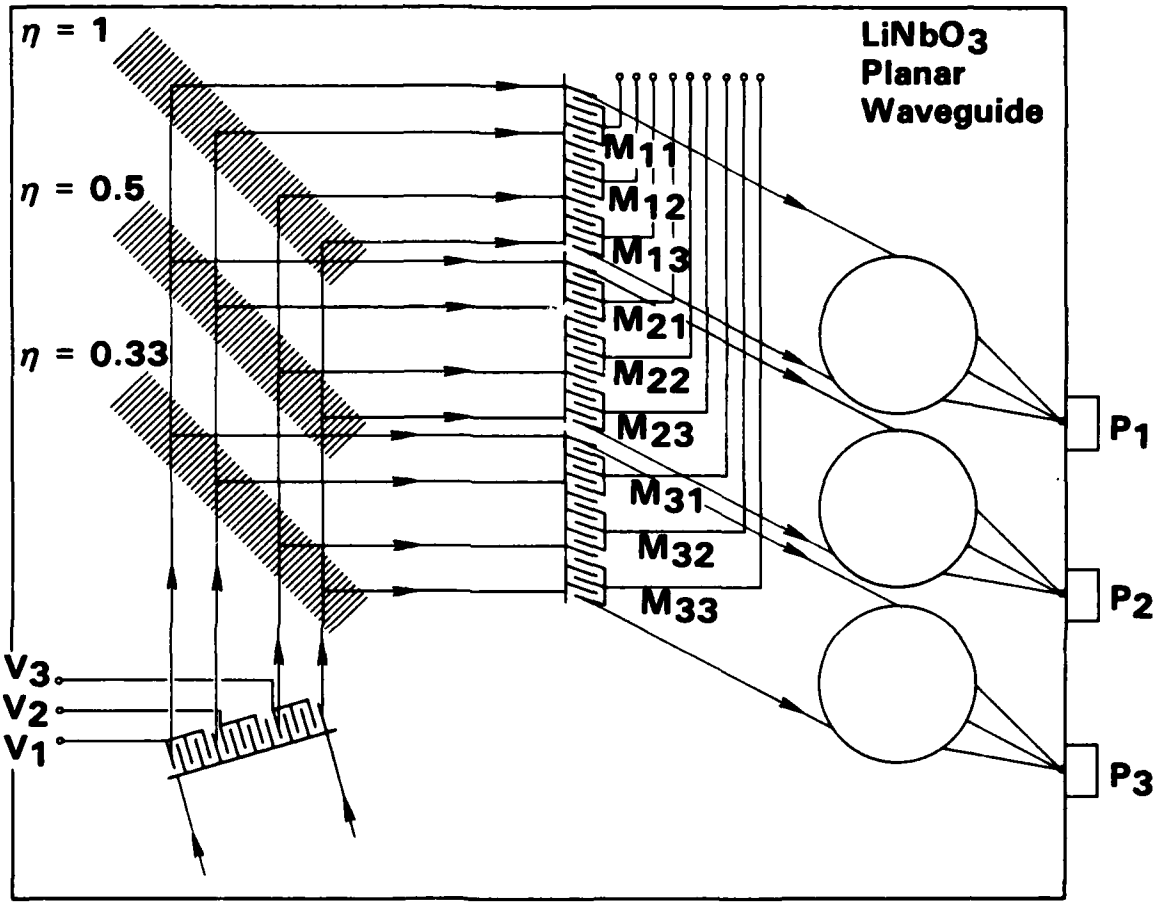

Figure 6-11. Schematic of an integrated optical circuit for performing vector matrix multiplication. The beamsplitters are holographically fabricated surface gratings and the lenses can be simple moderate quality As_2S_3 Luneburg lenses.

To operate the IOC shown in Fig. 6-11 the voltages corresponding to the 3 components of the vector are entered on the single IOSLM in the bottom left corner. Light incident on this structure is modulated and passes through 3 beamsplitters, each one of which directs one-third of the original beam intensity onto what amounts to three copies of the second half of the herringbone electrode structure. Each of these 3 structures has applied to it voltages corresponding to the components of one row of the matrix. The multiplication and summing operations are accomplished in a manner identical to that of the device shown in Fig. 6-10. Each of the components of the desired product vector appears at the appropriate output detector indicated P1, P2 and P3 in the figure.

Fabrication of the matrix-vector multiplication IOC could be accomplished in three basic steps. The first step is a single photolithographic step which would define all of the grating structures. The second and probably most difficult step would be the holographic exposure of the surface gratings which would act as the beamsplitters. The major difficulty here would be to attain the appropriate diffraction efficiencies and also to achieve the proper orientation so that the beams were incident at the Bragg angle on the second grating arrays. The third step would be to fabricate the lenses which could be fairly crude As_2S_3 Luneburg lenses. The quality of these lenses need not be very high since they are merely acting as light-gathering elements. They could be easily fabricated in a single step by simultaneous evaporation of As_2S_3 through a multiple mask. This device would therefore have the advantages of rather simple fabrication and high speed fully programmable operation. It would not however be possible to build a single chip which would be capable of handling very large matrices.

REFERENCES

1. R. Shubert and J. H. Harris, "Optical Surface Waves on Thin Films and Their Application to Integrated Data Processes", IEEE Transactions on Microwave Theory and Techniques, MTT16, 1048-1054 (1968).

2. C. S. Tsai and P. Saunier, "New Guided-Wave Acoustooptic and Electrooptic Devices Using $LiNbO_3$", Ferroelectrics 10, 257-261 (1976).

3. Michael W. Casseday, Norman J. Berg, Irwin J. Abrams, and John W. Lee, "Wide-Band Signal Processing Using the Two-Beam Surface Acoustic Wave Acoustooptic Time-Integrating Correlator", IEEE Transactions on Microwave Theory and Techniques, MTT-29, 483-490 (1981).

4. W. Richard Smith, Henry M. Gerard, Jeffrey H. Collins, Thomas M. Reeder, and Herbert J. Shaw, "Design of Surface Wave Delay Lines with Interdigital Transducers", IEEE Transactions on Microwave Theory and Techniques, MTT-17, 865-873 (1969), Table II, p. 869.

5. J. T. Milek and S. J. Welles, "Linear Electrooptic Modulator Materials", Electronic Properties Information Center (EPIC) Report S-14, Hughes Aircraft Company, (1970).

6. Simon Ramo and John R. Whinnery, Fields and Waves in Modern Radio, Second Edition, John Wiley and Sons, Inc. (New York) 1953, p 153 ff;
P. Vandenbulcke and P. E. Lagasse, "Static Field Analysis of Thin Film Electrooptic Light Modulators and Switches", Wave Electronics, 1, 295-308 (1974).

7. Helge Engan, "Excitation of Elastic Surface Waves by Spatial Harmonics of Interdigital Transducers", IEEE Transactions on Electron Devices, ED-16, 1014-1017 (1969).

8. Herwig Kogelnik, "Coupled Wave Theory for Thick Hologram Gratings", Bell System Technical Journal, 48, 2909-2947 (1969).

APPENDIX

PUBLISHED PAPERS AND TECHNICAL PRESENTATIONS ARISING FROM THIS PROGRAM

APPENDIX

PUBLISHED PAPERS AND TECHNICAL PRESENTATIONS ARISING FROM THIS PROGRAM

CONTENTS

APPENDIX 1

AN INTEGRATED OPTICAL SPATIAL FILTER

AN INTEGRATED OPTICAL SPATIAL FILTER*

C.M. VERBER, R.P. KENAN and J.R. BUSCH
Battelle Columbus Laboratories, Columbus, Ohio, USA

Received 28 December 1979
Revised manuscript received 19 February 1980

The demonstration of a static integrated optical spatial digital filter based upon the Bragg effect is reported and a design for a programmable filter is suggested.

The possibility of making an integrated optical correlator was first suggested by Schubert and Harris [1] in 1968. In its simplest form, a correlator consists of two spatial light modulators (SLM), traversed by an optical beam, together with some means of translating the signal modulating ones of the SLM's traversely to the beam. The amount of light passing both modulators, integrated over the beam width, then varies with the position of the translating signal according to the correlation of the two modulating signals. We call the SLM with the spatially translating modulation signal the "signal" modulator, and the other SLM, which serves to analyze (or filter) the output of the first SLM the "filter" modulator or simply the "filter". All of the components needed to construct a correlator are available in present-day integrated optics technology with the exception of a conveniently programmable filter modulator. In particular, surface acoustic wave (SAW) transducers are available that have sufficient bandwidth and efficiency to serve as a signal modulator; the translation of the input signal is then accomplished by the propagation of the SAW. We report here on the first step towards realization of a programmable binary (i.e., two-state) filter, the fabrication and testing of a static filter, and present suggestions for the design of a programmable filter.

The static binary filter consists of a segmented surface grating [2] operating in the Bragg regime. A broad beam of light incident upon the grating at the Bragg angle is deflected by $2\theta_B$ in the segments in which the grating exists (binary "ones") and is undeflected in the region where the grating is absent (binary "zeros"). The incident beam is thus diffracted into two beams separated by the angle $2\theta_B$. Each beam is amplitude modulated: the diffracted beam according to the pattern of ones and zeros in the segmented grating, at 100% modulation; and the transmitted beam according to the ones complement of this pattern and generally with less than 100% modulation (if the grating segments are less than 100% efficient). The operation of the filter modulator has been investigated in conjunction with a signal grating which is produced by a surface acoustic wave (SAW) transducer driven by a digitally-modulated r.f. signal, thus forming a correlator. The gratings are designed such that the presence of a "one" in both the signal and reference plane results in the deflection of one bit's worth of light into the detector. Any other combination will result in no light at the detector. The correlation signal appears at the detector as the digital SAW pattern moves past the stationary filter pattern.

As shown in fig. 1, the filter is composed of a permanent photoresist surface grating on a Ti-infused $LiNbO_3$ waveguide. It is formed by first exposing the resist to the interference pattern formed by two 4880 Å laser beams and then further exposing the resist through a bit mask before development. The signal is a pulse modulated 270 MHz surface acoustic wave. The pulse duration of 114 ns is chosen to match the

* Work supported by the Air Force Office of Scientific Research.

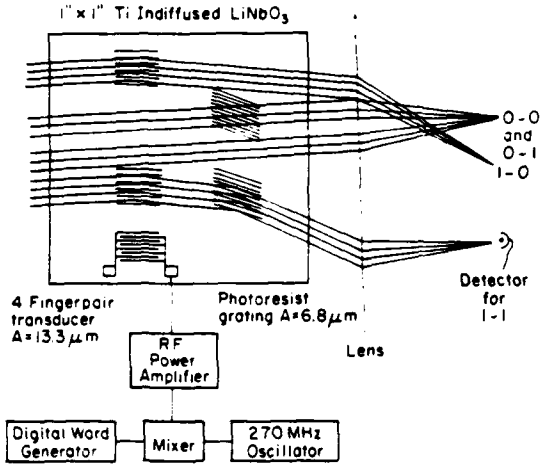

Fig. 1. Schematic of the digital filter showing the correlation of the signal word 1001 with the filter word 0101. The angle between the grating vectors of the SAW and photoresist gratings is equal to the sum of the two Bragg angles. The sound pulses emanating from the SAW transducer are traveling away from the transducers at the sound velocity. Only the one-one coincidence results in light at the detector.

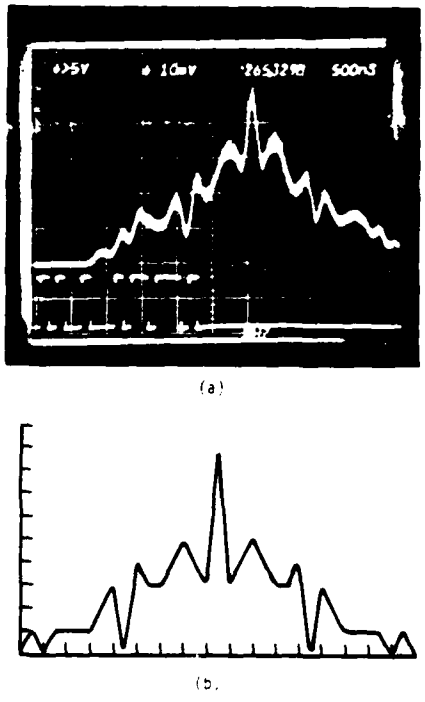

Fig. 2. (a) Observed and (b) computed autocorrelation of the digital word 1000100101101101. The digital word is also shown on the oscilloscope trace. The discrepancy on the leading edge of the correlation is due to a small filter segment with low diffraction efficiency.

400 μm segment length of the permanent filter. In fig. 2 the autocorrelation response of the filter to the 17-bit word 1000100101101101 is shown as well as the expected autocorrelation signal. As can be seen the device behaves as anticipated.

To generate the pattern shown in fig. 2, a 400 μm segment length was used. This requires a 6.8 mm-wide light beam to illuminate a 17-bit word. To increase the word length without increasing the beam width requires a decrease in segment length. Without modifying our present equipment, we have shown that 200 μm segment lengths can be used with no decrease in efficiency. Problems in maintaining a square r.f. pulse prevented us from attaining our goal of 100 μm segment lengths.

In the present experiment the filter and the signal grating periods were $\Lambda_f = 6.8$ μm and $\Lambda_s = 13.3$ μm, respectively. Two different grating periods were used so that only doubly-diffracted light would enter the detector. This results in good signal discrimination even if the gratings do not have very high diffraction efficiency. However, this type of correlator has a serious flaw. If the signal and filter patterns are identical, the output is maximum, as desired. But, adding additional "1"s (i.e., additional grating segments) to the signal grating will not decrease the correlation maximum. This situation arises because "0"s are, in essence, ignored in forming the correlation, that is, no weight is given to correct occurrence of a "0" in each grating. There are a number of ways to correct this problem, all of which involve some sacrifice of signal discrimination unless high (near unity) diffraction efficiencies are achieved. The simplest solution is to redefine the coding for the second grating so that a "1" corresponds to the *absence* of a grating segment and a "0" corresponds to the presence of a grating segment. Then, the singly-diffracted beams are detected. This corresponds to using the ones-complement code for the second grating. If the gratings have the same period, then singly-diffracted (0–0 and 1–1 coincidences) light passes in one direction, while undiffracted and doubly-diffracted light passes in a direction $2\theta_B$ away.

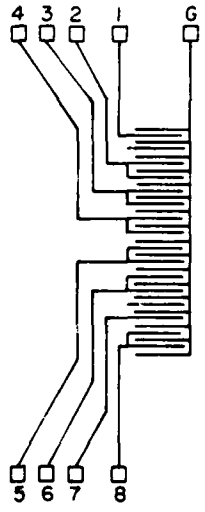

Fig. 3. Programmable 8-bit electrooptic Bragg filter. Electrode and fan-out patterns are shown. Drawing is not to scale.

Now excess "1"s in the signal do cause a decrease in correlation signal. Furthermore, if both beams are detected, they can be subtracted to effect a penalty for 0–1 and 1–0 coincidences. The loss in signal discrimination mentioned above occurs when the diffracted efficiencies of the gratings segments are low enough to allow significant zero-order energy to be transmitted through a grating segment that should be diffracting all of the light incident upon it into the first-order direction.

Having demonstrated that the digital integrated optical filter is a realizable device, it is reasonable to consider how a programmable filter could be constructed. One of the criteria for the programmable device is that it should operate on voltages low-enough to be compatible with semiconductor logic. This can be achieved in the manner of the large-angle optical waveguide switch first implemented by Verber et al. [3] and reported on in a later version by Kotani et al. [4]. These devices use the small deflection of a low-voltage electrooptic deflector to bring a light beam into Bragg incidence on a fixed phase grating. The fixed grating then imparts the required larger angular change. A programmable filter using this effect could consist of a row of N-shaped electrooptic deflectors [5] followed by a single permanent grating which extends across the entire width of the beam. Energizing a single deflector would bring a segment of the light beam into Bragg incidence upon the fixed grating which would then impart the required larger deflection. The set of "one" beams and the set of "zero" beams thus generated could then be used in the type of correlator already discussed. Alternatively, a larger Bragg angle could be used to further separate the two sets of beams and the "one" beams could be used as the input to a Fourier transform correlator of the type suggested in ref. [1].

An alternative approach to the implementation of a programmable spatial filter is to use a series of individually controlled electrooptic gratings [6] as shown in fig. 3. This approach is superior to the use of N-shaped deflectors in that a fixed grating is not required to achieve suitably large deflections. In addition, optical losses due to fringing effects are expected to be smaller in this case than for the N-shaped deflectors. In the design shown in fig. 3, one of the gratings is an acoustooptic one, as in the present experiments, while the other is the segmented electrooptic grating that can be addressed electrically for programming. The electrooptic grating is designed to have the same period as the acoustic grating so that the ones-complement coding can be used for one of the gratings as discussed above. A simple version of this design is presently being fabricated for preliminary testing.

References

[1] R. Shubert and J.H. Harris, IELE Trans. Microwave Theo. and Tech. MTT-16 (1968) 1048.
[2] W.W. Ng, C.-S. Hong and A. Yariv, IEEE Trans. Elec. Devices, ED-25 (1978) 1193.
[3] C.M. Verber, Van E. Wood, R.P. Kenan and N.F. Hartman, Ferroelectrics 10 (1976) 253.
[4] H. Kotani, S. Namba and M. Kawabe, IEEE J. Quant Elec. QE-15 (1979) 270.
[5] I.P. Kaminow and L.W. Stulz, IEEE J. Quant. Elec. QE-11 (1975) 633.
[6] J.M. Hammer, D.J. Channin and M.T. Duffy, Appl. Phys. Lett. 23 (1973) 176.

AD-A121 681 OPTICAL WAVEGUIDE SPATIAL FILTERS(U) BATTELLE COLUMBUS LABS OH C M VERBER ET AL. 30 JUN 82 AFOSR-TR-82-1000 F49620-79-C-0044

UNCLASSIFIED F/G 20/6 NL

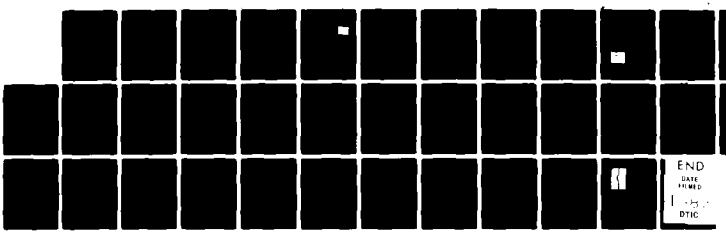

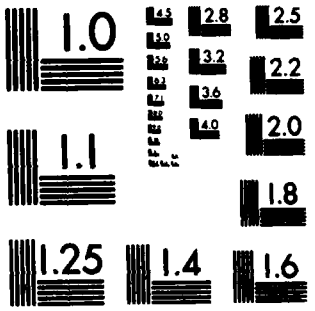

MICROCOPY RESOLUTION TEST CHART
NATIONAL BUREAU OF STANDARDS-1963-A

APPENDIX 2

CORRELATOR BASED ON AN INTEGRATED OPTICAL SPATIAL LIGHT MODULATOR

Correlator based on an integrated optical spatial light modulator

C. M. Verber, R. P. Kenan, and J. R. Busch

The fabrication and characterization of a 17.5-M bit/sec integrated optical correlator are described. The correlator makes use of a novel programmable electrooptic spatial light modulator in conjunction with a digitally modulated surface acoustic wave.

Introduction

A programmable integrated optical spatial light modulator (IOSLM) with sufficiently high performance characteristics would have the potential for forming the basis of a variety of integrated optical circuits for signal and data processing. For true utility the IOSLM should not only be easily and rapidly programmable, but should have high spatial resolution and should be capable of analog or binary operation. We report here the characteristics of an electrooptic IOSLM which demonstrates most of these desirable characteristics. The device consists of a number of adjacent but individually addressable interdigital electrode sets which, via the Bragg effect, deflect discrete portions of an incident guided wave proportionally to the voltages applied to the separate grating segments. The design and fabrication of a 32-segment IOSLM is described as well as its use in a 32-bit digital correlator.

There are, of course, a number of monolithic approaches to implementing the correlation operation, and it should be pointed out that the correlator is used here mainly as an example of the use of the IOSLM. The IOSLM-based correlator does, however, exhibit several interesting features. For example, it differs from the two-SAW space integrating correlator suggested by Tsai[1] in that a given reference function need be entered only once and does not have to be refreshed periodically. There is therefore no dead time except that required to shift in a new reference function. There is, of course, a sacrifice in analog bandwidth due to the finite size of the IOSLM windows.

The authors are with Battelle Columbus Laboratories, Columbus, Ohio 43201.

Received 6 November 1980.
0003-6935/81/091626-04$00.50/0.

© 1981 Optical Society of America.

In the sense that the present device is programmable, it should perhaps be compared to the acoustoelectric storage correlators discussed by Kino[2] and Ingebrigtsen.[3] The IOSLM-based correlator currently has a more limited bandwidth than the acoustoelectric devices. However it is capable of improvement in this regard, and has the advantage of ease of fabrication, requiring only a single photolithographic step.

Basic Grating Configuration

The IOSLM consists of an array of interdigital electrode sets fabricated on a thin buffer layer on the surface of a planar electrooptic waveguide as shown schematically in Fig. 1. The buffer layer serves to isolate the electrodes from the waveguide so that the guided wave is affected only by the applied electric fields and not by the presence of the metallization pattern. The tangential component of the electric field in the waveguide is the only field effective in altering the refractive index for the arrangement shown: TE-mode light propagating in the x direction in a Y-cut crystal of $LiNbO_3$. An expression describing this field has been derived by Engan.[4] The fundamental component is given by

$$E_z = (0.847)\left(\frac{V_0}{g}\right)\cos\frac{\pi z}{2g}, \tag{1}$$

where g is the electrode gap width, and z is the distance from the gap center. In the Bragg regime only this component is effective. In the electrooptic waveguide this field results in an index-of-refraction modulation

$$\Delta n = -\tfrac{1}{2} n_{\text{eff}}^3 r E. \tag{2}$$

The index of refraction n_{eff} is the effective index of guided mode, and r is the appropriate electrooptic coefficient. Since the electric field and the index modulation fall exponentially, it is desirable to use a waveguide which confines the light closely to the

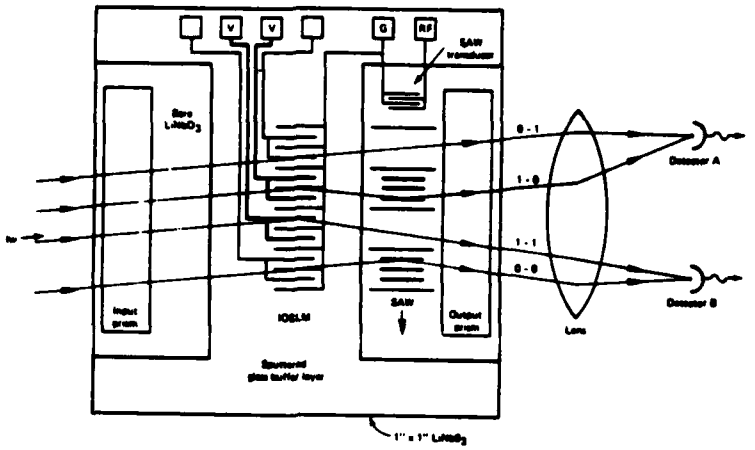

Fig. 1. Schematic drawing of an integrated optical correlator based on the programmable IOSLM. The IOSLM is the array in the center of the drawing. The notations (0–1, 1–0, etc.) on the output beams indicate the state of the IOSLM and SAW segments, respectively, that are encountered by the respective beams.

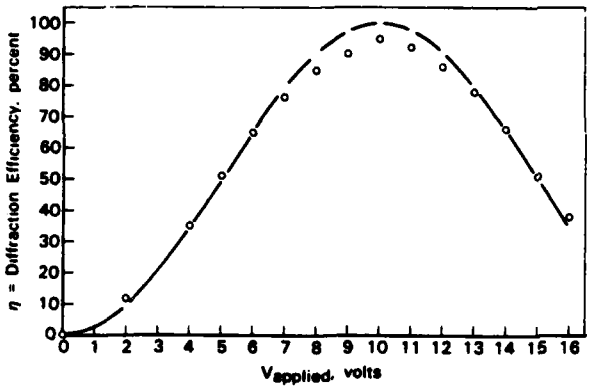

Fig. 2. Measured diffraction efficiency of the IOSLM grating array as a function of the applied voltage. Experimental data are indicated by the circles, and the solid curve is a fit to the form of Eq. (4).

waveguide surface. On a $LiNbO_3$ substrate, a Ti-infused guide is therefore perferable to an out-diffused guide.

If we ignore the falloff of the field in the y direction, we can treat the periodic index variation as a simple thick Bragg grating, the Bragg angle θ_B being given by

$$\sin\theta_B = \lambda_0/2n_{\text{eff}}\Lambda \tag{3}$$

and the diffraction efficiency by[5]

$$\eta = \sin^2 \frac{\pi \Delta n d}{\lambda_0 \cos\theta_B}, \tag{4}$$

where Λ is the wavelength of the electrooptic grating, and λ_0 is the vacuum wavelength of the light.

The electrooptic gratings used in this work have a wavelength $\Lambda = 13.33\ \mu$m and a corresponding Bragg angle of 0.62° for 0.633-μm He–Ne laser light in the $LiNbO_3$ waveguide. The depth d of the gratings is 2.86 mm. They are defined by standard photolithographic procedures on a 1500-Å thick buffer layer of Corning 7059 glass, which is sputtered onto the surface of a Ti-infused $LiNbO_3$ waveguide, which is then annealed at 650°C for 15 min in flowing argon. In Fig. 2 we show the diffraction efficiency of such a grating as a function of applied field. The maximum efficiency is seen to be 95%.

The maximum diffraction efficiency occurs at an applied voltage of 10 V. This value is close to the value of 9 V observed by Hammer and Phillips[6] in a $LiNb_xTa_{1-x}O_3$ waveguide with properties similar to ours, using a similar electrode structure and geometry. The fact that the efficiency does not reach 100% can be attributed to the failure to reach the Bragg regime fully. The geometric factor here is

$$Q = \frac{2\pi\lambda_0 d}{n_{\text{eff}}\Lambda^2} = 29. \tag{5}$$

Usually values of $Q > 8$ indicate operation in the Bragg regime. However, a ray impinging on the grating at the Bragg angle of 0.62° actually traverses only 2 or 3 periods of the grating, so we are not fully in a multiple-scattering regime. In fact, weak Raman-Nath peaks are observed, in support of the argument given here.

The IOSLM consists of N identical units, such as those pictured in Fig. 1, having a common ground electrode and separately addressable interdigitated electrodes. The structure divides a single broad beam incident at the Bragg angle into two angularly separated beams with complementary transverse amplitude modulation. Although there are a variety of applications for this structure, we will limit our discussion to its use in an integrated optical digital correlator. We have previously discussed[7] the use of a nonprogrammable grating structure for use in the same type of correlator.

Digital Correlator

The correlator based on the IOSLM is shown schematically in Fig. 1. Light is incident from the left upon the electrooptic structure and those segments of the incident beam which encounter a one (i.e., an energized grating) are deflected through $2\theta_B$. The deflected beam therefore consists of a series of bright bands (ones) and dark bands (zeros). This beam, which is now encoded with the filter word, is incident upon a surface acoustic wave interaction region, again at the Bragg angle which in the present experiment is the same for both the SAW and the IOSLM. Propagating through the interaction region is a SAW which is amplitude modulated with a binary data pattern. Beam segments which encounter either no gratings or two gratings exit the SAW region in the original input direction, while beams which encounter only one of the gratings are deflected by $2\theta_B$. Since any part of the original beam which is undeflected due to gratings of less than perfect diffraction efficiencies will enter detector A, it is preferable for the sake of noise reduction to take the correlation output at detector B. In this case, a ones-complement encoding is used for SAW. That is, if the presence of an active grating represents a one in the IOSLM, then the absence of the SAW in a given region is taken to represent a one.

The correlator was fabricated on a Ti-infused waveguide on a $LiNbO_3$ substrate. Each bit in the IOSLM consists of 15 finger pairs with a period of 13.33 μm so that each bit is represented by a 200-μm wide window. The SAW is generated by a 4-finger-pair transducer with the same period and finger length as in the IOSLM. The SAW frequency is 263 MHz, corresponding to the center frequency of the transducer, and the bit duration is 57 nsec, so at a SAW velocity of 3.5×10^5 cm/sec the lengths of the SAW bits and IOSLM windows are matched. The data rate for the present version of the correlator is 17.5 Mbit/sec. This data rate could easily by increased several fold, but the speed of the device will ultimately be limited either by the SAW bandwidth or by the necessity to exceed some minimum window dimension in the IOSLM. The limiting data rate is not yet known.

The correlator was exercised using the arrangement shown in Fig. 3. A preselected filter word was loaded into the IOSLM from the HP word generator via a data register which performs a 32-bit serial-to-parallel conversion. After loading the filter word, the word generator was then used to generate the 17.5-M bit/sec modulation signal for the SAW. The autocorrelation signal at detector B for the 32-bit word is shown in Fig. 4 along with the calculated autocorrelation.

Improved Correlator Design

The main sources of error in the correlator design discussed above are imperfect diffraction in both the SAW and the electrooptic grating and the presence of a background of diffracted light from the electrooptic grating even in the absence of a SAW signal. The latter source of error is the most serious and is responsible for the asymmetry in the autocorrelation shown in Fig. 4.

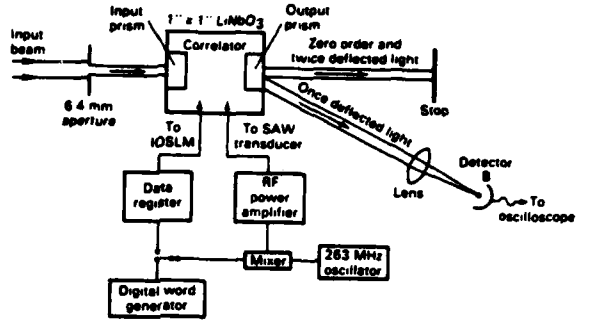

Fig. 3. Schematic drawing of the experimental arrangement used for testing the correlator.

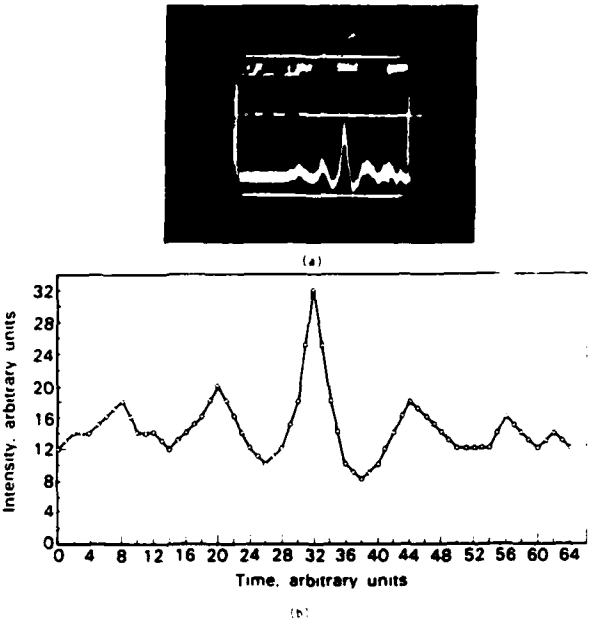

Fig. 4. Autocorrelation profile for the 32-bit word 11001111000011111100000011111111 (a) as generated by the correlator, and (b) as calculated. Note the asymmetry in both curves, produced by the presence of a signal from the IOSLM in the absence of a SAW signal. The digital word used is indicated by the top trace in (a) photograph.

We discuss here an improved design that eliminates the background diffraction and reduces the impact of <100% diffraction efficiency in the SAW. This design resulted from attempting to satisfy two major criteria:

(1) The output signal should be zero when the SAW and the E-O gratings do not overlap.

(2) The output directions should be well separated angularly from the incident direction and from any spurious diffraction-like Raman-Nath regime diffracted beams.

The first requirement implies that the E-O (stationary) grating must be ineffective when illuminated by the incident light beam with no SAW present. It also implies that we cannot use the absence of a SAW segment in the coding scheme, since then the E-O grating

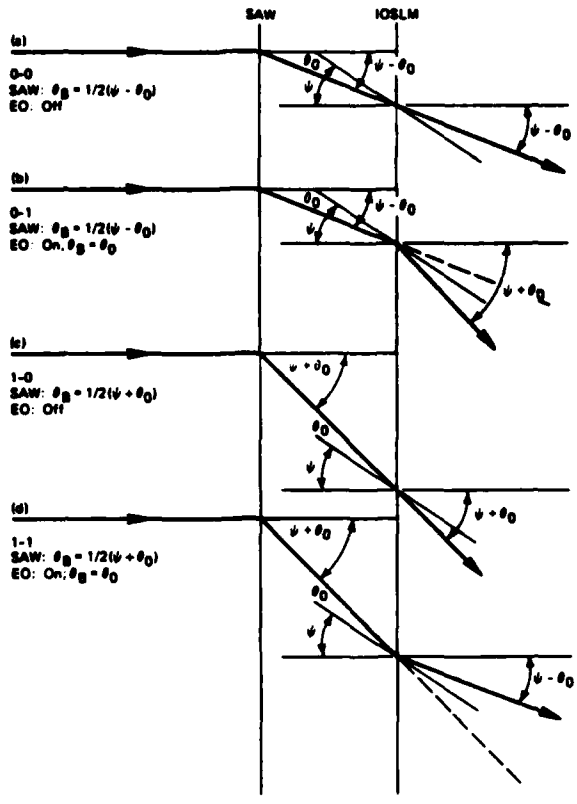

Fig. 5. Drawing to show the geometrical relationships for the improved correlator design. The IOSLM grating fingers are now tilted by the angle ψ. The left vertical line represents the SAW and the right one represents the IOSLM. The frequencies are now refined for the SAW.

would have to respond directly to the incident beam. The second requirement implies that the E-O grating segments must be slanted relative to the direction of the input light to avoid Raman-Nath beams in the output.

Since we cannot encode a zero in the SAW stream by the absence of a grating, we will need to interleave two SAW streams, one for zero bits, with period Λ_0, and one for one bits, with period Λ_1. Since it is inconvenient to use two electrooptic periods, we will continue to encode a zero using an off (no voltage applied) segment, and a one using an on segment. Denote the slant of the electrooptic grating fingers by ψ, as in Fig. 5, and define

$$\theta_0 = \sin^{-1}(\lambda_0/2\, n_{\text{eff}}\Lambda). \tag{6}$$

θ_0 is the Bragg angle for the electrooptic segments, measured relative to the electrode fingers. Because zero is encoded by the absence of an electrooptic grating (no applied voltage), it is necessary for an on segment, i.e., a one, to respond to both SAW codes. We accomplish this by arranging the gratings so that light diffracted from the SAW impinges on the electrooptic grating segments at either of two complementary Bragg angles. The four possible situations are illustrated in Fig. 5(a)–(d). In (a) and (b) the SAW code is a zero, while in (c) and (d) the SAW code is a one. The required angular relations and the corresponding state of the electrooptic grating segments are summarized in Fig. 5. Note that the light that encounters a 0–0 or 1–1 situation emerges in a single direction, θ'; similarly, 0–1 and 1–0 situations send light in another single direction. If ψ is carefully chosen, stray light from the incident beam will not contaminate either of the output beams.

Implementation of this improved correlator design is planned for the near future.

The authors thank R. Ridgway for designing and building the data register used in this work, which was supported by the Air Force Office of Scientific Research.

References

1. C. S. Tsai, IEEE Trans. Circuits Sys. CAS-26, 1072 (1979).
2. G. S. Kino, Proc. IEEE 64, 724 (1976).
3. K. A. Ingebrigtsen, Proc. IEEE 64, 764 (1976).
4. H. Engan, IEEE Trans. Electron Devices ED-16, 1014 (1969).
5. H. Kogelnik, Bell Syst. Tech. J. 48, 2909 (1969).
6. J. M. Hammer and W. Phillips, Appl. Phys. Lett. 24, 545 (1974).
7. C. M. Verber, R. P. Kenan, and J. R. Busch, Opt. Commun. 34, 32 (1980).

APPENDIX 3

PASSIVE AND ACTIVE INTEGRATED OPTICAL SPATIAL FILTER

Proceedings SPIE, Guided-Wave Optical and Surface Acoustic Wave Devices, Systems and Applications, 239, 128 (1980).

Passive and active integrated optical spatial filter*

C. M. Verber, R. P. Kenan and J. R. Busch

Battelle, Columbus Laboratories
505 King Avenue, Columbus, Ohio 43201

Abstract

A programmable spatial filter which could be used to impose an arbitrary intensity pattern on a guided optical wave would be generally useful in a number of integrated optical devices. As a first step in the development of such a filter, a static filter consisting of a segmented photoresist Bragg grating on a $LiNbO_3$:Ti waveguide has been fabricated. The static grating was tested by performing correlations using a modulated SAW. Plans for a 32-channel programmable filter using electrooptically induced Bragg grating are discussed.

Introduction

The possibility of making an integrated optical correlator was first suggested by Schubert and Harris[1] in 1968. In its simplest form, a correlator consists of two spatial light modulators (SLM), traversed by an optical beam, together with some means of translating the signal modulating one of the SLM's traversely to the beam. The amount of light passing both modulators, integrated over the beam width, then varies with the position of the translating signal according to the correlation of the two modulating signals. We call the SLM with the spatially translating modulation signal the "signal" modulator, and the other SLM, which serves to analyze (or filter) the output of the first SLM the "filter" modulator or simply the "filter". All of the components needed to construct a correlator are available in present-day integrated optics technology with the exception of a conveniently programmable filter modulator. In particular, surface acoustic wave (SAW) transducers are available that have sufficient bandwidth and efficiency to serve as a signal modulator; the translation of the input signal is then accomplished by the propagation of the SAW. We report here on the realization of a static binary filter[2] and the progress toward the fabrication of a 32 bit programmable filter.

The Static Filter

We have fabricated a 17-bit static filter which consists of a segmented surface grating[3] operating in the Bragg regime. A broad beam of light incident upon the grating at the Bragg angle is deflected by $2\theta_B$ in the segments in which the grating exists (binary "ones") and is undeflected in the region where the grating is absent (binary "zeros"). The incident beam is thus diffracted into two beam separated by the angle $2\theta_B$. Each beam is amplitude modulated: the diffracted beam according to the pattern of ones and zeros in the segmented grating, at 100% modulation; and the transmitted beam according to the ones complement of this pattern and generally with less than 100% modulation (if the grating segments are less than 100% efficient). The operation of the static filter modulator has been investigated in conjunction with a signal grating which is produced by a surface acoustic wave (SAW) transducer driven by a digitally-modulated r.f. signal, thus forming a correlator. The gratings are designed such that the presence of a "one" in both the signal and reference plane results in the deflection of one bit's worth of light into the detector. Any other combination will result in no light at the detector. The correlation signal appears at the detector as the digital SAW pattern moves past the stationary filter pattern.

As shown in Figure 1, the filter is composed of a permanent photoresist surface grating on a Ti-infused $LiNbO_3$ waveguide. It is formed by first exposing the resist to the interference pattern formed by two 4880 Å laser beams and then further exposing the resist through a bit mask before development. The signal is a pulse modulated 270 MHz surface acoustic wave. The pulse duration of 114 nsec is chosen to match the 400 μm segment length of the permanent filter. In Figure 2 the autocorrelation response of the filter to the 17-bit word 10001001011101101 is shown as well as the expected autocorrelation signal. As can be seen the device behaves as anticipated.

Alternative Configurations

The filter and signal grating periods used in the static filter were $\Lambda_f = 6.8$ μm and $\Lambda_s = 13.3$ μm, respectively. The gratings are oriented so that only doubly diffracted light enters the detector, i.e., the detector sees only 1-1 light. There is a serious problem with this kind of correlator, namely, the generation of false correlations. Careful examination of the expected signal from the device as tested shows that it does produce a maximum signal when the filter and signal codes are dientical and aligned. Unfortunately, an arbitrary signal consisting of the filter code plus ones in any position will generate the same, maximum, signal. This difficulty is caused by the neglect of 0-0 alignments, that is, the output signal is generated by coincidences of "1"s in both the filter and the signal codes, and by these coincidences alone. What is needed is a configuration that also takes 0-0 coincidences into account.

The 0-0 coincidences can be taken into account by using grating segments for filter and signal that have the same period. This is pictured in Figure 3(a), where ray paths for the four kinds of coincidences are indicated. It is seen that now 0-0 and 1-1 light is passed into one direction, while 0-1 and 1-0 light is passed into a different direction. The penalty paid for this separation is that imperfect gratings will cause some mixing of the two outputs. This mixing is illustrated schematically in Figure 3(b). It is seen that the presence of a grating segment in the signal code will introduce an error whenever the segment has less than unit diffraction efficiency, and that other errors are introduced if the filter segments have less than unit efficiency. These error terms appear to be unavoidable if the simple "on-off" type of codes (presence or absence of a grating segment) are used.

One further modification of the design should also be mentioned. Because the signal and filter regions are of necessity spatially separated, there will usually be some light that passes directly through the correlator at the segment boundaries, where the diffraction efficiency is lower, even if the diffraction efficiency in the center of a segment is unity. It is therefore desirable to detect the deflected light (the 0-1 and 1-0 beams). This beam is a perfectly acceptable correlation signal; its use requires merely that we reinterpret the filter coding as the ones complement of the desired filter code. This means that a "1" is now signified in the filter as the absence of a grating segment and a "0" by the presence of a grating segment.

Programmable Filters

The programmable filter is based upon the use of a segmented electrooptic Bragg deflector[4] in which a thick phase grating is formed under a set of interdigital electrodes whose geometry is similar to that of a SAW transducer. The grating exists by virtue of the electrooptic effect in the waveguide material and is therefore present only when the electrodes are energized. A schematic illustration of an 8-bit programmable electrooptic grating is shown in Figure 4.

In order to fabricate this type of filter on a $LiNbO_3$ waveguide, it is necessary to first deposit a dielectric buffer layer so that the guided wave is not affected by the metallized grating pattern. Preliminary tests were conducted using a simple four-finger-pair interdigital transducer with $\Lambda = 13.3$ μm to demonstrate the utility of such an electrooptic Bragg deflector. A 1500 Å layer of Corning 7059 glass was deposited onto a 1" x 1" $LiNbO_3$ waveguide by a r.f. sputtering technique. The sample was then annealed at 650°C for about 15 minutes in an argon atmosphere. The transducer was fabricated on the surface of the glass buffer layer by standard photolithographic techniques. The effective isolation of the guided wave from the interdigital SAW transducer by the dielectric layer was demonstrated by the absence of diffraction from the unenergized metallized grating pattern. As expected the intensity of the diffracted light was proportional to $\sin^2 V$, V being the applied voltage. The maximum diffraction occurred at odd multiples of 9 volts.

Masks for a 32-bit programmable filter are being fabricated by Ahmed Naumaan of the University of Cincinnati, Electrical Engineering Department, by the photoreduction of machine-cut Rubylith. The mask contains the pattern for both the 32-bit filter and a SAW transducer. Since each bit consists of 15 finger pairs, there are a total of 960 lines 3.33 μm wide by 3 mm long in the electrooptic filter. The SAW transducer, which has the same period and width is offset by 5 mm from the E-O array. The total area over which high resolution is must be maintained is therefore 8 mm wide by about 8.4 mm long, the latter dimension being determined by the separation between the two SAW transducers. Maintaining high resolution on this area has proved to be quite challenging, and no usable masks have yet been produced. Experimental results for the programmable filter are therefore not available at this time.

References

*Work supported by Air Force Office of Scientific Research, Contract No. F49620-79-C-0044.

1. Shubert, R. and Harris, J. H., IEEE Trans. Microwave Theo. and Tech., MIT-16, 1048-54 (1968).
2. Verber, C. M., Kenan, R. P., and Busch, J. R., Optics Comm. (1980) to be published.
3. Ng, Willie W., Hong, Chi-Sain, and Yariv, A., IEEE Trans. Elec. Devices, ED-25, 1193-2000 (1978).
4. Hammer, J. M., Channin, D. J., and Duffy, M. A., Appl. Phys. Lett., 23, 196 (1973).

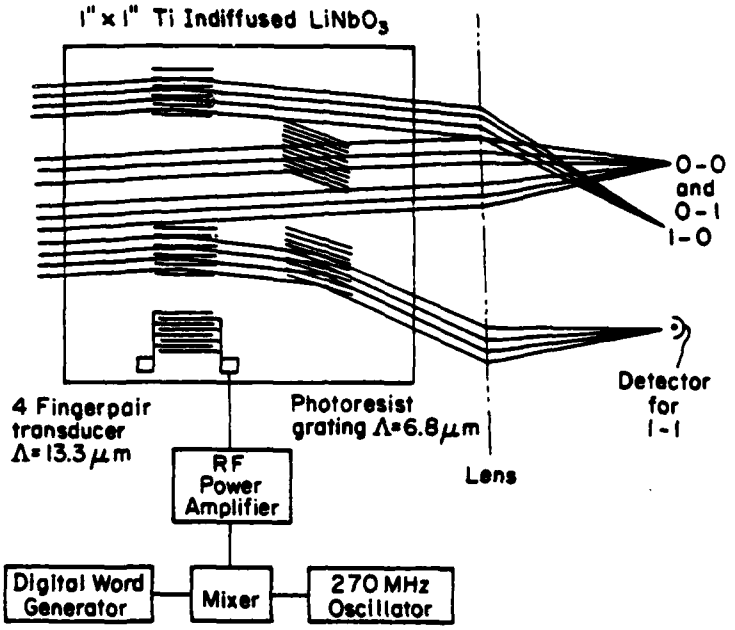

Figure 1. Schematic of the digital filter showing the correlation of the signal word 1001 with the filter word 0101. The angle between the grating vectors of the SAW and photoresist gratings is equal to the sum of the two Bragg angles. Only the one-one coincidence results in light at the detector.

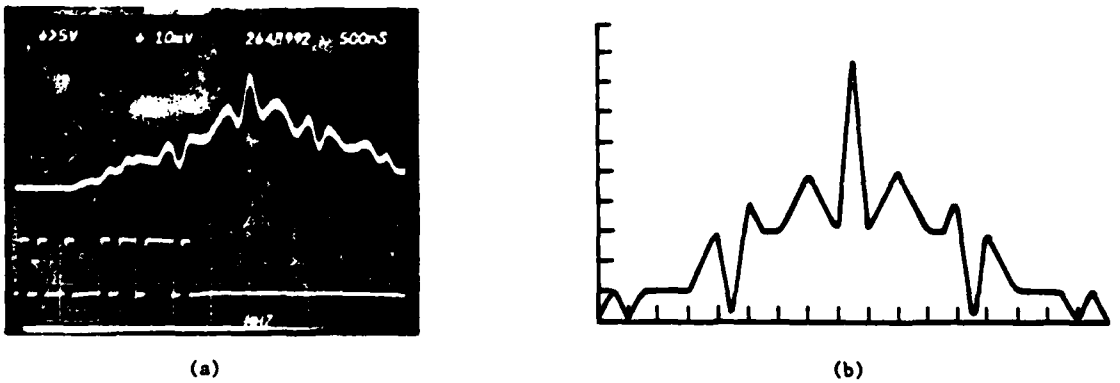

(a) (b)

Figure 2. (a) Observed and (b) computed autocorrelation of the digital word 10001001011101101. The digital word is also shown on the oscilloscope trace.

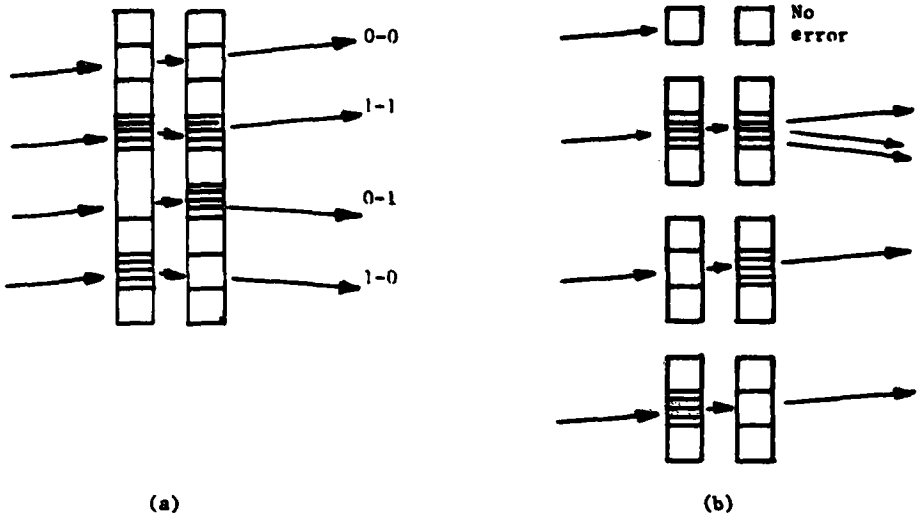

Figure 3. Correlator in which signal and reference "ones" are represented by identical gratings. The ideal response (a) separates the guided optical wave into two beams, one representing correlations (+) the other anticorrelations (+). Errors which occur unless the diffraction efficiencies are unity are shown in (b); only the error beams are indicated. In the 1-1 picture, the upward beam results from partial transmission by both gratings while the two downward beams result from partial transmission by one grating and reflection from the other.

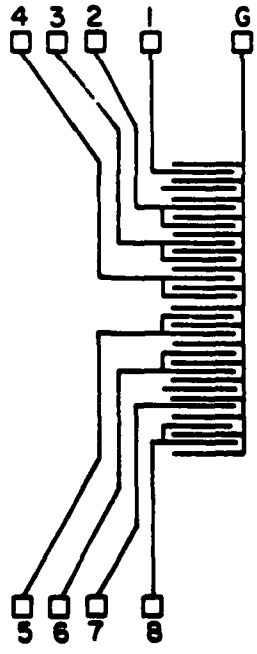

Figure 4. Programmable 8-bit electrooptic Bragg filter. Electrode and fan-out patterns are shown. Drawing is not to scale.

APPENDIX 4

APPLICATION OF ADDRESSABLE ELECTROOPTIC GRATING TO INTEGRATED OPTICAL CIRCUITS

Paper presented at IOOC'81, Third International Conference on Integrated Optics and Optical Fiber Communication, San Francisco, CA, April 27-29, 1981

APPLICATION OF ADDRESSABLE ELECTROOPTIC GRATING TO INTEGRATED OPTICAL CIRCUITS*

C. M. Verber & R. P. Kenan
Battelle Columbus Laboratories
505 King Avenue
Columbus, Ohio 43201

ABSTRACT

An integrated optical spatial light modulator using electrooptic grating arrays is described. It can be used for both analog and digital data. Applications to correlation, voltage comparison, and optical logic are discussed.

APPLICATION OF ADDRESSABLE ELECTROOPTIC GRATING TO INTEGRATED OPTICAL CIRCUITS*

C. M. Verber & R. P. Kenan
Battelle Columbus Laboratories
505 King Avenue
Columbus, Ohio 43201

We have fabricated an integrated optical spatial light modulator (IOSLM) which consists of an electrooptic grating[1] structure addressable in 32 separate segments. It has been successfully used as a component in a 32 bit, 17.5 MBit/sec digital correlator. In this paper we report the operation of the correlator and discuss other uses of the grating structure in forming components for integrated optical circuits. A non-programmable version of the correlator has been reported earlier.[2]

The basic IOSLM structure is shown in Figure 1. A broad optical guided wave which passes under the device is divided into two beams which propagate in directions θ_B and $-\theta_B$, respectively. The beams have complementary transverse amplitude modulations which are determined by the voltages applied to the IOSLM electrodes.

The structure used for the correlator consists of 32 segments each containing 15 finger pairs. The electrooptic grating period is 13.33 μm so each segment is 200 μm wide and $\theta_B = 0.62°$ for 0.628 μm light in a $LiNbO_3$:Ti waveguide. A diffraction efficiency of 95% was achieved at an applied voltage of 9.5 volts when the electrodes were applied over a 1000 Å sputtered-glass buffer layer. Lower voltages are required for thinner glass layers and for no glass at all, maximum diffraction efficiency is reached at 4 volts.

The correlator consists of the IOSLM and a 4 finger-pair SAW transducer of the same period mounted on the same substrate. The SAW is digitally modulated so that the SAW and E-O bit lengths are identical. Various correlator configurations are possible. The first one demonstrated (Fig. 2) uses a ones-complement notation. That is, a one is designated by the presence of an E-O grating or the absence of a

SAW grating. The (0-0) and (1-1) coincidences are then both singly diffracted and proceed in the $-\theta_B$ direction, while the (0-1) and (1-0) anticoincidences both proceed in the $+\theta_B$ direction. Discrimination between the programmed filter word and a series of random words has been demonstrated.

The number of resolution elements in the IOSLM can easily be increased to at least 64. The number will ultimately be limited by the area required for the electrical connections. The size of a resolution element can be reduced to 40 μm without significant loss of diffraction efficiency, so spatial frequencies of up to 12 lp/mm are possible. Since the IOSLM can be used either in a digital or in an analog mode it could be used as an element for introducing either data or filter functions into an integrated optical Fourier-transform processor.

Another application of the electrooptic grating structure is in the implementation of a variety of computational devices. Two of these structures are illustrated in Figure 3 along with the truth tables for the gratings used as logic elements. The voltages A and B can also be analog voltages in which case the diffraction efficiency of the EXOR configuration is easily shown to be proportional to (A - B) as long as the diffraction efficiency is less than 0.1. A large number of such structures can be fabricated in a line in the IOSLM configuration and addressed by a single light beam. In this case the intensity of the diffracted light is proportional to $\vec{A} - \vec{B}$ where $\vec{A}$ and $\vec{B}$ are two N-dimensional vectors whose components are introduced on the left and the right sides of the grating electrodes respectively.

* Research supported by Air Force Office of Scientific Research under Contract No. F49620-79-C-0044

1. J. M. Hammer and W. Phillips, "Low-Loss, Single Mode Optical Waveguide and Efficient High-Speed Modulators of $LiNb_xTa_{1-x}O_3$ on $LiTaO_3$", Appl. Phys. Lett. 24, 545-547 (1974).

2. C. M. Verber, R. P. Kenan and J. R. Busch, "An Integrated-Optical Spatial Filter", Opt. Comm. 34, 32-34 (1980).

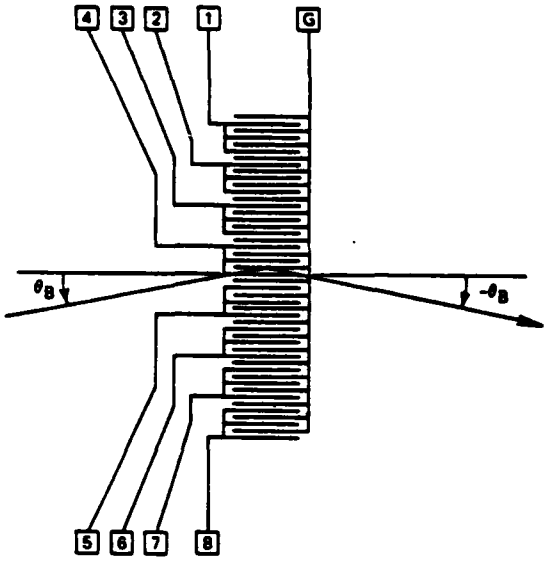

Figure 1

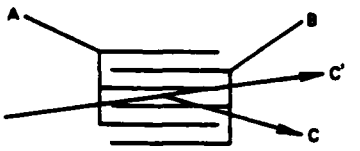

A	B	C	
0	0	0	C is EXOR
1	0	1	
0	1	1	
1	1	0	

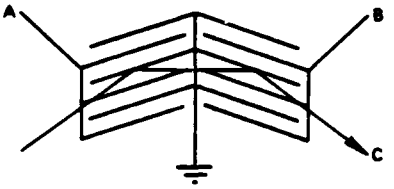

A	B	C	
0	0	0	C is AND
1	0	0	
0	1	0	
1	1	1	

Figure 3

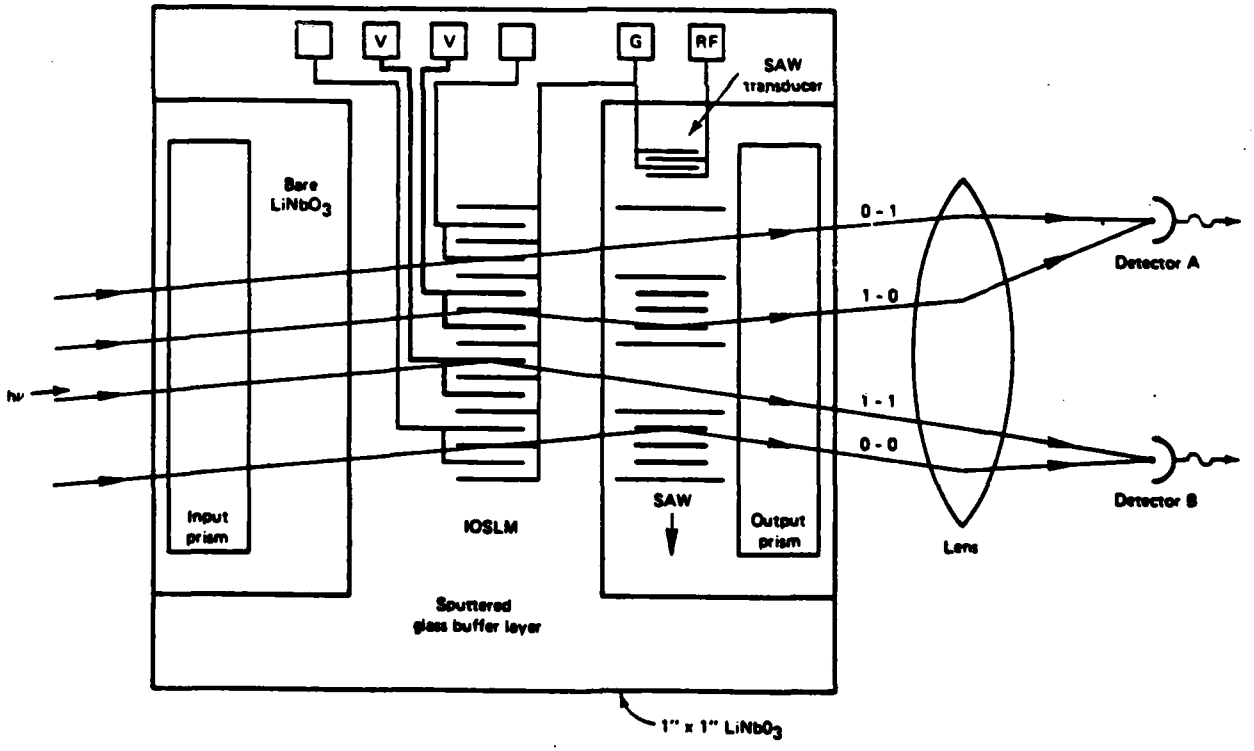

Figure 2

APPENDIX 5

APPLICATIONS OF ELECTRO-OPTIC GRATINGS IN INTEGRATED OPTICAL SIGNAL PROCESSING DEVICES

Paper presented at the Optical Information Processing for Aerospace Applications Conference, Hampton, VA, August 1981.

APPLICATIONS OF ELECTRO-OPTIC GRATINGS IN INTEGRATED OPTICAL SIGNAL PROCESSING DEVICES*

Carl M. Verber
Battelle Columbus Laboratories
505 King Avenue
Columbus, Ohio 43201

SUMMARY

The electro-optic grating is an easily fabricated component which allows a rapid and efficient interaction with an optical wave in a planar electro-optic waveguide. The operation of such gratings and their use as intensity modulators, spatial light modulators, and components in correlators and in a variety of computational units is described.

INTRODUCTION

The electro-optic effect has been the most important interaction mechanism used in the design of the active integrated optical devices employing channel waveguides.[1] In these devices, the designer is able to take advantage of the lateral confinement of the light which allows long interaction lengths and consequently low voltages. In the present paper we will, in contrast, be concerned with the use of the electro-optic effect in planar integrated optical structures. In this planar geometry, the guided light is confined to a several micrometer-thick waveguide at the surface of a suitable electro-optic substrate. Lateral diffraction is not inhibited, but the confinement close to the surface allows the use of moderate voltages to obtain a strong interaction with the guided light. In particular we will show how the interaction of a relatively broad guided beam with an electro-optically induced thick phase (Bragg) grating[2] can be used to advantage in a variety of integrated optical devices. We begin by describing the properties of the gratings and then discuss a number of modulators, correlators and computational units which incorporate these gratings.

THE ELECTRO-OPTIC GRATING

The basic geometry of the I.O. grating electrodes is shown in figure 1. The electrodes are defined by standard photolithographic techniques upon the surface** of a planar electro-optic optical waveguide such as Ti-indiffused[4] $LiNbO_3$. It is conventional to make the electrode line-wide equal the spacing between adjacent fingers, so the required photolighographic resolution is $\Lambda/4$.

* Work supported in part by Air Force Office of Scientific Research.

** Often a sputtered glass buffer layer is employed[3] to isolate the guided wave from perturbation due to the metallization pattern.

The application of a voltage across the electrodes results in a periodic electric field which, via the electro-optic effect, gives rise to a periodic modulation of the index of refraction of the waveguide material and thus to the mode index of the guided wave. The guided wave sees this periodic perturbation as a thick phase grating and will be diffracted as indicated in figure 1 when incident upon the grating at the Bragg angle, defined by

$$\sin\theta_B = \frac{\lambda}{2\Lambda} \tag{1}$$

where λ is the optical wavelength in the medium.

The diffraction efficiency[5] is

$$\eta = \sin^2 \frac{\pi \Delta n d}{\lambda_o \cos\theta_B} \tag{2}$$

where Δn is the amplitude of the periodic index modulation. The magnitude of Δn is determined by the product of the applied field strength E, and the appropriate electro-optic coefficient r_{ij} according to[6]

$$\Delta n = \frac{1}{2} n^3 r_{ij} E \tag{3}$$

where n is the average index of refraction. Inclusion of geometric effects[7] results in an index modulation

$$\Delta n = \frac{1}{2} n^3 r_{ij} \frac{2}{\pi} \left(\frac{V}{\Lambda/4}\right) \tag{4}$$

or a diffraction efficiency of

$$\eta(V) = \sin^2 \left(\frac{4n^3 r_{ij} d}{\lambda_o \cos\theta_B} V\right) \tag{5}$$

Ignoring buffer layer effects, eq. (5) indicates that for $\Lambda = 8$ μm, a He-Ne laser and $d = 2$ mm, we get 100% diffraction efficiency for $V = 3.1$ volts. Since high diffraction efficiencies are readily achieved and the electrode capacitances are quite low, it is evident that the electro-optic Bragg effect can be utilized to make a high performance modulator. This device was originally suggested by Hammer and Phillips,[2] and has more recently been employed by Holman[8] to make a high performance planar modulation with a 69% optical throughput.

THE INTEGRATED OPTICAL SPATIAL LIGHT MODULATOR

The basic grating structure can be extended as shown in figure 2 by introducing electrodes which allow segments of the grating to be individually addressed. In this manner, one can impose a transverse amplitude modulation upon the diffracted beam. The undiffracted beam will of course have a complementary modulation. The grating structure is now operating as an electrically addressable integrated optical spatial light modulator (IOSLM) and can, in principle, be used to modulate an arbitrarily wide guided wave. The modulator can be used in an analog or a binary mode, although there will obviously be a finite number of addressable segments. The largest such IOSLM we

have fabricated thus far[9] is composed of 32 segments 200 μm wide and spans a 6.4 mm-wide guided wave.

It should be possible to reduce the width of each grating segment to 50 μm or less. It would then be possible to use the IOSLM in the signal and filter planes of a planar optical Fourier transform device.[10] However, even with the larger grating segment size, several useful functions can be performed by incorporating a SAW transducer on the same substrate as the IOSLM. If the orientations of the EO and acoustic gratings are chosen so that only doubly diffracted light is detected, then by introducing a single acoustic pulse which is shorter than a single IOSLM element, the transverse modulation produced by the IOSLM is converted to a temporal modulation of the output (doubly diffracted) beam. Parallel-to-serial conversion is thus accomplished. Another application involving the combined IOSLM SAW structure is the correlator, which is shown schematically in figure 3. Such a device has been constructed[9] and operates on a 32 bit word at a data-rate of 17.5 Mbit/sec.

COMPUTATION WITH GRATINGS

Consider once again the simple grating structure shown in figure 1. If voltage V_A is applied to one electrode and voltage V_B to the other, the diffracted light intensity is given by

$$I = I_o \sin^2 [a(V_A - V_B)] \tag{6}$$

where a is a constant. For $I \lesssim 0.1\ I_o$ we have

$$I = I_o\, a^2 (V_A - V_B)^2 \tag{7}$$

Now arrange N such electrode sets in a vertical line so that they can each be addressed by the same broad optical beam. If the N components of the vector $\vec{A}$ are applied to one electrode of each set and the corresponding component of the vector $\vec{B}$ is applied to the opposed electrodes then the total deflected intensity is

$$I = \sum_{i=1} I_i = \sum_{i=1} a^2 (V_{Ai} - V_{Bi})^2 \tag{8}$$

We have therefore calculated the magnitude of the difference of the two vectors.

Vector multiplication can also be performed as is suggested in figure 4. In this structure the diffracted intensity from the i^{th} segment is

$$I_i = I_o\, \eta_{Ai}\, \eta_{Bi} \tag{9}$$

Of course, each η is actually proportional to the square of the voltage difference but it can be shown that by a simple signal processing technique, the desired A_iB_i term can be extracted from I_i. The structure shown in figure 4 is therefore capable of performing the scalar product of two vectors.

It should also be noted that if binary signals are applied to the grating structures then standard logic operations may be performed. The structure used for subtraction can be used to generate the EXCLUSIVE OR operation, or the NOT operation, while the structure used for multiplication can be used for the logical AND. These operations may also be carried out in parallel, and in the case of binary signals, the complications arising from the the $\sin^2$ response are no longer present.

SUMMARY

We have shown a variety of applications of electro-optically induced Bragg gratings in integrated optical signal processing and computation devices. The gratings are easy to fabricate and operate efficiently on relatively low voltages. The design principles are well known and reliable. It is therefore quite likely that a large number of additional devices employing similar grating structures will be developed.

REFERENCES

1. Alferness, R. C.: Guided Wave Devices for Optical Communication. IEEE J. of Quant. Electr., vol. QE-17, no. 6, June 1981, pp. 946-959.

2. Hammer, J. M. and Phillips, W.: Low-Loss Single-Mode Optical Waveguides and Efficient High-Speed Modulators of $LiNb_xTa_{1-x}O_3$ on $LiTaO_3$. Appl. Phys. Lett., vol. 24, no. 11, June 1974, pp. 545-547.

3. Tangonan, G. L., Persechini, D. L., Lotspeich, J. F., and Barnoski, M. K.: Electrooptic Diffraction Modulation in Ti-diffused $LiTaO_3$. Appl. Opt., vol. 17, no. 20, Oct. 1978, pp. 3259-3263.

4. Schmidt, R. V. and Kaminow, I. P.: Metal Diffused Optical Waveguides in $LiNbO_3$. Appl. Phys. Lett., vol. 25, no. 8, Oct. 1974, pp 458-460.

5. Kogelnik, H.: Coupled Wave Theory for Thick Hologram Gratings. Bell Syst. Tech. J., vol. 48, no. 9, Nov. 1969, pp. 2909-2947.

6. Kaminow, I. P.: Introduction to Electrooptic Devices. Academic Press, New York, 1974, 409 pp.

7. Kaminow, I. P. and Stulz, L. W.: A Planar Electrooptic-Prism Switch, IEEE J. of Quant. Electr., vol. QE-11, no. 8, August 1975, pp. 633-635.

8. Holman, R. L. and Cressman, P. J.: A Very High Throughput Damage-Resistant Lithium Niobate Waveguide Modulator. Technical Digest, Topical Meeting on Integrated and Guided-Wave Optics, Incline Village, NV, January 28-30 (1980), paper TuE6.

9. Verber, C. M., Kenan, R. P., and Busch, J. R.: Correlator Based on an Integrated Optical Spatial Light Modulator. Appl. Opt., vol. 20, no. 9, May 1981, pp. 1626-1629.

10. Verber, C. M., Kenan, R. P., and Busch, J. R.: An Integrated Optical Spatial Filter. Opt. Commun., vol. 34, no. 1, July 1980, pp. 32-34.

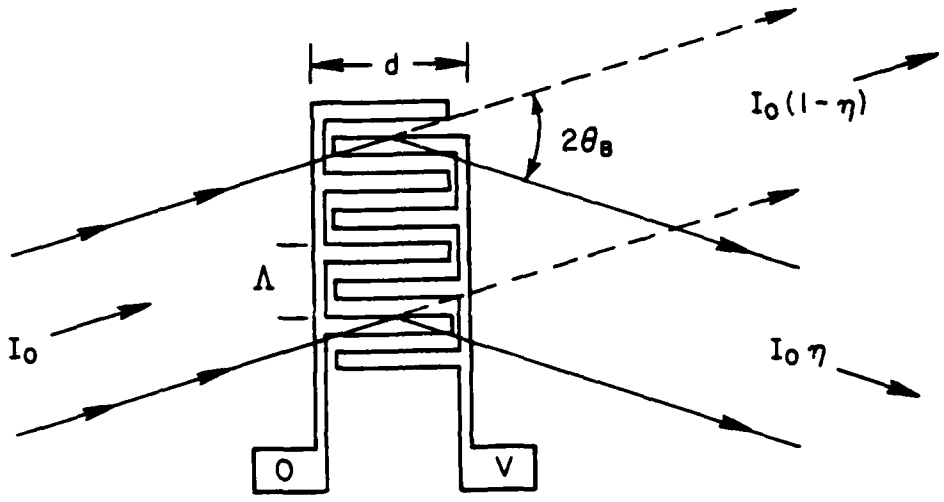

Figure 1.- Basic electrode structure. The grating wavelength Λ and depth d are indicated.

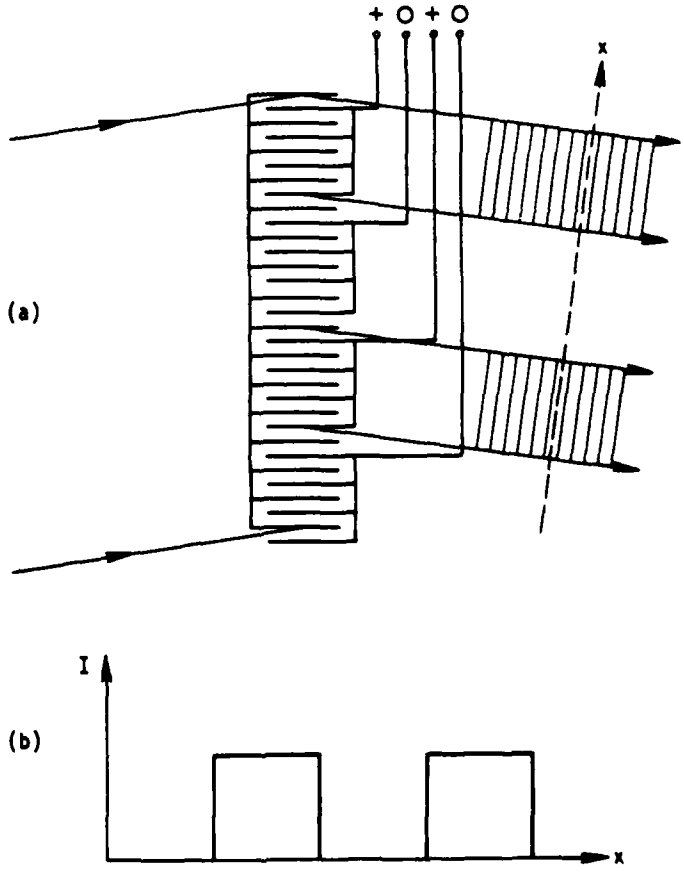

Figure 2.- The electrode structure is addressable in segments to form an integrated optical spatial light modulator. If the common electrode is at zero potential then the voltage pattern indicated in (a) produces the transverse amplitude modulation shown in (b).

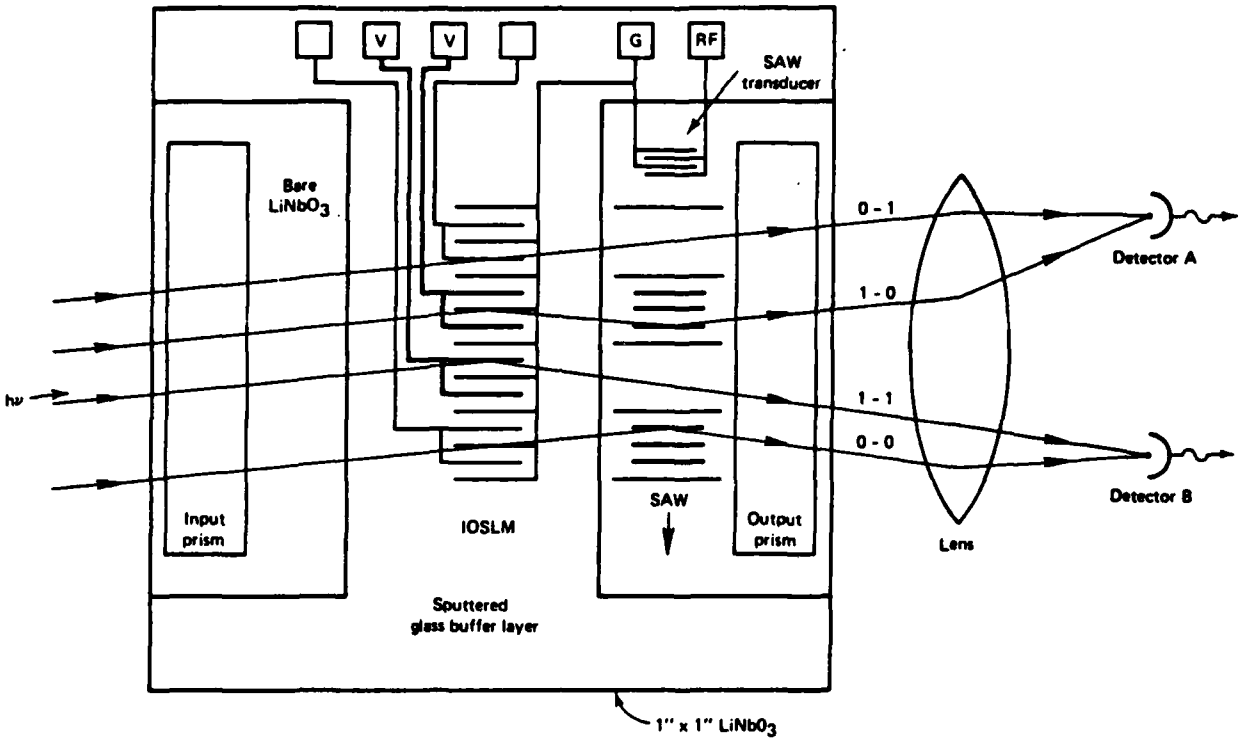

Figure 3.- Correlator incorporating a programmable IOSLM and a SAW transducer with digital modulation.

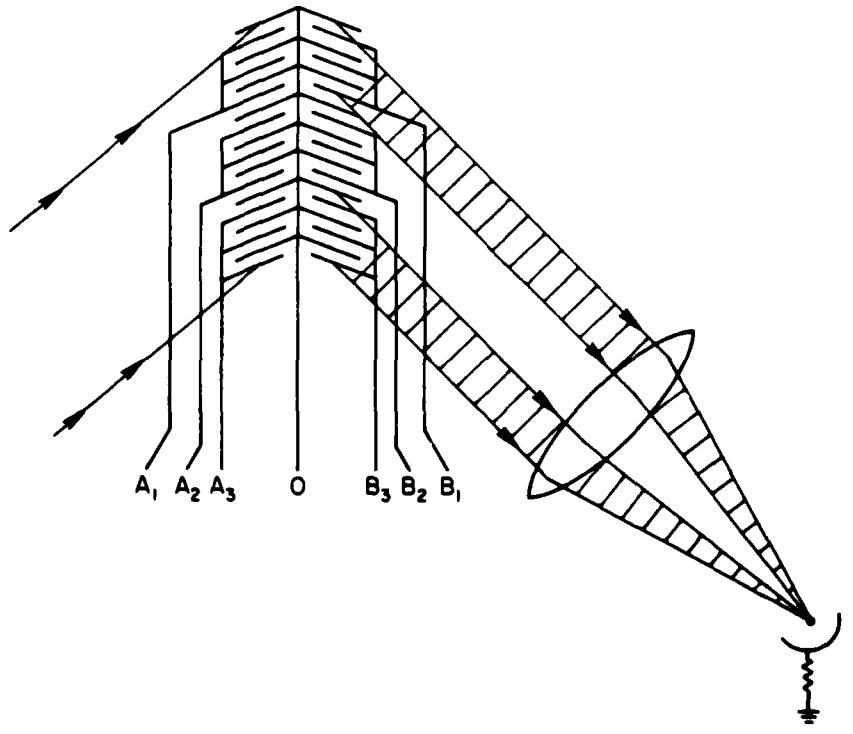

Figure 4.- Electrode structure for vector multiplication.

APPENDIX 6

APPLICATIONS OF THE INTEGRATED-OPTICAL LIGHT MODULATOR

Paper presented at the SPIE Conference on Integrated Optics and Millimeter and Microwave Integrated Circuits, Huntsville, AL November, 1981.

Applications of the integrated-optical light modulator*

C. M. Verber, R. P. Kenan, and J. R. Busch

Battelle-Columbus Laboratories
505 King Avenue, Columbus, Ohio 43201

Abstract

The electrooptic grating is an easily-fabricated component for integrated-optical applications that allows high-speed, efficient interaction with a guided optical wave in a planar waveguide. The use of these components in arrays allows implementation of several interesting and useful functions like spatial light modulation, correlation, parallel-to-serial conversion, and vector subtraction. We describe research on such devices; some potential applications in computation are also described.

Introduction

The electrooptic effect has been widely used in integrated optics for the fabrication of active devices, especially in conjunction with channelized waveguide structures in the surface of ferroelectric substrates like $LiNbO_3$ and $LiTaO_3$. In channelized structures, the lateral confinement of the light allows the use of electrode structures having a very large length/width ratio, enabling very long interaction lengths and low drive voltages. For example, in a channelized vector comparator constructed for NASA this ratio was 775.[1] In contrast to this situation, we will describe here the use of the electrooptic effect in planar waveguides, where the lateral spread of the light by diffraction is not inhibited. The light is still, of course, confined to within a few micrometers of the crystal surface, so one can still anticipate the effective use of fringing fields from surface-electrode structures to control the light with moderately low drive voltages required.

Our particular concern is with interdigital electrode structures that create induced phase gratings when they are energized. No claim to novelty in the basic structure is made--a modulator based on the basic grating structure was described by Hammer and Phillips[2] as long ago as 1974, and a patent on the structure issued to C. F. Buhrer[3] in 1972. We have used this basic structure in arrays to achieve several devices that are novel as well as useful.

In the next sections, we will describe the operation of the elementary electrooptic phase grating. In the following sections, we describe the use of grating arrays for spatial light modulation, correlation, parallel-to-serial conversion, vector subtraction, and, finally optical logic.

The Electrooptic Grating

The geometry of the electrooptic grating electrode structure is shown in Fig. 1. The structure is formed using standard photolithographic methods on the surface of a $Ti:LiNbO_3$[4] waveguide. Typically, the spacing between the fingers of the electrodes is made the same as the width of the fingers, so that the required photolithographic resolution is $\Lambda/4$. This choice is made partially as a holdover from the fabrication of similar structures for launching surface acoustic waves (SAWs), where this choice suppresses the excitation of certain harmonics, and partially from the intuitive feeling that it is just as difficult to make a space as to make a line, so making them equal minimizes the resolution. Equality is not required for operation of the gratings.

The application of a voltage across the electrodes results in a periodic fringing electric field that, via the electrooptic effect, causes a periodic modulation of the refractive index in the waveguide region. This modulation comprises the phase grating. The operation of such a grating in the Bragg regime is dominated by the fundamental Fourier component of the electric field distribution. Engan[5] has derived expressions for these components; he finds the amplitude (at the waveguide surface and for finger-width/gap ratio of 1)

$$E_o = 3.389\ V/\Lambda \qquad (1)$$

where V is the potential difference applied and the numerical factor can be compared to $8/\pi = 2.546$, which applies to the field in a slotted plane with the same applied potential and a slot width of $\Lambda/4$. For this geometry, the next non-zero harmonic is the fifth, for

*Work supported in part by the United States Air Force Office of Scientific Research.

which the amplitude is -1.695 V/Å, reduced only by a factor of one-half. However, when the fundamental is addressed at Bragg incidence, the fifth harmonic grating will be addressed well away from Bragg incidence, which accounts partially for the dominance of he fundamental.

The Bragg angle for a grating of period Λ is

$$\mathrm{Sin}\theta_B = \frac{\lambda_o}{2n\Lambda} \tag{2}$$

where λ_o is the vacuum wavelength of the light and n is the effective refractive index of the guided mode. The diffraction efficiency is given by[6]

$$\eta = \mathrm{Sin}^2\left[\frac{\pi \Delta n d}{\lambda_o \cos\theta_B}\right] \tag{3}$$

where d is the length of the finger overlap in Fig. 1 and Δn is the index modulation induced by the field of Eq. (1):

$$\Delta n = \frac{1}{2} n^3 rE.$$

where r is an electrooptic coefficient. Combining Eq. (4) with Eq. (1) and (3) gives for the efficiency

$$\eta = \mathrm{Sin}^2\left[\frac{5.32\ n^3\ r\ d\ V}{\lambda_o\ \Lambda\ \cos\theta_B}\right] \tag{4}$$

In practice, this result is followed in form, but somewhat higher voltages than implied by Eq. (5) are usually required to reach the maximum diffraction efficiency. The increase in voltage is not large for electrodes deposited directly on the waveguide surface and is probably caused by a combination of the finite depth of the waveguides and alteration of the conductivity of the waveguide surface by the various heat treatments and depositions involved in fabrication. However, a bare waveguide has a fixed grating of half the period of the electrooptic one, induced by the metal electrode structure. This fixed grating can weakly diffract light even when the electrodes are not energized; the metal electrodes also cause unwanted losses, scattering, and mode conversion. Hence, one commonly uses a buffer layer of glass or SiO_2.[7] This layer protects the light from the metal, but is thin enough that the field should not be seriously reduced from its surface value. In fact, it is typically observed in our experiments that voltages about 2.5 times larger are required to obtain maximum diffraction efficiency when a buffer layer is used. Some of this can be attributed to the finite thickness of the buffer layer and waveguide; however, such a large increase is not satisfactorily understood at present. It should be noted that these buffer layers must be annealed, preferably in oxygen to insure complete oxidation of the glass. Otherwise even larger differences are found.

The integrated optical spatial light modulator

The electrode structure of Fig. 2, in which one of the electrodes has been divided to allow access to individual segments of the grating structure, can be used to impress spatial information onto a guided wave, i.e., it can be used as an integrated-optical spatial-light modulator (IOSLM). The largest spatial frequency that can be transferred in this way depends on the width of the grating segments. If efficient operation is desired, then there must be enough fingers in each segment to insure operation in the Bragg regime. For many signal-processing applications, however, efficient operation is not absolutely necessary, and the number of fingers per segment can be reduced. We have fabricated a 32 channel array having 200 μm channels[8]; it spans a 6.4 mm wide optical guided wave and operates at 95% efficiency with an applied voltage of 4 volts without buffer and 10 volts with a buffer layer.

It should be possible to reduce the width of each grating segment to less than 25 μm, especially if smaller periods are used. The 25 μm figure corresponds to a spatial frequency maximum of 20 line pairs/mm in terms of the Nyquist sampling criterion (2 samples/period). Better photolithography (smaller periods) would allow further reductions and resolutions of 50 lp/mm or more should be possible. These are not remarkable figures, but are sufficient for performing several useful functions.

Correlation and parallel-to-serial conversion

The IOSLM described above has been used in conjunction with a surface acoustic wave transducer to construct a space-integrating correlator for discrete data. The layout of the original device is shown in Fig. 3. The SAW is modulated in an on-off fashion by the signal word at a data rate of about 16 Mb/sec, and its propagation across the crystal serves to

produce the offset needed for correlation. The reference word to be correlated with the signal is held statically in the IOSLM. In order to avoid the necessity for detecting light from the direction of the source, the ones complement of the reference word is actually used, so the correlation is obtained as a time sequence at detector B. Data on the operation of this correlator have been published.[8] With this simple layout, the autocorrelation of a signal appears to be asymmetric, because the IOSLM can diffract the incident light even when there is no SAW present. To correct this, the layout shown in Fig. 4 was devised. Here, two SAWs of different frequency are used to encode ones and zeros. They operate by deflecting the incident light into complimentary Bragg directions for the IOSLM. The arrangement is such that undeflected light is not affected by the IOSLM, and the resulting autocorrelation should be symmetric.

The correlators described above perform as expected and serve to illustrate the function and utility of the IOSLM. Data rates of 64 Mb/sec are well within current capabilities without changing the grating period. Reducing the grating period should permit data rates up to 100 Mb/sec. It should also be noted that because of the parallel entry of reference (or "filter") words, the downtime while reference words are changed can be made negligible. Indeed, since typically the capacitance per channel for the IOSLM will be smaller than 10 pf, this downtime will be determined by external circuitry and not by the correlator.

Another illustration of the utility of the IOSLM is obtained by considering the time sequence generated when the SAW signal is simply a single pulse having the same length as one of the grating segments. Then, as the pulse traverses the IOSLM region, a time sequence of pulses, replicating the reference word in the IOSLM, is obtained, that is, a parallel-to-series data conversion has been accomplished. Because the IOSLM can be parallel-loaded very rapidly, this conversion can be accomplished at a rate determined by the transit time for the pulse across the IOSLM width. For the improved correlator, the segments are about 110 μm wide so the data rate is about 32 Mb/sec and the conversion time is about 1 μsec.

Vector subtraction

The second electrode of Fig. 2 could also be segmented, so that the array truly was an array of the structures of Fig. 1. If we examine the diffraction from one of these elementary gratings, we find by Eq. (5) that the diffracted intensity is

$$\eta = \mathrm{Sin}^2\,[a(V_1 - V_2)] \qquad (6)$$

where a is a constant. For small signals, this response is proportional to the square of the voltage difference. In an array of N such elements, we can regard the voltages applied to, say, the left-hand electrodes as the components of an N-dimensional vector and those applied to the right-hand electrodes as the components of a second such vector. The diffracted intensity is then proportional to the summation of the squares of the component differences, that is, to the squared magnitude of the difference of the two vectors represented by the voltage sets. Such a vector subtractor can be operated at very high speeds and can be used for such operations as data classification or for rejection of redundant of already-observed data. The speed of operation of such a subtractor is limited mainly by the electrode capacitance, which can be very small.

Optical computation

The elementary electrooptic grating of Fig. 1, operated in a discrete, two-voltage system, performs the operation of logical difference (exclusive OR). An array of N such elements can perform this operation on two binary words of length N, and do so very rapidly. This is the simplest application of these gratings to numerical computation. For analog voltages, we simply obtain the vector subtractor described above.

To perform multiplication, we can use the structure pictured in Fig. (5). As indicated in the figure, the diffracted light is proportional to the product of the diffraction efficiencies of the two gratings. For binary (two-voltage) systems, the diffracted light will be the logical AND of the applied signals; for an array of N elements like this one, we can obtain the AND of the two binary words. If the total diffracted light is focused onto a detector, the output from the detector will be proportional to the number of ones in the AND. For analog signals, the operation can be used to produce the product of two vectors. However, the operation is not as simple. The diffracted intensity is really proportional to the square of the product of the signals, but the use of signal voltages modulated at some fixed frequency enables one to retrieve the desired product of signal voltages in a simple way.

Conclusion

We have described the use of electrooptic grating arrays in integrated optics to perform several useful functions. The most significant of these currently are correlation, spatial

light modulation, parallel-to-serial conversion, and vector comparison. Efforts are under way to examine the computational uses of these arrays experimentally.

References

1. Hartman, N. F., Verber, C. M. and Chapman, C. M., "Fabrication of a 16 Channel Integrated Optical Data Preprocessor", Paper presented at the 31st Electronics Components Conference, Atlanta, GA (May 11-13, 1981).
2. Hammer, J. M. and Phillips, W., "Low-Loss Single-Mode Optical Waveguides and Efficient High-Speed Modulators of $Li_xTa_{1-x}O_3$ on $LiTaO_3$", Appl. Phys. Lett., Vol. 24, pp 545-547. 1974.
3. Buher, C. F., United States Patent No. 3,813,142, 1972. (Assigned to GTE).
4. Schmidt, R. V., and Kaminow, I. P., "Metal Diffused Optical Waveguides in $LiNbO_3$", Appl. Phys. Lett., Vol. 24, pp 458-460. 1974.
5. Engan, H., "Excitation of Elastic Surface Waves by Spatial Harmonics of Interdigital Transducers", IEEE Trans. on Electron Devices, Vol. ED-16, pp 1014-1017. 1969.
6. Kogelnik, H., "Coupled-Wave Theory for Thick Hologram Gratings", Bell Syst. Tech. J., Vol. 48, pp 2909-2947. 1969.
7. Tagonian, G. L., Persechini, D. L., Lotspeich, J. F., and Barnoski, M. K., "Electro-optic Diffraction Modulation in Ti-Diffused $LiTaO_3$", Appl. Opt., Vol. 17, pp 3259-3263. 1978.
8. Verber, C. M., Kenan, R. P., and Busch, J. R., "Correlator Based on an Integrated-Optical Spatial-Light Modulator", Appl. Opt., Vol. 20, pp 1626-1629. 1981.

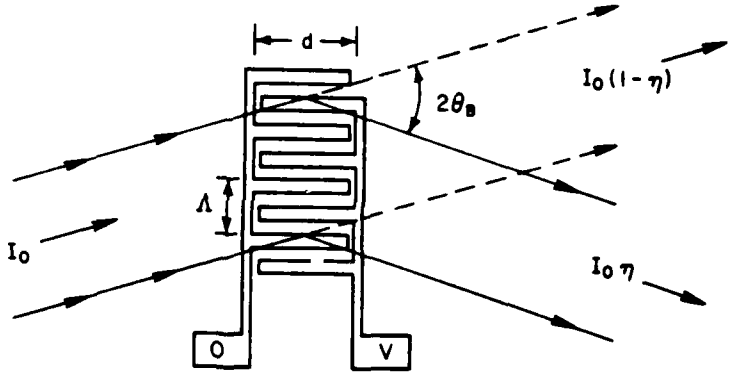

Figure 1. Basic electrode structure.

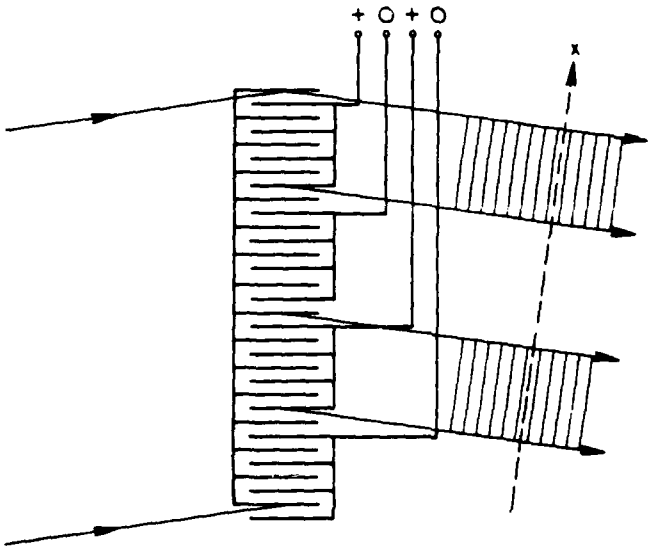

Figure 2. The electrode structure for the integrated optical spatial light modulator.

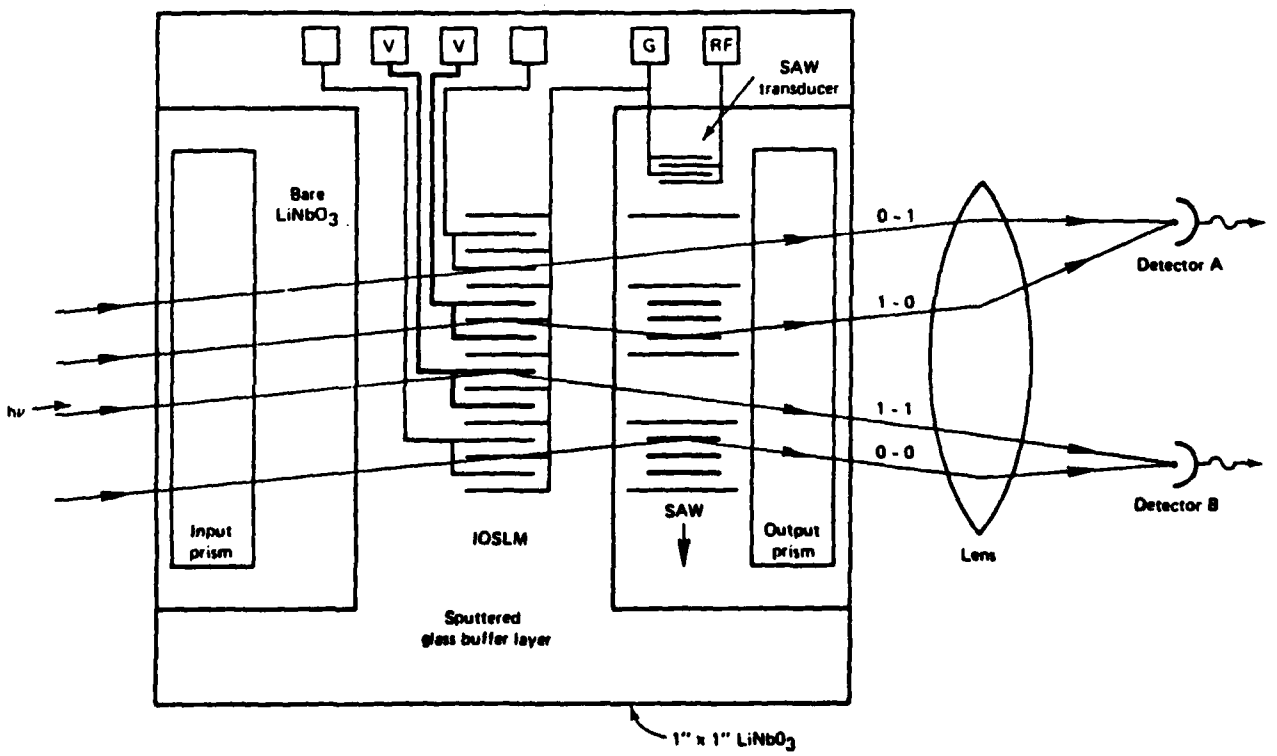

Figure 3. Correlator incorporating a programmable IOSLM and a SAW transducer with digital modulation.

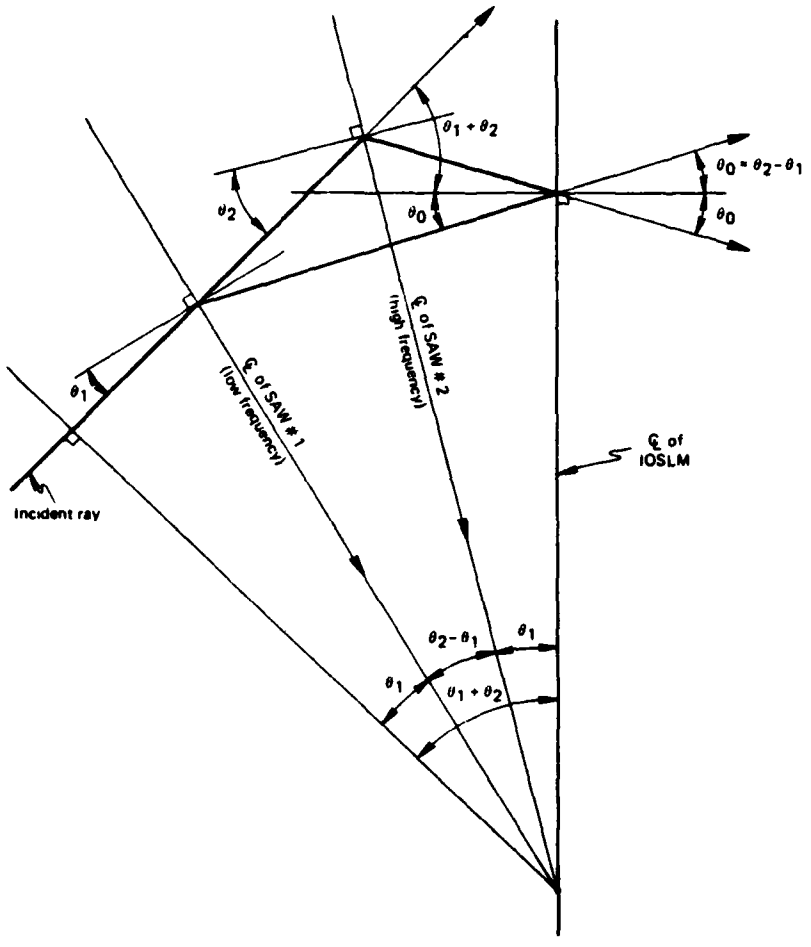

Figure 4. Geometric layout of the improved correlator, showing angular relationships in the small-angle approximation.

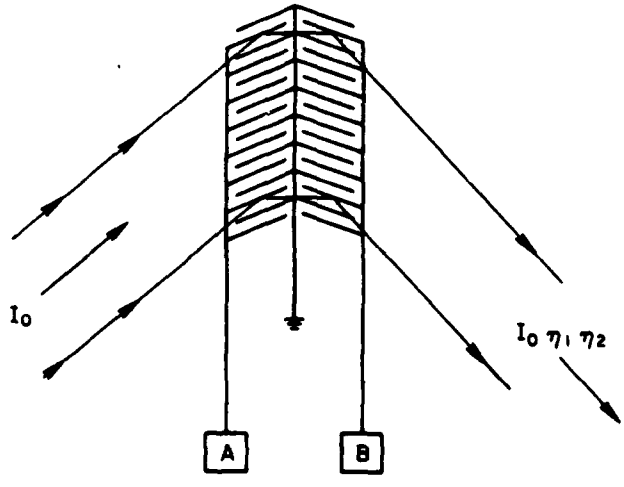

$\eta_1 \eta_2 = \sin^2 \alpha A \sin^2 \alpha B$

Figure 5. Grating structure for performing multiplication.

APPENDIX 7

GRATING ARRAYS FOR INTEGRATED OPTICS APPLICATIONS

Paper presented at Conference on Lasers and Electro-Optics (CLEO '82), Phoenix, AZ, April 14-16, 1982.

Grating Arrays for Integrated Optics Applications

R. P. Kenan, C. M. Verber, and J. R. Busch
Battelle Columbus Laboratories
505 King Avenue
Columbus, Ohio 43201

Abstract

The design and operation of two integrated-optical devices utilizing grating arrays are discussed.

Grating Arrays for Integrated Optics Applications

R. P. Kenan, C. M. Verber, and J. R. Busch
Battelle Columbus Laboratories
505 King Avenue
Columbus, Ohio 43201

Introduction

Electrooptic gratings have been used in integrated optics to form deflectors, modulators, and switches by a number of researchers. Recently, we have demonstrated a correlator based on an array of such individually addressable elements in conjunction with a modulated surface acoustic wave (SAW).[1] The device performed as predicted by theory, generating the correlation of two 32-bit binary words at a data rate of 17.5 Mbits/sec.

Electrooptic gratings are capable of other uses as well. In particular, it is possible to use them to generate an optical signal that is proportional to the difference between the voltages applied to the electrodes. For two-voltage systems, this becomes the logical difference, usually called the exclusive OR (EXOR) operation.

In this paper, we present two applications of arrays of electrooptic gratings. We report the design of an improved version of the correlator discussed in the first paragraph; and we discuss the operation of a 16-channel vector comparator that can generate an output proportional (for small signals) to the magnitude of the difference vector of the two sets of voltages applied to the structure, where we regard each voltage set as forming a 16-dimensional vector.

Improved Correlator

The original correlator layout is shown in Fig. 1. The complement of one of the signals to be correlated is applied to the 32 electrodes of the grating array (IOSLM, for integrated-optical spatial light modulator), while

the other is used to modulate (as a binary signal) an rf generator connected to a SAW transducer. During the time when there is non-zero overlap between the SAW and the grating array, the singly-diffracted light generates the correlation of the two signals, superimposed upon a signal that arises because of the light diffracted from the array in the absence of the SAW. This part of the light is spurious. The geometry used in the improved version of the correlator is shown in Fig. 2. Here, the parts are arranged so that the grating array is ineffective in diffracting the undeflected input light. Two SAWs of different frequency are arranged so that light diffracted by either SAW will also be diffracted by an activated grating segment. The two complimentary Bragg directions of the gratings are used for this purpose. Arrangement of the two SAWs and the grating array as shown, radiating from a common point, allows a ray of light to enter the same part of the IOSLM independently of which SAW it is diffracted from. This arrangement should restore the symmetry expected in an autocorrelation, since now there is no signal output unless the SAWs and the array overlap, and the output comes only from the overlap region.

A sample correlator has been fabricated and tested. It utilizes a 32-window IOSLM and SAW frequencies of approximately 416 MHz and 875 MHz and performs correlations at a data rate of 32Mbits/sec. A preliminary sample correlation is shown in Fig. 3. More complete evaluations will be presented.

Voltage Comparator

A grating array similar to the one used with the correlator, except that both electrodes of each array element are individually addressable, can be used to perform vector subtraction. When the grating electrodes are connected to two voltage sets, those gratings for which the applied voltages differ become activated, but gratings for which the applied voltages are the

same are not activated. For small applied voltage differences, the response of a grating element is proportional to the square of the difference of the applied voltages. If the diffracted light is imaged onto a photodetector, so that light from the different gratings falls on different parts of the detector, then a photocurrent that is proportional to the sum of the squares of the voltage differences, thus generating the square of the magnitude of the vector difference between the two applied voltage sets, regarded as 16-dimensional vectors.

A prototype of this device has been fabricated for evaluation. Detailed data from this evaluation will be presented. Preliminary evaluation of a faulty sample indicates performance will be as expected from theory.

Reference

(1) C. M. Verber, R. P. Kenan, and J. R. Busch, "Correlator Based on an Integrated Optical Spatial Light Modulator", Applied Optics, 20 (9), May 1, 1981, pp 1626-1629.

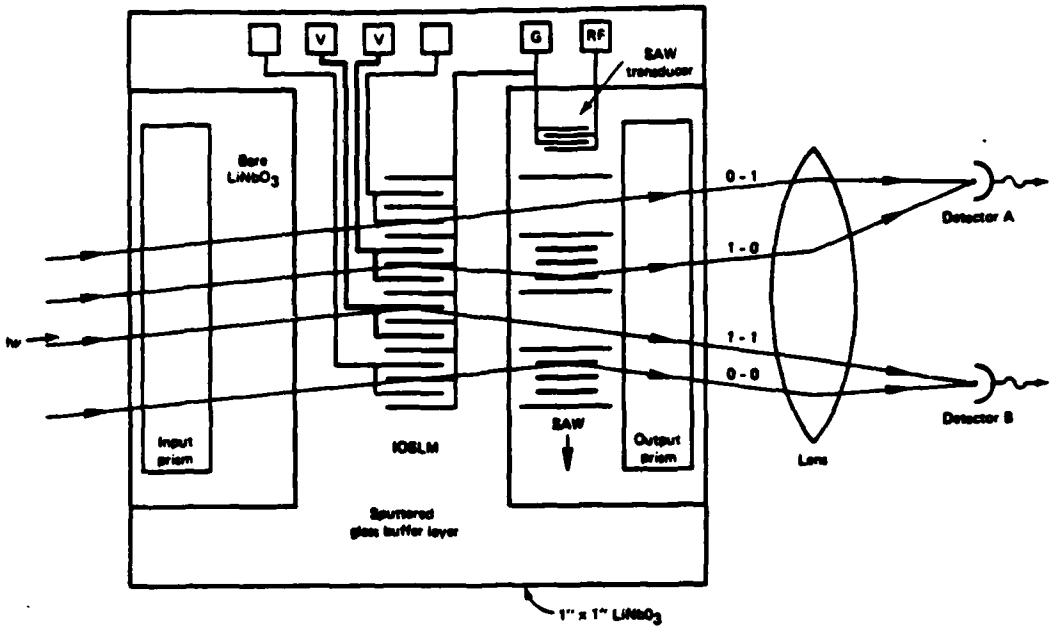

Fig. 1. Schematic drawing of an integrated optical correlator based on the programmable IOSLM. The IOSLM is the array in the center of the drawing. The notations (0-1, 1-0, etc) on the output beams indicate the state of the IOSLM and SAW segments, respectively, that are encountered by the respective beams.

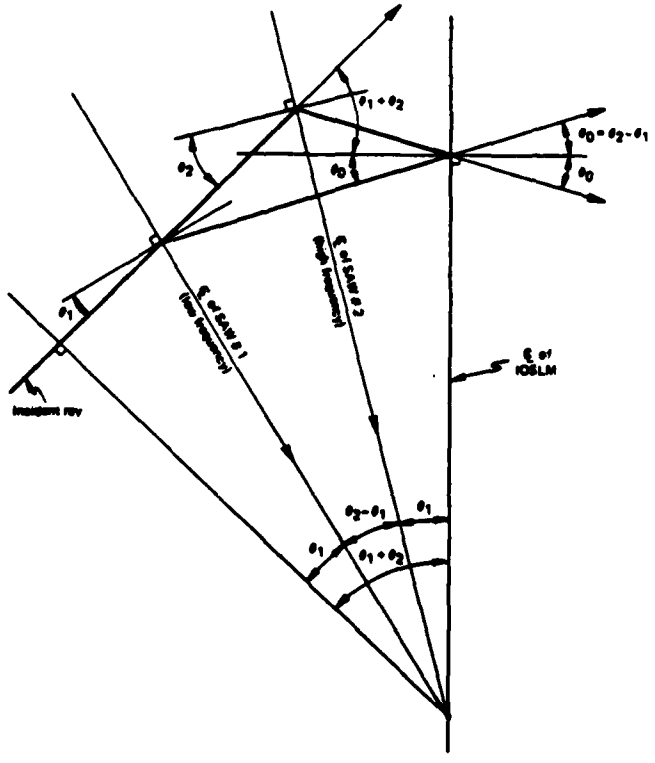

Fig. 2. Geometric layout of the improved correlator, showing angular relationships in the small-angle approximation.

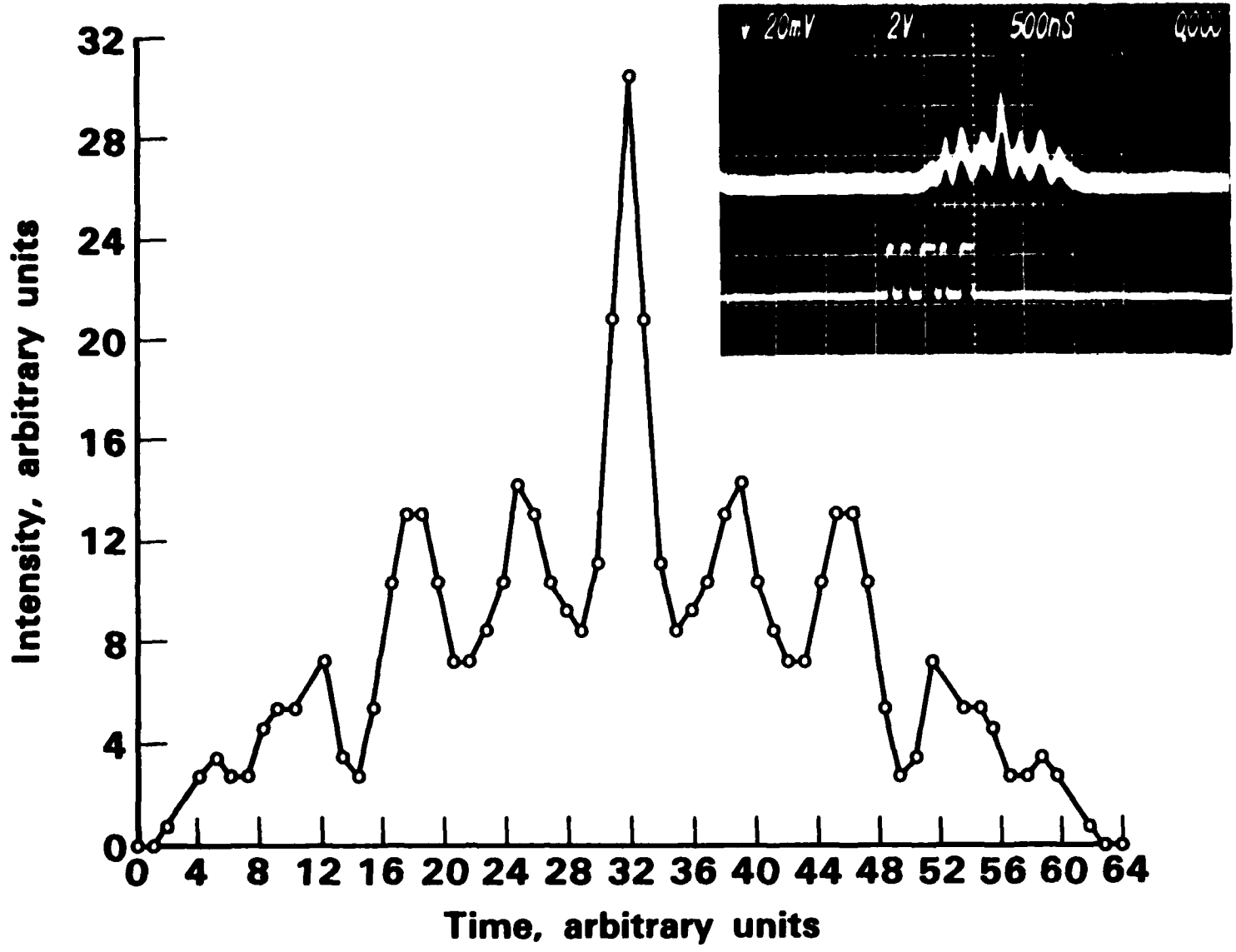

Fig. 3. Calculated autocorrelation function for the 32 bit binary word 11001110001111000001100111110000 and oscilloscope trace from the actual device (inset). This preliminary data was taken on a damaged grating array.


LME